uOttawa

L'Université canadienne
Canada's university

FACULTÉ DES ÉTUDES SUPÉRIEURES ET POSTOCTORALES

uOttawa

L'Université canadienne
Canada's university

FACULTY OF GRADUATE AND POSDOCTORAL STUDIES

Laura Petrescue

AUTEUR DE LA THÈSE / AUTHOR OF THESIS

M.A.Sc. (Mechanical Engineering)

GRADE / DEGREE

Department of Mechanical Engineering

FACULTÉ, ÉCOLE, DÉPARTEMENT / FACULTY, SCHOOL, DEPARTMENT

An Investigation of Defect Evolution in Foam Core Sandwich Structures Produced Using Vaccum Assisted Resin Transfer Moulding

TITRE DE LA THÈSE / TITLE OF THESIS

Dr. Michael Munro

DIRECTEUR (DIRECTRICE) DE LA THÈSE / THESIS SUPERVISOR

Dr. Pascal Hubert

CO-DIRECTEUR (CO-DIRECTRICE) DE LA THÈSE / THESIS CO-SUPERVISOR

EXAMINATEURS (EXAMINATRICES) DE LA THÈSE / THESIS EXAMINERS

Dr. F. Robitaille

Prof. P. Straznicky

Gary W. Slater

Le Doyen de la Faculté des études supérieures et postdoctorales / Dean of the Faculty of Graduate and Postdoctoral Studies

AN INVESTIGATION OF DEFECT EVOLUTION IN FOAM CORE SANDWICH STRUCTURES PRODUCED USING VACUUM ASSISTED RESIN TRANSFER MOULDING

Laura Petrescue

Thesis submitted to the
Faculty of Graduate and Postdoctoral Studies
in partial fulfillment of the requirements to the degree of

Masters of Applied Science

Ottawa-Carleton Institute for Mechanical and Aerospace Engineering

Department of Mechanical Engineering
Faculty of Engineering
University of Ottawa

Your file Votre référence
ISBN: 978-0-494-49263-5
Our file Notre référence
ISBN: 978-0-494-49263-5

Abstract

In this work, a resin infusion process used by Flight Dynamics Corp. was investigated for the fabrication of low-cost composite sandwich structures. Trials were performed to establish a complete set of potential defects that could develop during the manufacture of E-glass epoxy vinyl ester sandwich panels. A series of non-destructive evaluation techniques were examined for their potential to identify two representative defects. It was found that thermography and bondline analysis were effective at detecting defects such as dry spots and incomplete resin infiltration. However, due to technical limitations of these methods visual inspection of high quality digital images proved to be the most accurate method for evaluating the specimens. The effect of these defects was also evaluated through a selection of compression tests. These tests showed that the sensitivity of this test to the presence of defects is low. A parametric study of the infusion process was performed to evaluate the potential of defect evolution under controlled conditions. The evolution of defects was most affected by the vacuum pressure level and the method for distributing resin through the thickness of the sandwich panel. As part of this study, the resin flow front was evaluated to determine the effect on the evolution of defects. A series of defect metrics were developed for a variety of resin distribution methods. In general, it was found that defect evolution due to a single variable was limited and that further evaluation of the interaction of process parameters would be useful to optimize the process.

Dedication

To my husband Grant for his constant love, support, and encouragement.

Table of Contents

List of Figures

List of Tables

Acknowledgements

I would like to thank my supervisors Prof. Pascal Hubert and Prof. Mike Munro for their technical, financial and professional support. Their expertise has been invaluable and I would especially like to thank them for their patience throughout this process.

I also extend my thanks to Loleï Khoun, Mike McGrath, and Eric St-Amant for their tremendous support in performing experimental trials and conducting mechanical testing. Your help was greatly appreciated.

My sincere gratitude goes to the National Research Council and the people at the Institute for Aerospace Research in Ottawa for providing me with the time and resources to pursue this work. Special thanks go to Mike Brothers, Phil Vesely and Marc Genest for their assistance in performing non-destructive evaluation and Tom Kay for his help in specimen preparation.

I would also like to express my appreciation to Flight Dynamics Corporation for providing materials and financial support to this work.

Finally, thank you to the National Sciences and Engineering Research Council of Canada grant program for its financial support.

Chapter 1 Introduction

The application of composites on aircraft involves a range of advantages offset by a number of challenges. The ability to tailor the distribution of loads and integrate components enables the fabrication of more efficient structures with reduced weight and fewer manufacturing steps. Conversely, the application of any new material or process on aircraft requires a great deal of effort during the certification phase. Certification authorities need to be "convinced" that a structure made with a new process and/or material is safe to fly. The application of composite materials is not a simple design alteration. The basic material properties are developed in conjunction with the fabrication of the structure. Therefore, depending on the manufacturing process and the quality of operators, there can be variability of the final parts. The key to decreasing variability is to understand the process parameters affecting key characteristics such as fibre volume fraction and surface quality, as well as the evolution of defects such as porosity and resin starved areas. Besides the application of composite materials themselves the choice of manufacturing process contributes to the final part quality by using different methods for the introduction of the matrix to the reinforcement, application of consolidation pressure, automation, etc.

The Vacuum-Assisted Resin Transfer Moulding (VARTM) process has been used primarily in the marine industry as a method to reduce exposure of workers to hazardous volatiles by replacing hand layup processes. Since VARTM is not generally used in the aerospace industry, it is necessary to develop an understanding

of how this processing method affects the quality of composite aircraft structures. This manufacturing method is different from conventional composite processing methods for aircraft in that liquid resin must flow through the fibre preform and result in a uniform fibre volume fraction. Conventional methods make use of preimpregnated fibres or prepregs that have a premetered, partially-cured resin content. The use of liquid resin makes a number of other variables such as viscosity, temperature, gel time, and vacuum pressure potentially more influential on the resulting quality. By understanding how various process parameters affect part quality it is possible to design a robust process with key variables identified. A successful process design will allow for high quality, defect-free parts with control of only select variables.

1.1 Literature Review

1.1.1 Fibre-Matrix Composites

A composite is a material that is made up of two or more distinct components. Composites encompass a wide range of materials including wood, metal alloys and concrete. However, for the purpose of this work composites are considered to consist of a fibre reinforcement within a polymer resin matrix. The main objective for design of a composite material is to combine the properties of each individual component with final properties being higher than both constituents [1]. To outperform other material choices in a given application composites have the advantage of specific strength or stiffness. Specific strength and stiffness are the strength and stiffness of the composite divided by the density of the composite. Lightweight continuous fibres

with a high tensile strength or Young's modulus provide the load bearing or stiffening component of the material. A polymer matrix is used to bind the fibres together into a structure and transfer stresses between fibres. The resin can be formulated to provide a variety of properties such as toughness, fire resistance, and temperature performance. Another important function of the matrix is to protect fibres from abrasion or chemicals that would weaken or fracture them [1]. The mechanical properties of a composite material are a combination of the matrix and reinforcement properties.

The reinforcement phase of a composite material can come in a variety of forms, but generally, for aerospace applications the reinforcement is made up of continuous fibres aligned in one or two planar directions. The fibres can be aligned along one direction or woven in orthogonal directions into a variety of styles. Each planar arrangement of fibres makes up one lamina or ply. The plies are then stacked to form a laminate [2]. The polymer matrix material may be added prior to lamination to form a preimpregnated material, a prepreg, or after stacking of the laminate to produce a preform into which resin is injected, infused, or pressed.

Each lamina with fibres aligned in a particular direction(s) has enhanced mechanical properties such as stiffness or strength that are coincident with the direction of fibre alignment. The benefit of these types of composite materials is that anisotropic laminae can be strategically arranged to accommodate known loads on a structural component. Therefore, the design of a composite structure may be optimized to

accommodate stresses or strains in (given) directions without needing to have fibres (extra weight) in non-critical directions [2].

The methods of imparting the matrix phase onto the reinforcement phase are discussed in the following sections.

1.1.2 Manufacturing Processes

1.1.2.1 Traditional Processes

The key to successfully using fibre and matrix materials in constructing parts used in structural applications is the design of the manufacturing process. The main issues associated with a successful manufacturing process are the ability to achieve uniform consolidation with minimal porosity and to reach the desired degree of cure [3]. Over time, new methods of fabrication are developed and the technology of earlier methods is improved all with the goal of reducing cost, increasing efficiency, and improving quality. A number of fabrication methods have been developed and successfully used to manufacture composite parts. This section provides an overview of these methods including some of their advantages and disadvantages as well as potential applications.

One of the most basic fabrication techniques is manual hand layup. This process involves placing dry fibre materials into a mould and using rollers and brushes to distribute liquid resin. This manufacturing process is used in applications ranging from fabrication of surfboards to structural repair of critical aircraft structure such as

a wing leading edge. This is a low cost method because there is no large equipment expense and tooling can be very inexpensive. A schematic of the process is shown in Figure 1. The limitations of this technique are that there is no applied consolidation method so the resin volume fraction (V_m) can be quite high and the uniformity of resin deposition is low. From this basic fabrication method a number of other methods have been developed that either provide greater automation of the process or additional steps to improve quality such as controlled consolidation.

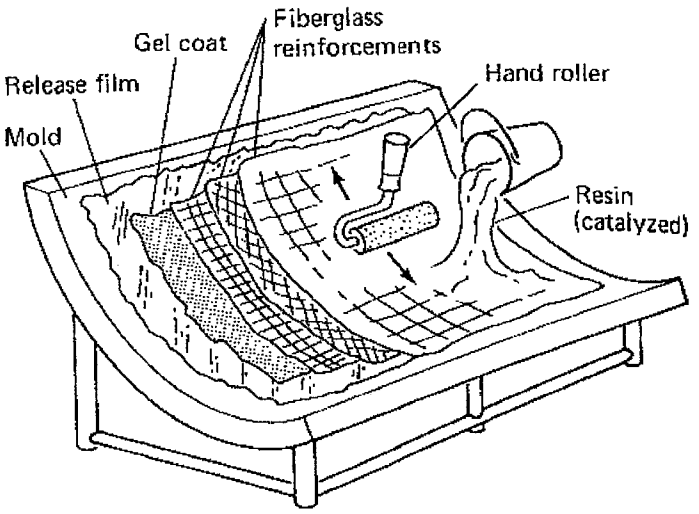

Figure 1 Schematic of manual lay-up process [4]

Spray-up is used to automate the application of fibres and resin. Continuous strands are fed into a chopper that cuts the fibres into shorter strands. The strands are then mixed with resin and sprayed onto a mould surface. Resin is initiated for curing as it is applied to the fibres thereby eliminating pot-life difficulties with pre-mixed resin [5]. This method results in very quick deposition, but the discontinuous fibres are applied randomly and there is no additional consolidation to increase the fibre volume

fraction [3]. The spray-up technique is commonly used for commercial products such as canoes and bathtubs. A schematic of this technique is shown in Figure 2.

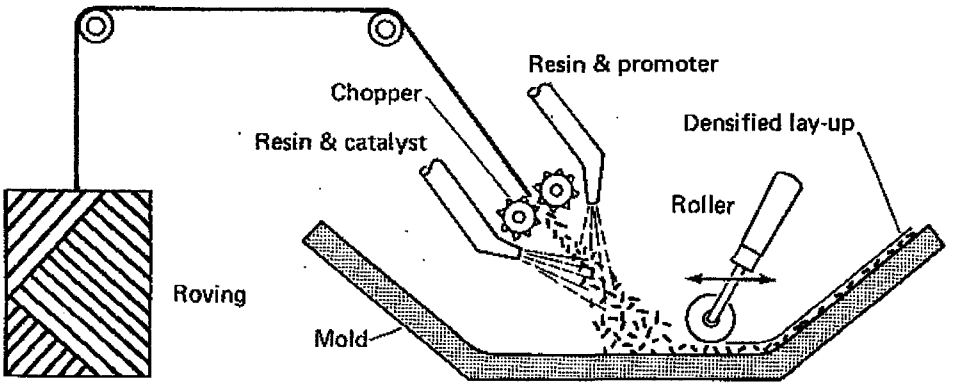

Figure 2 Schematic of spray-up process [4]

Pultrusion makes use of continuous fibres that are impregnated with resin and drawn through a die and cured in-situ. The result is a uniformly controlled cross-section with high unidirectional strengths [5]. This method has both automated impregnation and layup which is attractive for reduction of labour costs [6]. However, the manufactured part is generally used as stock material, but not for final finished parts. Pultrusion is useful for fabrication of commercial products such as window frames and ladders [6]. Recently, there has been work done to fabricate aircraft parts such as stringers and floor beams [7].

Filament winding is an automated method whereby a continuous fibre strand is wound around a mandrel. The mandrel can either become an integral part of the manufactured product or can be removable as in the case of an inflatable or soluble mandrel. Resin is automatically metered onto the fibre and the winding path is programmed to use a predetermined pattern. Figure 3 shows a schematic of this

process. The drawback of this method is that consolidation of the layup relies on fibre tension; therefore, concave surfaces cannot be fabricated and surface finish can be poor. Also, there is a restriction on the shape of the end of the part and 0° fibres cannot be applied [8]. However, due to the low labour and material cost of this method and the fact that very large structures can be fabricated, filament winding is an attractive method that is commonly used to fabricate pressure vessels [8].

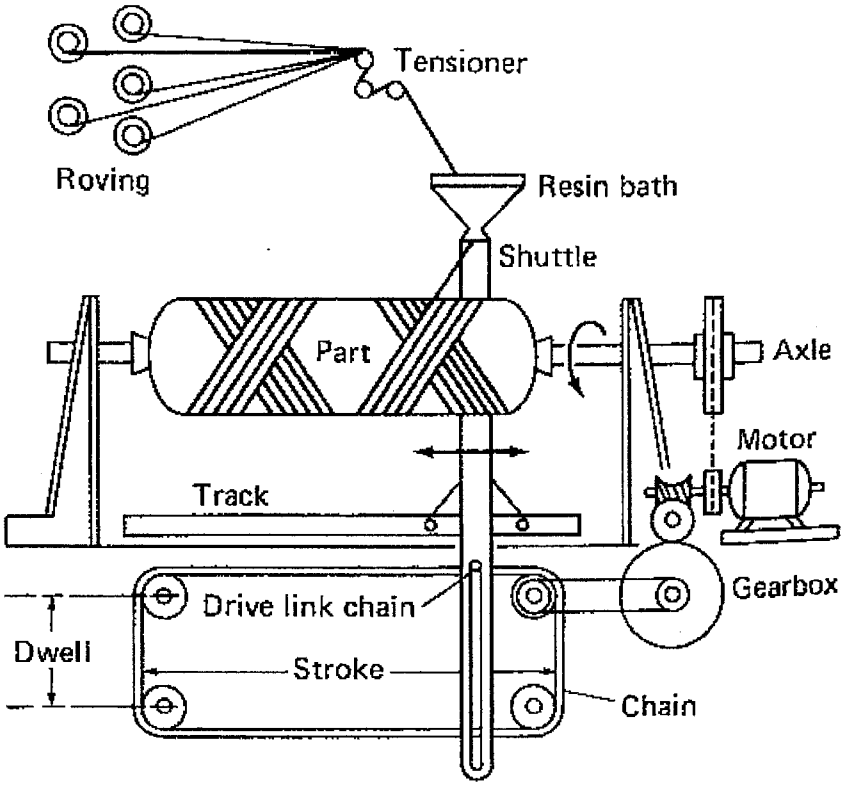

Figure 3 Schematic of filament winding process [4]

Vacuum bag forming is the same fundamental technique as hand layup with the added step of consolidation using a vacuum bag to promote a higher fibre volume fraction and more even resin distribution [5]. A nylon bag is sealed over the tool and vacuum is applied to evacuate the air from the bag and vacuum is maintained until the

resin has gelled. The vacuum bag method can be applied to a variety of different manufacturing methods including hand layup, filament winding, and spray up to increase laminate quality. A disadvantage of this method is in the fact that if the resin has a high volatile content the volatiles could tend to evaporate under applied vacuum and increase the porosity of the part [3].

An automated method of consolidating resin and fibre simultaneously without the application of a vacuum bag is press moulding. This method uses matched male and female moulds and high pressures to consolidate the layup and distribute resin throughout the dry fibres. This method has limitations on the size of part that can be manufactured since the size of the part is proportional to the amount of pressure required to consolidate the layup. Another disadvantage is that the amount of resin and the initiator and accelerator proportions must be very accurately measured to accomplish the correct final fibre volume fraction (V_f) and degree of cure [3].

The previous methods can be considered to be wet layup methods where liquid resin is applied to the fibres during the fabrication of the final part and the two material components are cured together directly after. To control the application of resin to the fibres prepreg is used whereby fibres are impregnated with resin in a hot-melt process which results in resin that is partially cured to a B-stage. Prepreg can then be stored at sub-zero temperatures until fabrication of a part begins. At this stage the prepreg is thawed to room temperature and cut into the appropriate ply orientations. The plies are applied to a mould surface sequentially and consolidated through the

use of a vacuum bag. Depending on the type of prepreg used the layup can be cured in an oven, or to attain a higher quality, in an autoclave which applies both heat and additional pressure up to 100 psi [3],[5]. Autoclave moulding has been used for decades as the main manufacturing method for aerospace parts.

More recently, parts that are too large to be manufactured cost-effectively using the autoclave method have been fabricated using automated tape layup to apply prepreg in the form of uniaxial tape to a mould. A robotic head with several axes of motion is used to apply the tape which allows concave curvatures to be manufactured. The part is then cured in an oven. The labour associated with this method is low due to the use of a programmable controller, but the software and the robotic arm must be capable of placing the prepreg accurately [5],[3]. This method is generally used for military and civil aircraft wings and empennages and helicopter blades [3].

Autoclave moulding and automated tape layup, however, require the purchase of expensive equipment and prepreg material. There is also a high expense associated with labour and processing time using the autoclave method. Because the autoclave and tooling have a large thermal mass, the cure cycle is generally five hours long in order that all parts heat up to the required temperature [3]. Due to the economic constraints of aircraft manufacturers there is a push towards the use of low cost methods to replace current techniques. There are a wide variety of potential liquid composite moulding techniques that result in parts having varying degrees of cost and

quality. These methods and their possibility to replace conventional techniques are discussed in the next section.

1.1.2.2 Liquid Composite Moulding processes

The use of closed mould LCM in the marine industry has the benefits of reducing labour on large-scale structures and exposure to hazardous chemicals caused by traditional hand layup techniques. The development of LCM processes for aircraft has been driven more by the need to reduce costs for materials and manufacturing. Large original equipment manufacturers (OEM) are commonly out-sourcing many of their products. Where originally they maintained all of the large high-capital cost equipment, such as autoclaves and automated tape layup machines, smaller companies are now required to produce high quality parts at a fraction of the cost. With the market now open for competition companies are adopting low-cost methods rather than investing in expensive equipment. This has paved the way for out-of-autoclave processing. The original LCM process, resin transfer moulding (RTM), uses the technique of hand layup to assemble a dry preform in the bottom half of a closed mould. Alternatively, preforms can be prepared in advance and stored until needed. A matching mould is placed on top and clamping pressure is used to seal the two halves together. Resin is injected into the mould under low pressures between 1 and 7 bar. A schematic of the RTM process is shown in Figure 4.

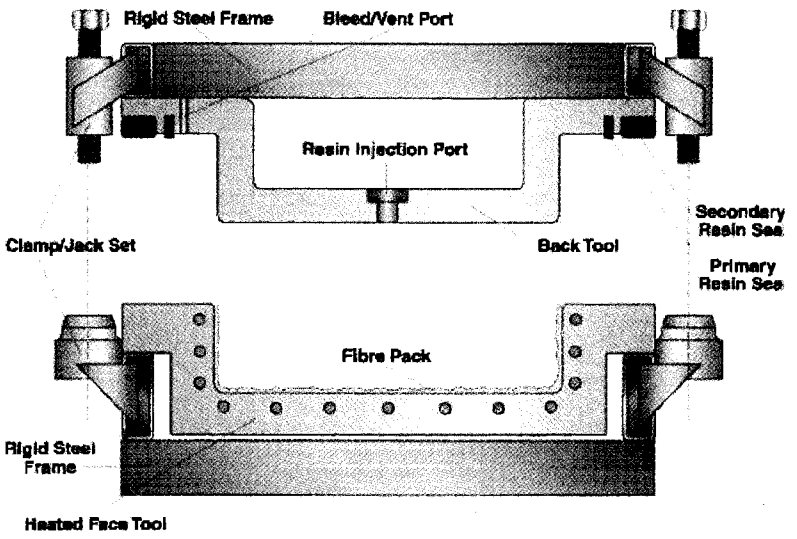

Figure 4 Schematic of RTM process [9]

Other advantages of RTM include tight tolerances, use of low cost materials, predictable fibre volume fractions, and low emission of solvents and volatiles [3]. The resulting part has two surfaces with tightly controlled tolerances and high quality surface finishes. The speed of production and quality of surface finish make this processing method good for medium volume automobile parts. Disadvantages include the high compaction of the reinforcement that results in a low permeability preform. Additionally, resin racetracking occurs where gaps exist between the preform and mould [3]. Racetracking is where resin circumvents the fibre preform and instead follows the path of least resistance to flow. Vacuum may be applied to aid in the removal of air from the mould in a process called vacuum-assisted resin injection (VARI). In 1982, Adolf le Compte patented a version of the VARI technique for manufacturing large thin-walled structures such as a ship's hull [10]. However, as with vacuum bagging methods, low pressures can result in porosity due to volatilization of the resin constituents [3]. Because of the expense of RTM tooling,

single sided liquid moulding processes are preferred for lowering manufacturing costs. In many aircraft applications only a single control surface is required. Wing skins, leading edges, fairings, radomes, nose cones, etc., all have the potential to use single-sided LCM methods. Thus, single-sided tooling on which a part can be cured in an oven or in-situ is very desirable.

It is not the intention of this thesis to outline all of the possible LCM manufacturing methods, but to pinpoint those that are considered potential for fabrication of aircraft parts. LCM methods such as reinforced Reaction Injection Moulding (RRIM) use low-cost, low property materials such as polyester and random mat that are typically unsuitable for aircraft structural parts [4]. Thus, methods such as Resin Film Infusion (RFI), Seemann Composites Resin Infusion Molding Process (SCRIMP), and vacuum infusion can provide significant cost benefits over autoclave processing for aircraft parts.

1.1.2.3 Resin Infusion Processes

Williams et al. [11] and Karbhari [12] provide reviews of resin infusion development from its inception in 1950 to the state-of-the-art in 2001. In 1950, I. E. Muskat patented a number of different moulding methods incorporating features that make up today's compression, RTM and VARTM methods [13]. In particular, one method involves drawing the resin into the two-sided mould using a vacuum pump. Saturation of the part was indicated by the resin exiting the tool at the location of vacuum draw. While this method is not considered single-sided it represents one of

the first closed mould infusion processes [13]. A schematic of this process is shown in Figure 5.

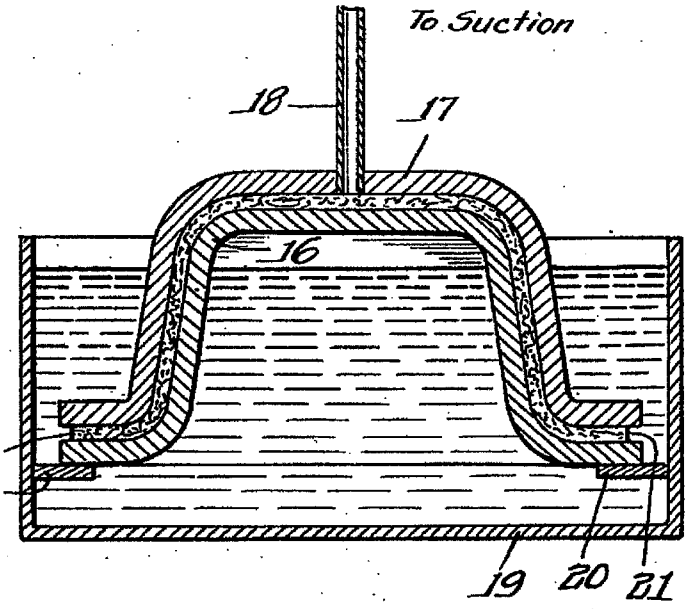

Figure 5 Schematic of I.E. Muskat's patented liquid composite moulding technology [13]

The current basic method of resin infusion involves placing dry fabric or fibres into a single-sided mould and sealing within a vacuum bag. Air is evacuated from the preform using vacuum pressure to consolidate the plies. Resin is introduced into the vacuum bag at atmospheric pressure and the differential pressure serves to draw the resin through the preform. This simple method shown in Figure 6 requires very little capital cost [14],[15].

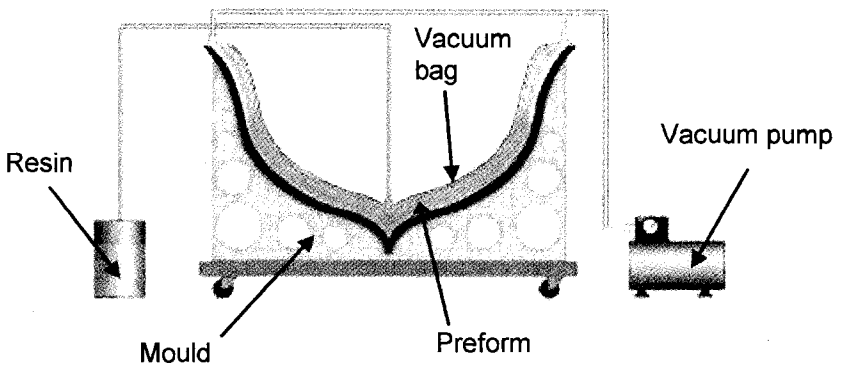

Figure 6 Schematic of resin infusion process [16]

Resin film infusion is a method where dry fibres are placed onto a single-sided tool with resin film either below the preform or interleaved between layers of fabric [3]. A vacuum bag is applied to the layup and then heat is often added to soften the resin while vacuum is applied. Figure 7 shows a schematic of the RFI process. An advantage of this method is that resin has only to travel through the thickness of the preform in order to fully saturate the dry fibres. This fact makes RFI desirable for use with higher viscosity resin systems and high fibre volume fraction (V_f) fabrics.

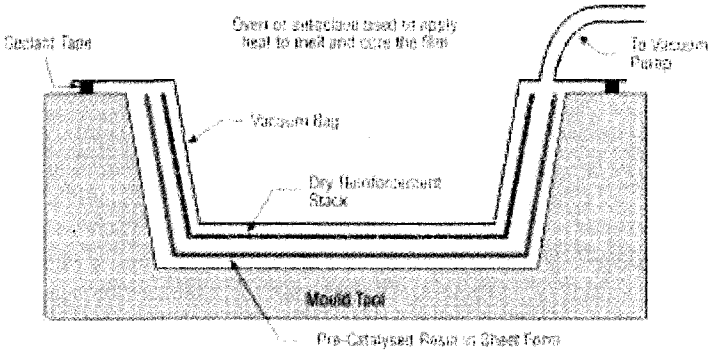

Figure 7 Schematic of RFI process [17]

The FASTRAC method [18] uses a double bagging technique and a rigid or flexible non-contacting tool that creates resin distribution channels in the primary vacuum bag. During infiltration, the non-contacting tool is held on the outside of the primary vacuum bag by the secondary vacuum bag. Vacuum draws the primary bag into the channels of the non-contacting tool creating resin flow paths. Once the resin has infiltrated the primary bag, the secondary vacuum bag and non-contacting tool are removed and vacuum draws the primary bag tightly over the preform thereby saturating the part. The benefit of this method over other resin infusion techniques is the speed of infiltration. A schematic of this process is shown in Figure 8.

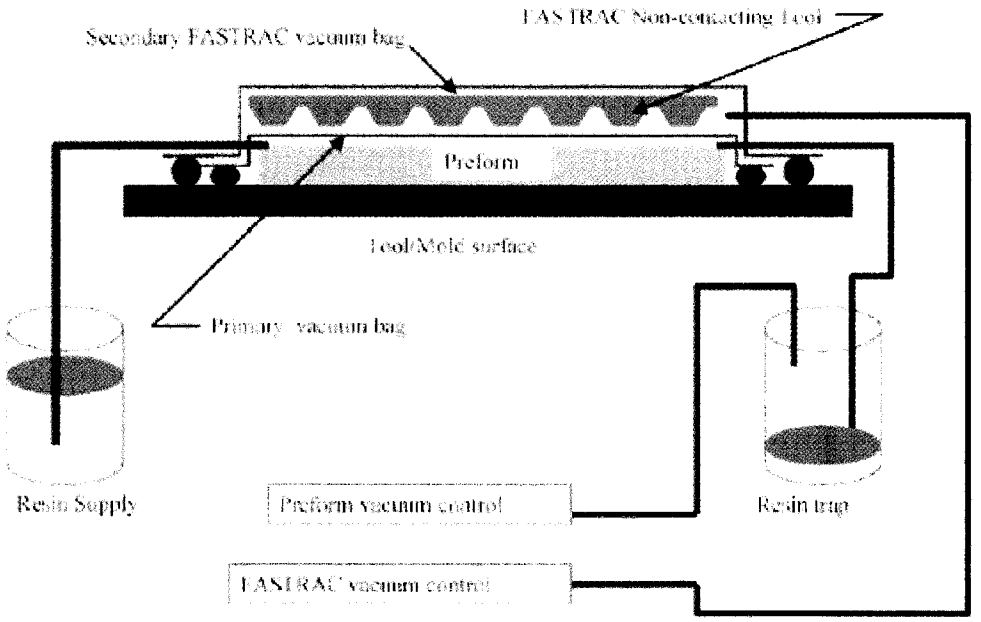

Figure 8 Schematic of the FASTRAC process [18]

The SCRIMP process addresses the issue of limited resin flow due to the driving force of atmospheric pressure. This process makes use of a high permeability consumable layer in the layup to distribute resin quickly over the surface of the

preform. The resin is then drawn through the thickness of the preform. With a shorter resin flow path parts can be saturated more quickly than without the distribution layer [14],[19]. Figure 9 shows a schematic of the SCRIMP lay-up.

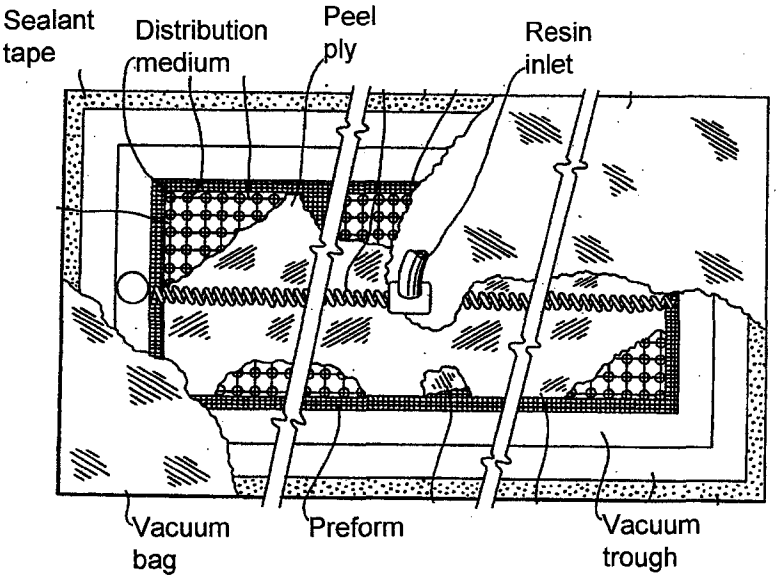

Figure 9 Schematic of SCRIMP process [20]

Another resin infusion process that is promoted as a technique that contributes to higher part quality is single-line injection. Resin is injected under pressure into a preform on a single-sided tool which is under autoclave pressure. A high part quality can be achieved with low material cost compared to prepreg; however, it requires investment in an autoclave which significantly raises the cost over typical liquid moulding methods. Manufacturers that currently work with prepreg in an autoclave would find that they could create similar quality parts with lower cost material. While material costs are a significant component of the manufacturing process, using

the single-line technique does not allow small companies to become part suppliers for aircraft OEM's without a significant startup cost [21].

The major challenge in using liquid composite moulding processes in aerospace applications is the attainment of the high quality necessary for these parts. The following section presents the research performed to understand liquid moulding process parameters, particularly for resin infusion, and to predict the evolution and effect of process-induced defects.

1.1.2.4 Research on Resin Infusion Process Parameters

The resin infusion process possesses the advantages of low cost materials, tooling, and capital equipment; however, as stated by Advani and Sozer [14] the V_f is limited by the application of only one atmosphere of pressure. In order to improve the structural properties a number of studies have been performed to examine methods to increase the V_f under the restrictions imposed by this LCM process.

Thomas et al. [22] applied a double bagging technique whereby a layer of breather was placed between two vacuum bags and evacuated with an independent vacuum line. They found that by using the double bag and thoroughly degassing the resin they were able to achieve a fibre V_f of 58% for a high temperature VARTM process compared to 60% for an autoclave process. They were able to fabricate parts that had zero void content and compressive strength similar to autoclave materials.

Gama et al. [23] performed processing trials to improve the compaction and thickness uniformity of VARTM processed parts. They found that multiple debulking cycles prior to infusion increased the final V_f, but did not improve the thickness gradient between the resin inlet and vacuum end of the part. To reduce the thickness variations two processing methods were investigated, one in which the resin inlet was closed after saturation and vacuum was allowed to draw the resin through the part. This method resulted in a high V_f part with fairly even resin distribution, but was prone to resin starvation. The other method made use of a secondary vacuum bag over the first to apply pressure to the part after the part was saturated and the main vacuum and resin ports were closed. This method resulted in less even resin distribution with a lower V_f, but the appearance of the part was improved over the former method.

Williams et al. [15] observed compaction of fabric preforms during infusion. In some of the experiments they observed that there was an initial decrease in the thickness of the preform at the resin flow front possibly caused by the lubricating effect of the resin. They found that the results are variable and possibly depend on the pre-existing nesting of the preform plies or the resin flow rate. They believed that increased resin flow rate through the preform did not allow time for the lubricating effect to take place. These observations improved the understanding of how a soft-sided mould impacts the compaction of resin-infused parts.

Daval and Bickerton [24] showed that the vent pressure during mould filling and post-mould filling has an effect on the final V_f of the part and the fill time. The part V_f also varies locally with the highest V_f being closest to the vacuum port. This was also observed by Rigas et al. [25]; however, they did not evaluate the effect of the pressure on the void content.

Rigas et al. [25] also showed that varying the infusion pressure to simulate poor pressure or vacuum bag leak had a direct effect on the of the final preform V_f. Lower pressure on the order of 1/3 atm had a slightly lower V_f (46%) compared to full vacuum (49%) and pressure unload and reload (53%). They also showed that when the pressure was reduced from full atmosphere some of the compressibility was maintained even though infusion takes place at a lower pressure. A disadvantage of higher compressibility is the corresponding lower permeability of the preform.

Rohatgi et al. [26] studied the formation of voids during RTM. They found that the incidence of macrovoids versus microvoids was influenced by the resin flow rate, flow pattern and the capillary number of the preform. In this case the capillary number is defined as the ratio of viscous to capillary forces multiplied by the contact angle. Microvoids within the fibre tows formed more readily at higher flow rates while macrovoids generally formed below a critical capillary number. As the capillary number decreases, macrovoids can be trapped between the fibre bundles as the flow of resin within the fibers is faster.

Kang et al. [27] suggested that the amount of air in the preform, and therefore, the level of dry spots and microvoids is a direct effect of the level of vacuum pressure. While this may be true it is likely not the cause of all dry spots. Similar to reference [25], Advani and Sozer [14] identified a number of layup related reasons for dry spot formation during resin infusion. Similarly, Thomas et al. [22] found that transition from thick regions to thin regions were likely to cause localized dry spots if the thin region became saturated with resin prior to saturation of the thick section. Also, the ability of the fabric to nest and consolidate affects the amount of air left in the preform. Haque et al. [28] showed that thicker preforms which were less compacted than thinner preforms had fewer voids implying that resin was able to flow more freely through the preform due to a higher permeability. However, the result is a composite part with a lower fibre volume fraction. Therefore, there has been effort towards understanding and improving the consolidation of the preform both before and after resin infiltration [25],[15], but there is a limit to how much a part can be consolidated before the permeability is adversely affected.

1.1.3 Effects of defects and mechanical response

Mechanical properties and the failure response of VARTM processed parts have also been examined for comparison with those of other liquid composite moulding methods. Wu and Hahn concluded that E-glass epoxy vinyl ester composites fabricated by VARTM had comparable mechanical properties with tensile strength ranging from 144-664 MPa compared with 279-359 MPa for a part made by RTM.

Similarly, the shear strength of the VARTM parts ranged from 32-178 MPa compared with 44-55 MPa [29],[30].

Dai and Hahn [31] investigated the failure response of sandwich structures fabricated using VARTM. PVC foam core sandwich structures with E-glass face sheets were found to fail by yielding in the core. Predictions were made that estimated the failure of long beams to be caused by face wrinkling; however, experimental results showed that long beams failed by tensile failure of the bottom face. Fatigue tests on wood core sandwich structures showed that the short and long beams in fatigue failed similarly to those in static tests.

Previous work in the area of the effect of defects on composite structural performance has shown that tensile, flexural and shear strengths were reduced by between 6 and 30% in the presence of defects such as dry fibers, interfacial cracks, or inclusions in the skin [32]. Studies have shown that interfacial cracks artificially induced by Teflon inserts can have an adverse effect on shear strength after they reach a critical length between 25 and 30 mm [33]. However, only limited work has been performed specifically on the evaluation of process-induced defects. Majumdar, et al. [34] showed that the debond fracture toughness had higher variability when the vacuum pressure was lower and that there was an increase in average debond fracture toughness with a corresponding increase in foam density. Research into the effect of the layup on VARTM process parameters showed that the placement of a distribution medium affected the flow of resin during infusion [25]. The distribution medium

promoted a gradient in resin flow between the surface on which it was placed and the opposite surface. The arrival of resin at the vacuum port due to the presence of the distribution medium corresponded to a significant reduction in vacuum pressure. The result was a severe decrease in flow rate on the side that did not have a distribution medium. This situation could potentially lead to defects such as dry spots if the flow rate was too slow to saturate the part prior to resin gelation.

In preforms that contain cores, channels in the foam core may be used as an alternative to a distribution medium to enhance resin flow through the preform [14]. However, investigations have shown that the use of a high permeability distribution medium is preferred over channels in the core for part quality. The high permeability layer (HPL) is a disposable layer placed on the surface(s) of a preform to increase the resin flow rate. Channels in core (CIC) refers to grooves cut in the surface of the foam core in the resin flow direction to add inherently high permeability regions to the preform. The use of either the HPL method or the CIC method was intended to shorten infusion time. Dai et al. and Karbhari et al. [35],[12] demonstrated the occurrence of dry spots and/or voids with the use of channels or grooves in the core to distribute resin. Dai et al. [35] showed that when three different methods, CIC, HPL, and straight infusion are compared, the optimized HPL method was the quickest, most cost-effective and provided the best surface quality.

Mathur et al. [36] investigated the use of a performance index with weighted criteria to assess the optimization of manufacturing process parameters. They found that, for

aerospace applications where extra resin carries a weight penalty, a system of resin injection channels spaced incrementally along the length of the part provided the most efficient combination of filling time and resin weight in the part.

1.2 Motivation

As explained in the previous sections, the vacuum infusion process has long been used and improved for manufacturing large marine structures. Typical materials used have been fibreglass and polyester or vinyl ester resins with polyvinyl chloride (PVC) foam cores to fabricate sandwich panels. These materials are relatively inexpensive compared to typical aerospace materials such as carbon fibre and epoxy resin. In addition to being inexpensive the materials have been proven with time in marine environments due to their application on ships. These reasons make the choice of material suitable in many ways for the Seawind amphibious aircraft. Flight Dynamics Corporation developed the design for the amphibious aircraft, as shown in Figure 10, which uses a single-step hull structure for landing on water.

Figure 10 Seawind amphibious aircraft

This aircraft is currently sold as a kit airplane with parts made using hand layup which are then assembled by the customer. However, the goal of Flight Dynamics is to fabricate the complete aircraft using vacuum infusion. This aircraft falls under a different set of certification guidelines compared to the kit aircraft. It is necessary for the OEM to certify the aircraft with Transport Canada according to the Canadian Aviation Regulation, CAR 523 [37].

A series of certification tests was performed to assess the properties of the materials manufactured using the vacuum infusion technique. Compression, notched tension, and open hole compression tests were performed and the fibre volume fraction and void content were determined. It was found that in a typical solid laminate, the void content was on the order of <1% in the form of microvoids [38]. Research into the effect of the resin constituents on the mechanical properties was also examined [39]. Since the resin formulation makes use of styrene to reach the proper viscosity to allow infusion there is a question of the effect of the styrene on the quality of the composite. The research showed that while the compressive strength was unaffected the compressive modulus decreased by up to 21% with increasing styrene content.

The Seawind aircraft also includes sandwich structures in its design. The added complexity of these parts changes the simple resin flow path of a solid laminate. During infusion of such sandwich structures defects were found to arise from unknown sources when few process parameters were held in control. Thus, the objective of this work was to develop an understanding of process-induced defects in

E-glass/epoxy vinyl ester sandwich panels with a PVC closed cell foam core, fabricated using VARTM. By identifying common defects and determining which process parameters are responsible for their development it may be possible to develop a more robust process where only the critical parameters are controlled. If every aspect of the process can be tightly controlled it is likely that defects can be avoided; however, the effect of controlling process parameters has an adverse effect on the cost. For example, in order to maintain a tight tolerance on temperature and humidity an environmental control chamber must be fabricated. The size depends on the size of parts needed and ultimately limits the fabrication of any parts larger than this size. There must also be an adequate method for removing these parts from the controlled environment after fabrication. This example points to the complexity of controlling just two of the process parameters that may affect ultimate part quality. For this reason, it is most beneficial to identify the parameters that have a significant effect on defect evolution and determine the tolerances necessary to avoid defects. The wider the process window that can be allowed, the lower is the potential manufacturing cost.

1.3 Thesis Organization

The remaining chapters of this work present the experimental trials and analysis performed to evaluate the effect of process variables on the evolution of defects in resin infusion moulding. Chapter 2 presents the experimental process and set-up used to perform preliminary and parametric process trials. An explanation of the materials and instrumentation is included. Chapter 3 provides the definitions used for

classification of potential defects that evolve during resin infusion. A variety of conventional non-destructive evaluation (NDE) methods are described with their potential for identifying defects in resin-infused sandwich panels. Chapter 4 explains the parametric study that was performed to determine the influence of process variables on defect evolution. Chapter 5 presents a qualitative evaluation of resin flow characteristics during infusion of sandwich panels. The focus of this evaluation is on the flow of resin through patterns of holes through the core thickness. Chapter 6 examines the influence of defects on mechanical properties by comparison with conventional compression after impact (CAI) tests.

Chapter 2 Infusion Process and Experimental Set-up

Typically, marine structures make use of low-cost materials such as E-glass and polyvinyl chloride (PVC) foam. The successful application of these materials to aerospace structures could result in a significant cost advantage over conventional material systems. The materials and process examined in this work are based on those used by Flight Dynamics Corporation for their amphibious seaplane. The specifications for these materials are contained in the following sections.

2.1 Materials

Three plies of 0.5 mm thick 5-harness satin E-glass fabric from Northern Fiberglass Sales in a $[0/90]_3$ lay-up were used for the sandwich panel skins. The core was made from AirLite™ 5.00 PVC closed cell foam with a density of 86.5 kg/m^3 and a thickness of 6.4 mm. This sandwich structure was infused with Derakane Momentum 411-350 epoxy vinyl ester resin with a density of 1.046 g/mL. A promoter, Trigonox 239A and an accelerator, Cobalt(II) 2-ethylhexanoate with 1% Cobalt by weight in aliphatic ester, were added to the resin to make a three-component system. Trigonox 239A with a density of 1 g/ml was added in a percentage of 1.05% by weight. The 1% solution of Cobalt with a density of 0.949 g/mL was added at 0.66% by weight.

A schematic of the nominal layup for the test panels is shown in Figure 11. A layer of Style 56115/Code 52008 peel ply with Finish 067 from Northern Fiberglass Sales separated the single layer of Resin Distribution Netting, Style 1291-R from DelStar

Technologies from the top skin of the panel. A polyethylene spiral tube from M.M. Newman Corp. was placed at either end of the part for resin infiltration and vacuum extraction. The type MPS-300-93-31-011 tube in a diameter of 0.25 inch was used for the resin infiltration and a diameter of 0.375 inch was used for the vacuum extraction. In the controlled experiments the foam core was tapered at a 45° angle in order that bridging of the fiberglass did not occur. Bridging can lead to high-permeability gaps that cause resin to "racetrack" which can lead to anomalous results particularly in experiments used to study resin flow paths.

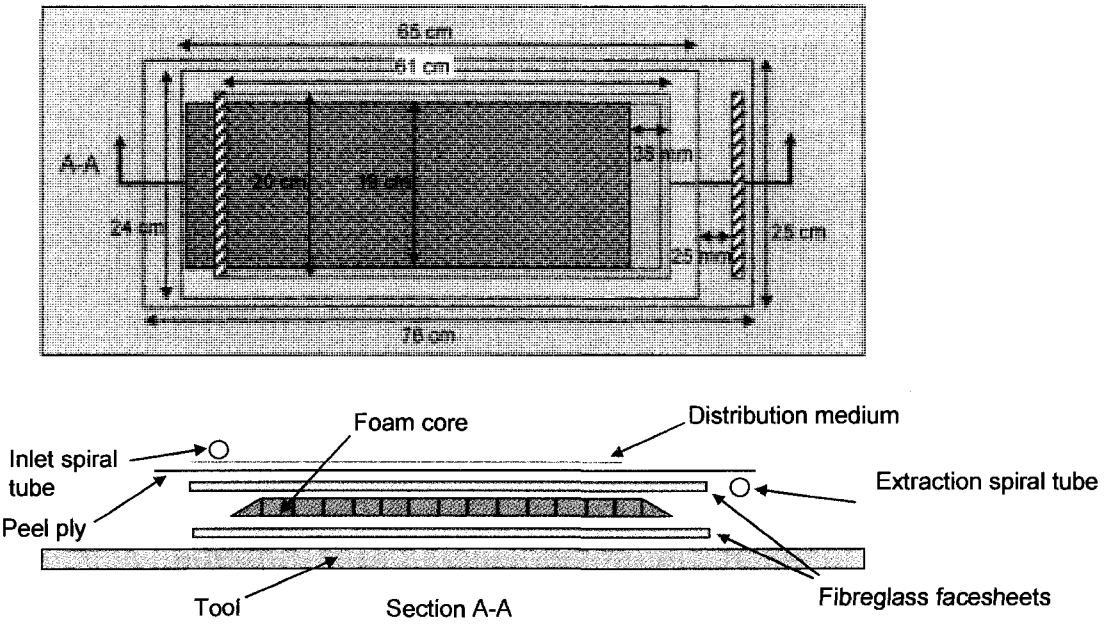

Figure 11 Schematic of experimental trial panels

The size of the test panels was chosen so that two experiments could be run simultaneously on the instrumented tool, but with as little edge effect as possible. Therefore, the maximum panel size possible was 65 cm long by 24 cm wide with a core of 61 cm by 20 cm.

2.2 Instrumentation

A modular station was built to support an instrumented glass tool and resin and vacuum chambers used for fabrication by resin infusion. The set-up was equipped with two CCD cameras to record the resin flow front on the bag and tool sides of the specimen during infusion. A LabView module was created to capture images from the cameras at 30 second intervals. A photo of the set-up is shown in Figure 12.

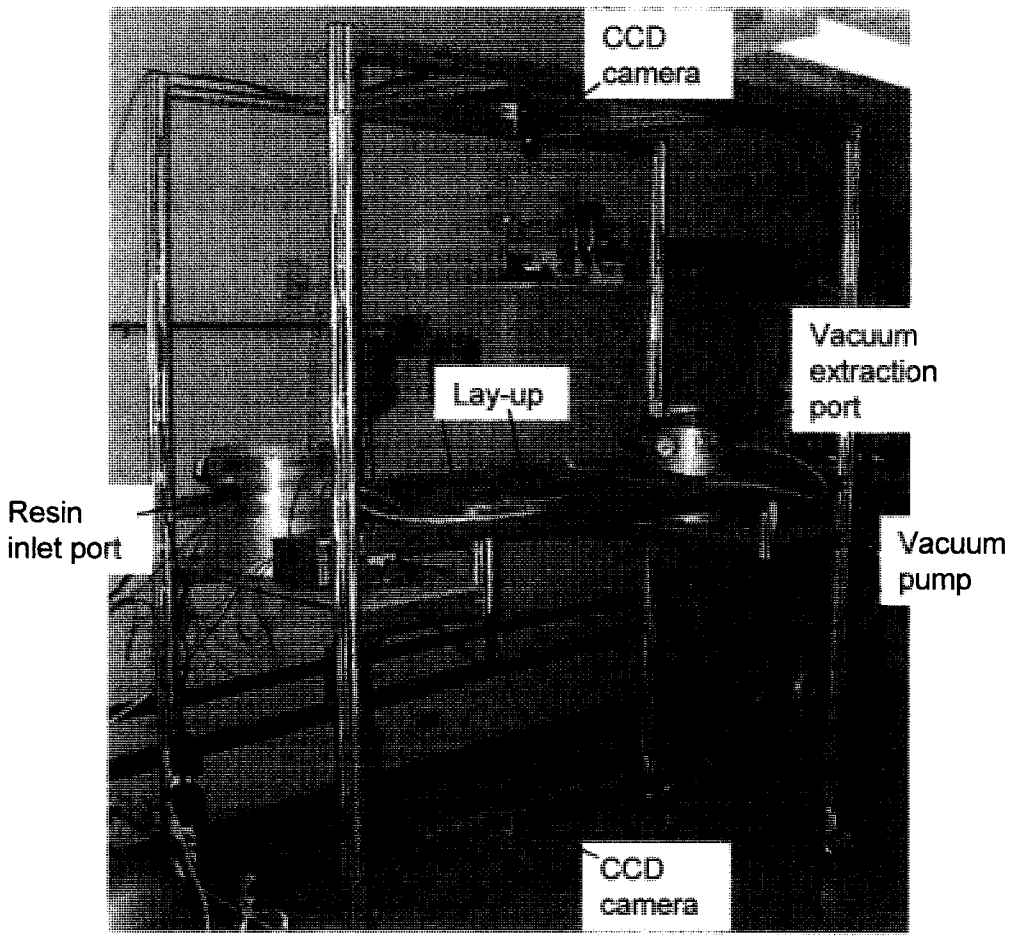

Figure 12 Photo of experimental trial set-up

A vacuum reservoir made of a metal container with a Plexiglas lid containing a silicone seal was connected to the vacuum end of the layup. The vacuum outlet from the vacuum bag was attached to a fitting on the side of the reservoir which was attached directly to the vacuum pump. The reservoir was used to prevent resin from overflowing into the vacuum pump. The vacuum pump was used to evacuate the reservoir until it reached the required vacuum level as measured on a gauge attached to the reservoir. The measurement was considered to be the exit pressure in the vacuum bag. The added benefit of this vacuum reservoir was in its ability to control the vacuum level. By allowing air to flow into the vacuum reservoir through a valve the pressure difference in the bag was reduced. This feature was used for evaluating the effect of the pressure difference on resin flow in the infusion pressure trials.

2.3 Flow Process

The flow process parameters used as a baseline for the experimental trials are outlined in Table 1. The values listed for each of the parameters are the default settings. Some of the parameters listed in Table 1 were used as variables for the experimental trials. See Appendix A for a list of the actual values used during each of the trials. The nominal values are based on two panels being fabricated simultaneously.

Table 1 Nominal flow process

Parameters	Value
Operator	record
Core length	61 cm
Core width	20 cm
Fibreglass length	65 cm
Fibreglass width	24 cm
# of plies	6
Peel ply length	76 cm
Peel ply width	25 cm
Resin tube length - panel to T connector	69 cm
Resin tube length - T connector to pot	51 cm
Spiral tube length	20 cm
Vacuum tube length - panel to T connector	69 cm
Vacuum tube length - T connector to pot	51 cm
Distance between end of media and start of core taper	38 mm
Media width	19 cm
Distance between vacuum tube and end of fibreglass	25 mm
Resin tube location	Shown in Figure 11, adjacent to taper
Vacuum pressure (gauge)	-96.5 kPa
Temperature	15.5-23.0 °C
Humidity	30-96 %RH
Flow front location when clamping resin tube	Core fully saturated
Flow front location when clamping vacuum tube	Fiberglass fully saturated
Viscosity of resin after mixing	0.275±0.025 Pa·s

Infiltration of the bottom skin was accomplished by an array of 2 mm diameter holes drilled through the foam core. The nominal hole array was in the pattern of a hexagon with a hole centred in the hexagon. The shortest distance between hole centres in any direction was 25 mm. In the direction of resin flow the closest holes along the same longitudinal axis were 44 mm apart. A schematic of the nominal hole array is shown in Figure 13.

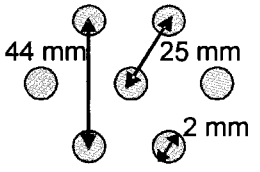

Figure 13 Nominal hole pattern for resin distribution through foam core

Chapter 3 Defect Characterization

The following sections describe the defects created from a set of preliminary trials and methods to accurately identify these defects.

3.1 Classification

A set of preliminary trials was performed to identify typical defects that occur during resin infusion. The process and materials used were as described in Chapter 2. With the exception of viscosity which was held to the nominal value of 0.275 ± 0.25 Pa·s and resin/accelerator/catalyst ratio which was as outlined in Sec. 2.1, processing parameters were not strictly controlled resulting in the worst case scenario for defect evolution while maintaining reasonable infusion results. From these trials four common defects were identified: dry spots, incomplete resin infiltration, air ingression, and pre-gelation. These four defects are pictured in Figure 14.

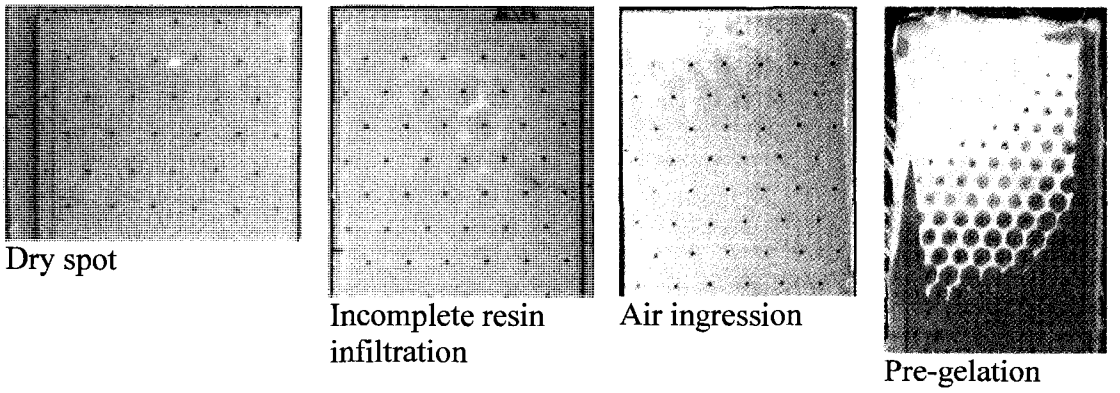

Figure 14 Images of defects occurring in resin infused sandwich panels

Dry spot defects consisted of fibres in the laminate skin that were completely unsaturated. Incomplete resin infiltration defects were predominantly saturated with

resin, but contained bubbles or voids. Air ingression defects were areas that were not completely consolidated and contained a mixture of resin and air saturating the fibres. Pre-gelation defects were where the resin gelled prior to full saturation of the panel. A list of the defects that evolved during the preliminary trials and the corresponding quantity of parts is shown in Table 2. It is clear from Table 2 that without adequate process control the probability of creating a defect-free part is very low. The probable causes of these defects are discussed below.

Table 2 Results of preliminary trials

Defect	Quantity of Parts
Dry spot	2
Incomplete resin infiltration	2
Air ingression	1
Pre-gelation	1
No apparent defects	1

In some of these trials the foam core was not tapered on each side, but was cut at a 90° angle to the bag and tool faces. When the fabric was draped over the core an elongated air (void) pocket remained along each edge. Resin racetracked along this high permeability region and reached the vacuum tube before the panel was fully saturated resulting in a dry spot. Incomplete resin infiltration (IRI) was caused when the resin flowing through the holes in the foam core did not fully coalesce before the part was saturated up to the vacuum tube. The difference between this defect and the dry spot defect was that fibres on the surface appeared to be saturated and the defect had the same texture as the surrounding fully saturated fibres. Air ingression defects occurred when a leak formed in the vacuum bag. In this case, air entered the bag at the origin of the leak then flowed through the part in the direction of the vacuum. This defect could also occur after the part was fully saturated, but before the resin had

gelled. The defect was in the form of widespread air bubbles on either the bag or tool side of the part or a combination of both. Conversely, the dry spot and IRI defects occurred exclusively on the tool side of the part usually near the vacuum tube.

After classifying defects into one of the three types trials were performed to create controlled defects. Rather than allow racetracking to create uncontrolled defects the methods for resin distribution on both the tool and bag sides of the parts were altered. A hole was cut in the distribution medium to inhibit resin flow in one area on the bag side of the part. In another area no holes were drilled through the foam core in order to inhibit resin flow from the bag side to the tool side. The purpose was to create a single dry spot on each of the top and the bottom of the panel. A schematic of the layup used to create dry spots is shown in Figure 15.

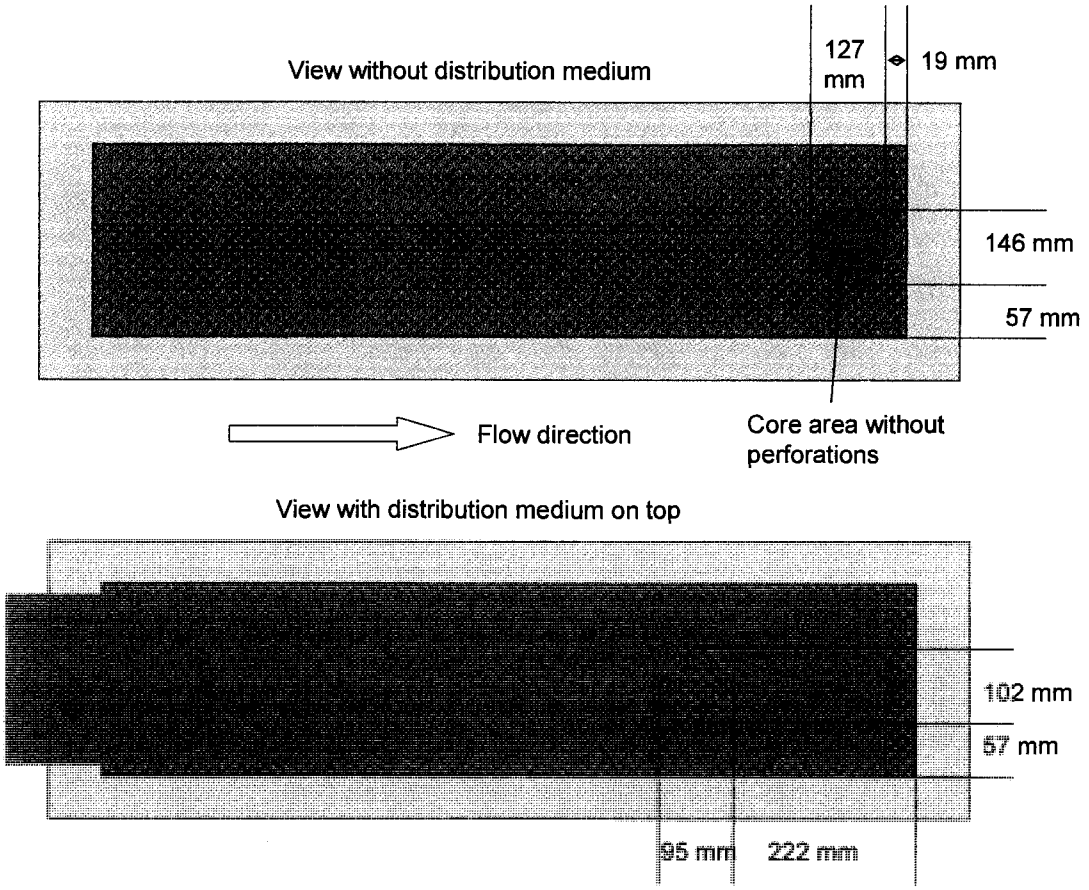

Figure 15 Schematic of lay-up used to fabricate experimental panels with dry spot defects. Details of layup can be found in Figure 11.

These trials resulted in dry spots that were slightly closer to the vacuum side of the area where resin flow was altered. In general, the defects located on the tool side were larger in area than those on the bag side due to the fact that resin flow on the tool side lagged that on the bag side. These parts were used for later analysis of the effect of defects on the compression properties of the sandwich panels.

During these trials the deleterious effect of air ingression was clearly observed. Two specimens were fabricated simultaneously under the same processing conditions. In one, a leak occurred in the vacuum bag during infusion. The result was a dry spot on

the order of 2.5 times larger than for the part without a vacuum bag leak. This effect is shown in Figure 16.

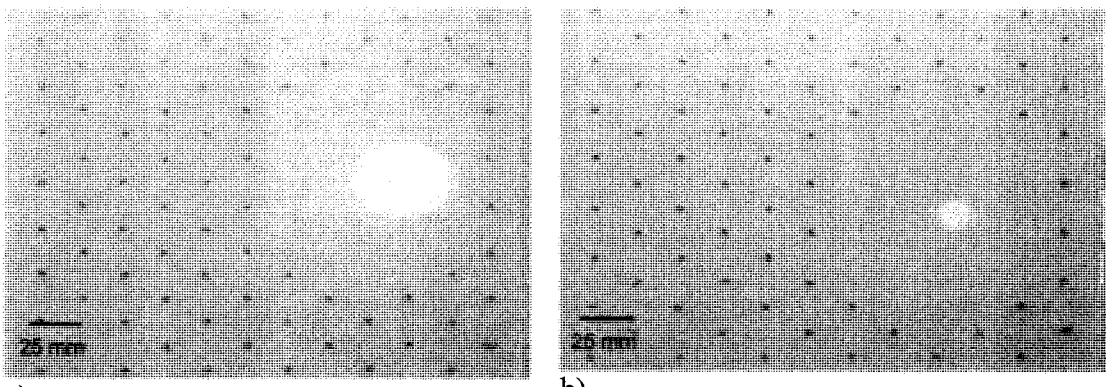

a) b)

Figure 16 a) dry spot defect with bag leak causing air ingression, b) dry spot defect without bag leak

In addition, the air that entered the vacuum bag was drawn to the dry region, thereby enlarging the localized defect. The reason for the attraction of the air to this region was likely due to this area having the lowest pressure in the part because it had not equalized with the atmospheric pressure of the resin. Because of the reduced vacuum pressure in the leaking bag the resin flow was reduced and the size of the dry spot defect was larger than the part that did not have a vacuum bag leak. Figure 17 shows graphically a comparison of the mold filling time for a part with a bag leak and one without.

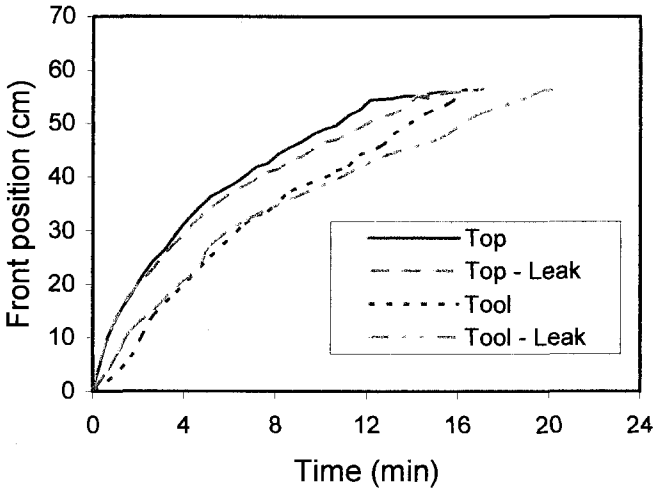

Figure 17 Comparison of resin flow front position versus time for resin infused panels with and without vacuum bag leaks

As shown in Figure 17, the part in Figure 16a) that was fabricated with a leaking bag had a 25% increase in mould filling time compared with the part shown in Figure 16b) that was fabricated in an air-tight vacuum bag. The leaking bag resulted in air being drawn into the part during infusion. Figure 17 also shows that the difference in the flow rate on the top of the part versus the tool side was greater for the leaking bag than for the non-leaking bag.

In all later trials, air ingression caused by a vacuum bag leak was avoided since it is not intrinsic to the process, layup, or geometry of the part, or a factor of the materials used. Therefore, further microscopy to determine the morphology of the defects did not include the examination of air ingression defects.

To examine the morphology of the defects panels containing dry spot and incomplete resin infiltration defects were cross-sectioned through the middle of the defects using

a diamond saw. Specimens were then polished by holding the cut surface firmly on a rotating disc with water as a lubricant. The first stage used 600 grit SiC-coated sandpaper to remove sawcut edges, then 800 grit sandpaper was used to remove grooves from the previous step. The final polishing was performed with 1200 grit sandpaper to achieve a smooth and reflective surface. The microscopic images shown in Figure 18 were then captured along the polished surfaces using a stereomicroscope.

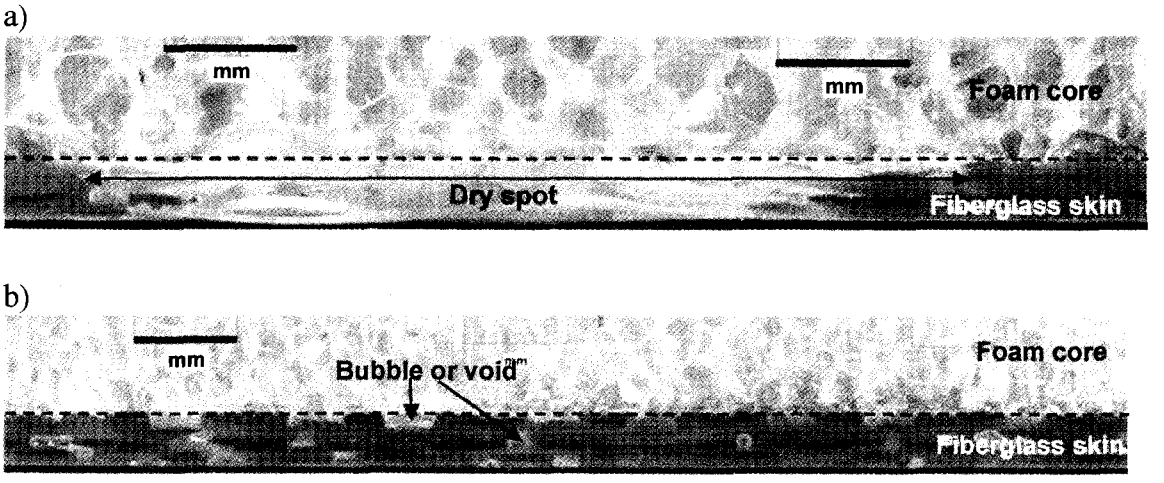

Figure 18 Cross-section image of a) dry spot defect and b) incomplete resin infiltration defect

The microscopic image of the dry spot shows that the defect consists of dry fibres in every ply of the skin adjacent to the tool surface. The cross-section of the specimen with incomplete resin infiltration reveals that this type of defect corresponds to a distribution of bubbles or voids throughout multiple layers of the laminate. The diameters of the defects range from approximately 0.125 mm to 0.5 mm.

3.2 NDE Methods and Microscopy

An investigation of a variety of non-destructive evaluation techniques revealed the most effective and efficient method to detect typical processing defects. The NDE methods examined included ultrasonic C-scan, bondline analysis, image analysis, edge-of-light, thermography, and X-ray. Microscopy was used to verify the results of the NDE techniques.

3.2.1 Ultrasonic C-scan

Ultrasonic C-scan is a non-contact technique whereby the inspected part is immersed in water and interrogated by an ultrasonic signal sent through transducer. The signal is either transmitted through the part to a receptor on the opposite side of the part, called through transmission, or reflected back to the emitting transducer, called pulse-echo. As the signal enters the part it is attenuated by various features such as voids, delaminations, discontinuities, pores, and resin-starved areas [23]. The measured signal, after it has passed through the part and returned to the transducer, indicates the extent of attenuation [5]. The C-scan is a measure of amplitude of the attenuated signal versus location of the transducer over the part [23]. To acquire the C-scan, the transducer moves over the part in a repeating pattern as shown in Figure 19. The result is a two-dimensional contour image showing the planar location of defects or discontinuities.

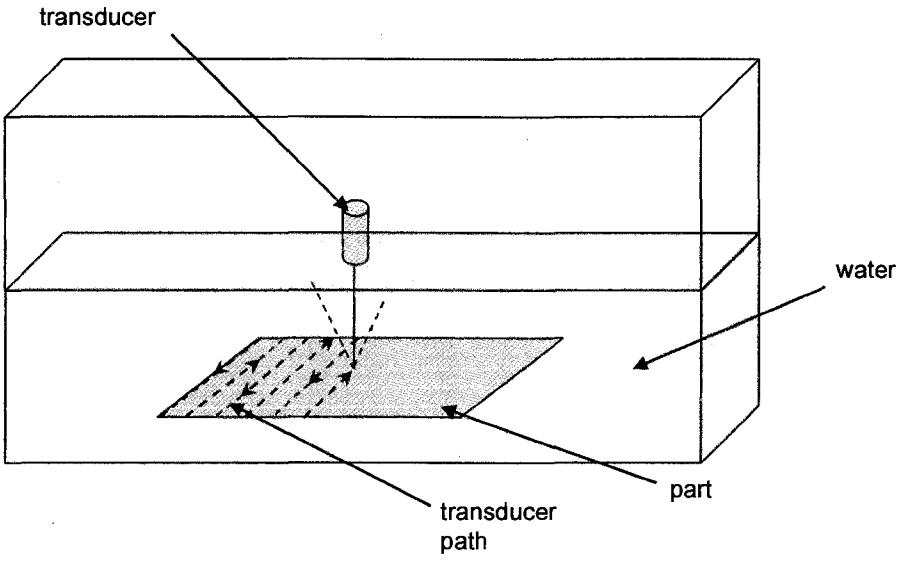

Figure 19 Schematic of ultrasonic C-scan operation

3.2.2 Bondline Analysis

The specific acoustic impedance of the specimen is monitored by amplitude/phase sensitive circuits [40]. A resonant transducer transmits and receives the ultrasonic energy into and from the panel. An oscilloscope is used as a visual indication of part quality. A schematic of the oscilloscope is shown in Figure 20. The center of the scope is the origin of the reference high quality region. A phase or amplitude shift of the energy is indicated by the position of the dot on the scope. If the dot is in a position other than the origin there is a potential defect present. The BondaScope 2100 does not have a recorded output so this method is useful for performing quick checks on suspect areas. However, it is possible to obtain a record of test results on newer equipment for documentation and analysis purposes.

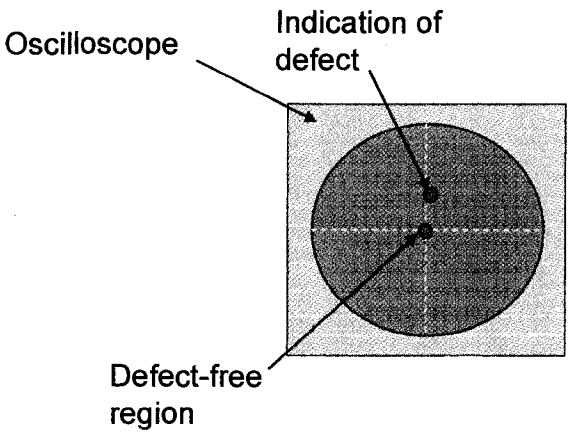

Figure 20 Schematic of oscilloscope used with BondaScope 2100

3.2.3 Image Analysis

To perform image analysis a photograph of the part is acquired and then imported into any common image analysis software. The most useful technique is to download a grayscale photo or a colour photo then use the software to convert it to grayscale. Once the photo is in grayscale a histogram of the pixels is used to produce a two-colour image (e.g. black/white or red/black), where one colour represents defective regions. The number of pixels in this colour region factored over the total number of pixels indicates the defect size. An example of a histogram obtained using this method is shown in Figure 21; however, image segmentation by the histogram method is subject to photo quality. It can be difficult to acquire an image without shadows or glare, particularly on the smooth tool surface.

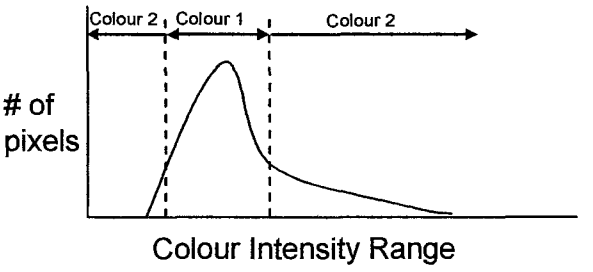

Figure 21 Schematic of histogram used to segment image

3.2.4 Edge of Light

A rectangular band of light is created on the surface of a part by passing incident light through a slit. A camera is used to examine this region at a set distance and angle to the incident light. At the edge of this band of light there is a region where the intensity quickly drops off. Within this band of light the slope of the surface is indicated by the intensity of the light reflected. Constant light intensity indicates that a smooth surface is being examined. A change in slope will be reflected by a change in light intensity. This method of inspection is relatively quick and easy to interpret [41],[42].

3.2.5 Thermography

The theory of thermography is that discontinuities in a material will affect its thermal conductivity [5]. The result is uneven heat flow with defective areas having higher temperatures than surrounding areas [43]. By applying heat to one side of the part and monitoring its dissipation the defects may be identified [43]. Measurement equipment consists of an illumination head containing two xenon flash lamps and flash reflectors. The controller synchronizes the triggering of the two flash lamps and

the infrared (IR) camera then acquires images at a rate of 0.94 Hz for 10 minutes which allows sufficient time for the thermal wave to propagate through the thickness of the composite. A schematic of the thermography system is shown in Figure 22 .

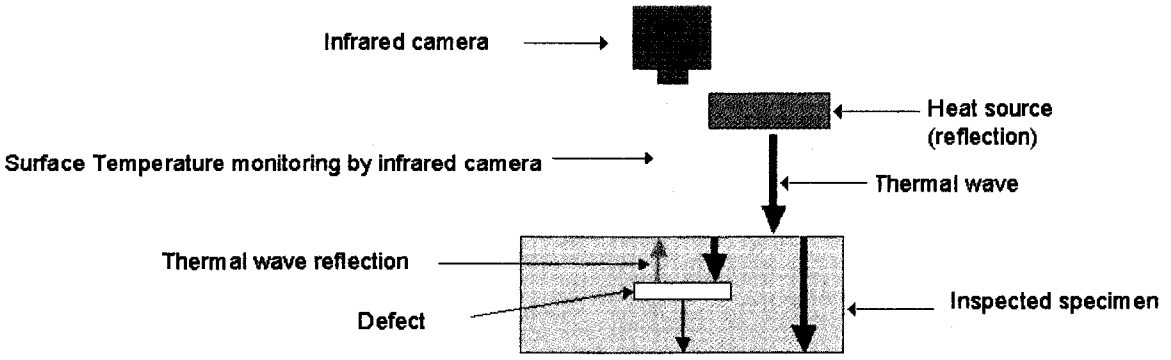

Figure 22 Schematic of thermography equipment and operation [44]

Once the thermal wave reaches a defect the temperature changes over this area, which is detected by the IR camera. Some advantages of thermography are its ability to detect disbonds between the skin and core of a sandwich structure and the speed of the inspection. This method also has the ability to detect defects at varying positions through the thickness and, with the help of image processing software, can determine the depth of the defect [43]. However, images of defects below the surface can be increasingly blurred with depth of the defect.

3.2.6 X-ray Inspection

Radiography involves bombardment of a part with X-rays. The X-rays that pass through the part are captured by photographic film placed on the opposite side of the part [43],[5]. Defects such as resin-rich or resin starved areas, non-uniform fibre

distribution, fibre misalignment, foreign particles, and voids in the part will absorb part of the energy which will appear as less exposed areas on the photographic film [43].

3.2.7 Visual Inspection

Visual inspection is performed on photographs of test panels acquired on a neutral background with even, matte lighting. The photos are digitized and defect sizes are measured using software such as ImageTool.

3.2.8 Microscopy

Microscopy is a destructive technique whereby the test panel is sectioned through the defects. The cross-section is then polished and examined in an optical microscope. The same software used for visual inspection may be used to measure defects on images of the cross-section.

3.3 NDE Results

The drawback of using the bondline analysis technique is that there was no capability for a recorded output. In contrast, thermography provided a colour image representing the location and extent of the defect and visual inspection provided an accurate image of the defect as it appeared to the naked eye. X-radiography also provided a recorded output in the form of an image on film, but the operator was unable to clearly identify the presence of defects on the film. In general, the image resulting from X-radiography may be scanned and digitized, but in this work the

defect was not visible even when the film was placed in front of a high intensity light. For the remainder of the evaluation methods with recorded outputs the results for evaluation of a dry spot defect and an incomplete resin infiltration defect are shown in Figure 23a) and b), respectively.

a)

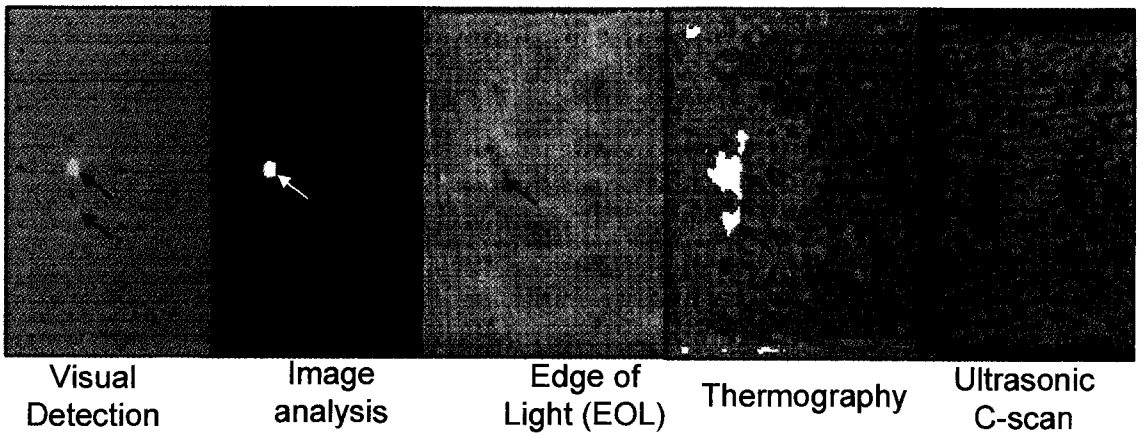

b)

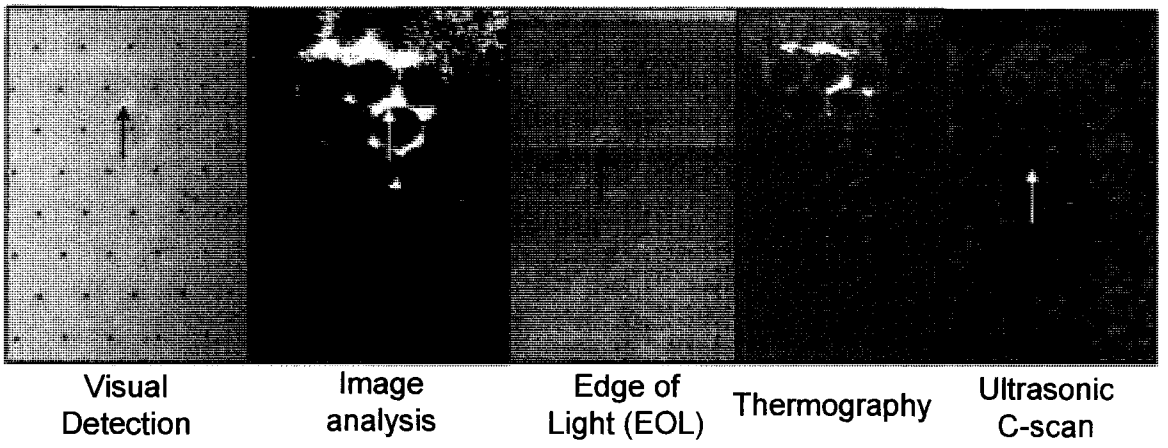

Figure 23 NDE of a part containing a) dry spot defect and b) incomplete resin infiltration defect

Based on the images shown in Figure 23 and on the comments made by NDE operators, the EOL and ultrasonic C-scan methods provided inconclusive results. It is obvious that it is difficult to identify the defect in the EOL images. This method is more useful for parts that have defects resulting in surface distortions. While the ultrasonic C-scan image appears to demonstrate a discontinuity corresponding to each type of defect, the attenuation of the C-scan signal was high. Also, this type of discontinuity appeared in other regions of the C-scan image where there were no corresponding defects. A typical problem with UT C-scan is that it cannot distinguish between defects that are at different positions through the thickness of the part, but overlapping in the x-y plane. Instead, it will tend to detect the closest defect to the transducer and be incapable of detecting any defect that is farther through the thickness [43]. Image analysis provided an adequate contrast between the most obvious defects and the rest of the panel. However, this method was not able to identify the less obvious dry spot defect and showed the incomplete infiltration defect to be much larger than was visually apparent. In addition, the determination of contrast for these images was subjective based on the operator's judgment. An example of the difficulty in acquiring a suitable image for image analysis is shown in Figure 24 and Figure 25.

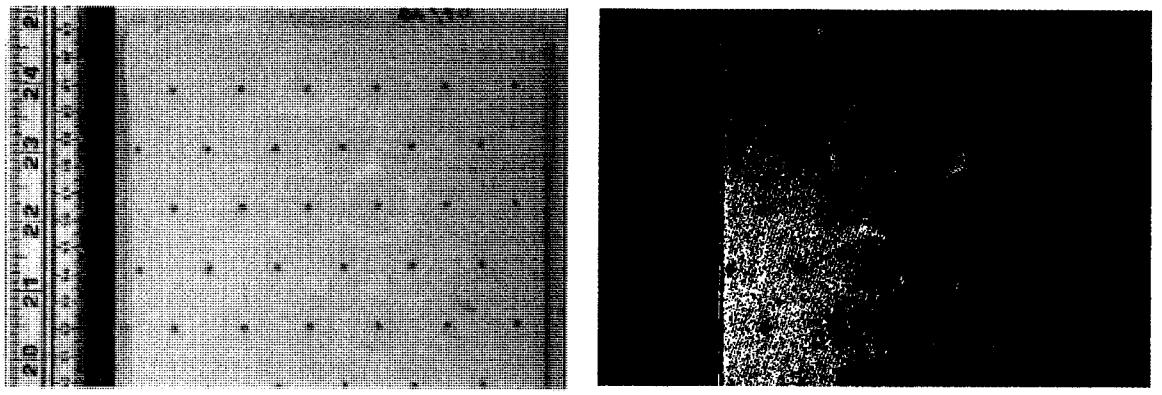

Figure 24 Over prediction of defect by image analysis due to glare

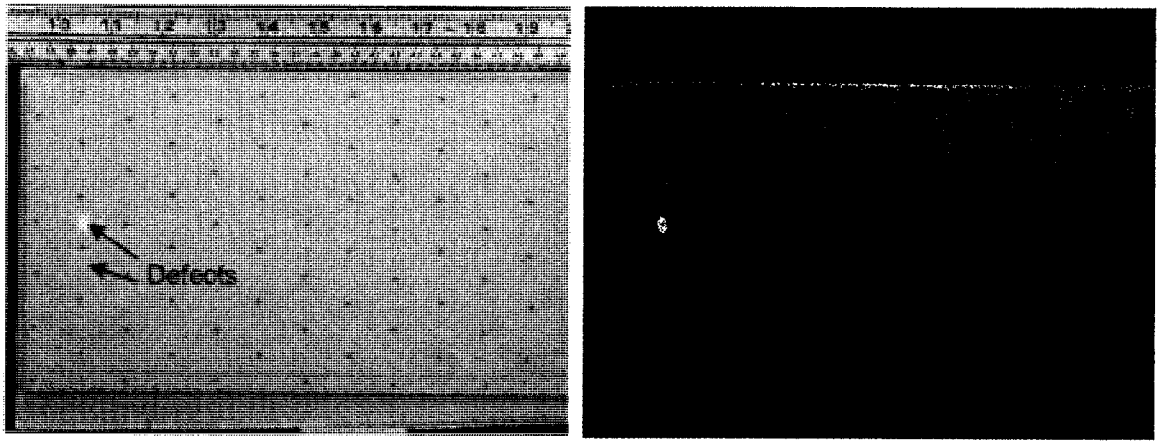

Figure 25 Under prediction of defect by image analysis

In Figure 24 the incomplete resin infiltration defect is apparent in the visual image, but uneven lighting of the part results in inaccurate image analysis. Figure 25 shows that the more subtle dry spot defect, which can be seen with both the naked eye and by a visual image, disappears when image analysis is performed. Therefore, due to the subjective nature of this evaluation method it was not pursued.

Thermography was successful in identifying both types of defects, but results showed apparent defects that were larger than could be observed from visual inspection,

which appeared to clearly identify both types of defects and their severity. For the two most promising methods offering recorded outputs, thermography and visual inspection, further analysis was performed to determine the accuracy of each method in identifying the extent of the defects.

3.4 Microscopy Results

Optical microscopy was used to validate that visual inspection was more effective than thermography for characterizing the extent of dry spot and incomplete resin infiltration defects. Cross-sections created to characterize the morphology of the defects were measured by ImageTool software. Figure 26 shows the location of the cross-sections relative to the defects.

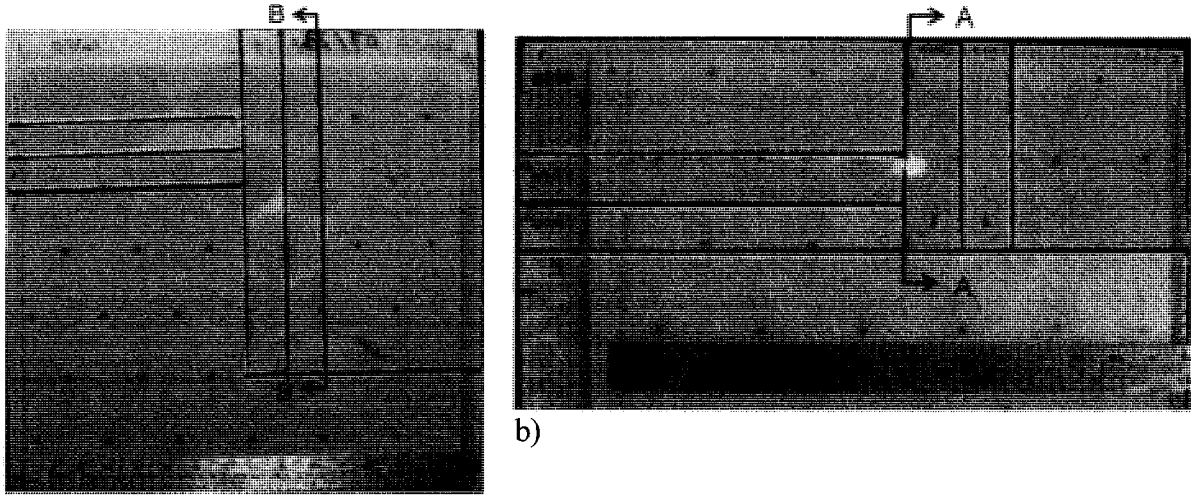

a) b)

Figure 26 Location of cross-sections through a) incomplete resin infiltration and b) dry spot defects

For cross-section B, ImageTool was used to measure the distances between points 1 and 2, and 3 and 4 on both the visual image and the thermography image as shown in

Figure 27. These measurements were then compared to the extent of the defect measured from microscopic images taken of the cross-section of the specimen shown in Figure 28.

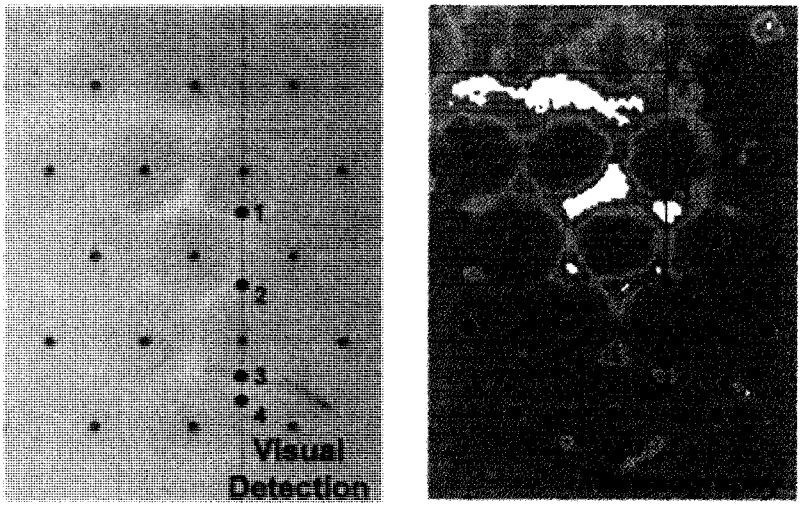

a) b)

Figure 27 Location of Image Tool measurements on a) visual image and b) thermography image

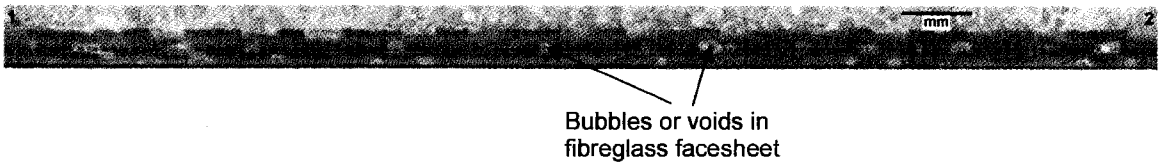

Figure 28 Microscopy of cross-section between points 1 and 2 (Figure 27)

The results of the measurements between each set of points are shown in Table 3.

Table 3 Results of Image Tool measurements at Section B

NDE Method	Size (mm)
Microscopy (1-2) (3-4)	18.0 2.3
Visual (1-2) (3-4)	17.7 3.5
Thermography (1-2) (3-4)	20.4 4.2

In both cases thermography overestimated the size of the defect, but visual observation was closer to the actual extent of the defect as measured by microscopy. The same process was used for the dry spot defect. Figure 29 shows the visual, edge-of-light, thermography, and microscopic images acquired.

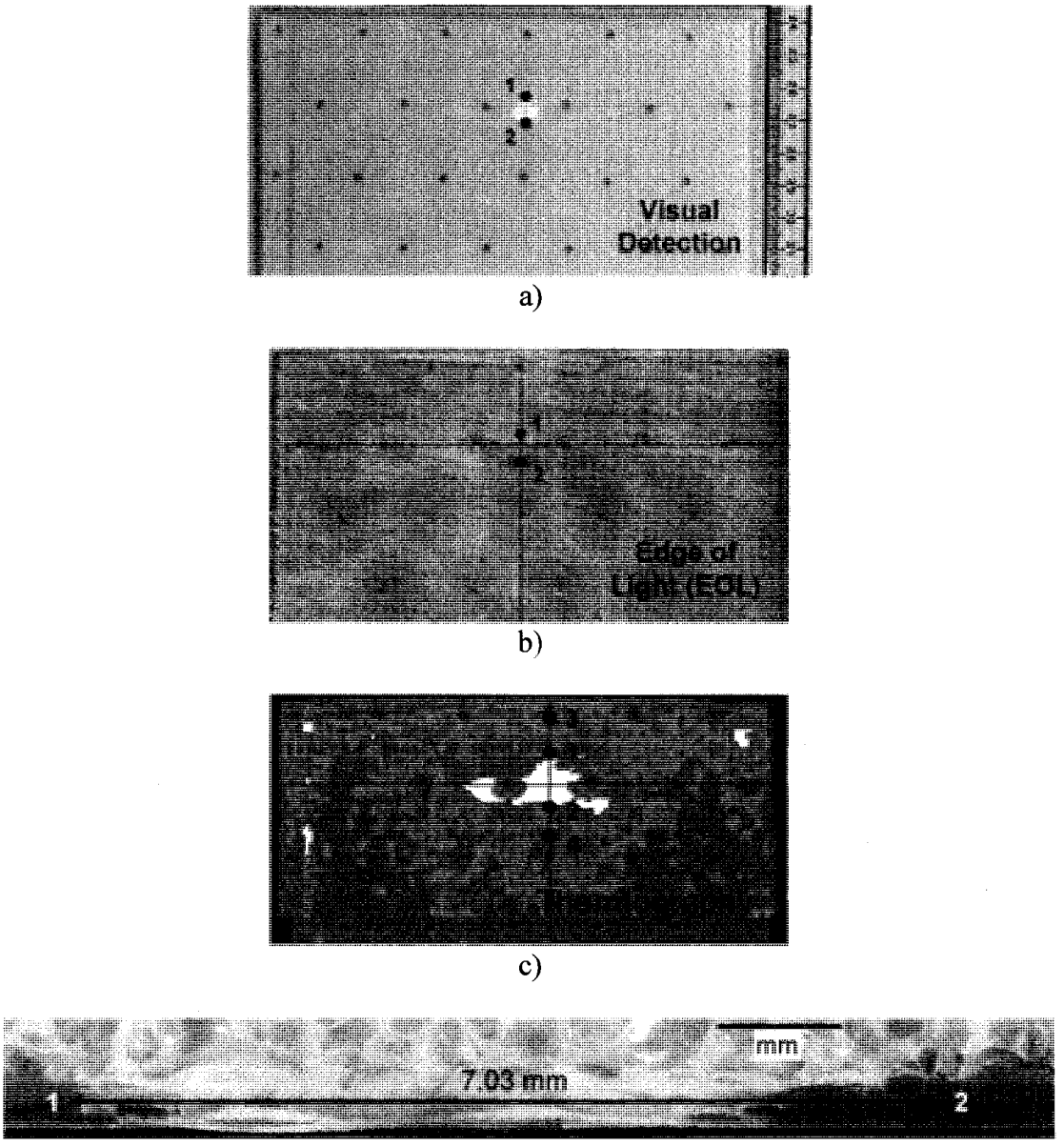

a)

b)

c)

d)

Figure 29 Location of Image Tool measurements on a) visual, b) edge-of-light, c) thermography, and d) microscopy images

The results of the measurements for the dry spot defect are shown in Table 4. The extents of the defect in both the white and red regions of the thermography image are provided for comparison.

Table 4 Results of Image Tool measurements at Section A

NDE Method	Size (mm)
Visual (points 1-2)	5.6
EOL (points 1-2)	6.0
Thermography (points 1-2)	13.8
Thermography (points 3-4)	32.5
Microscopy	7.0

The results from these measurements revealed that, in all cases, thermography overestimated the size of the defects. With close examination the results for edge-of-light appeared to be similar to the microscopic results, but this method was only useful if the defect was evident in the surface topography of the specimen. Visual inspection both overestimated and underestimated the defect extent in different locations. However, since visual inspection more closely characterized the defects, and it was simple and efficient, it was determined to be the method most suitable for analysis of the parametric process trials which will be described in Chapter 4.

Since thermography as an NDE technique is potentially very useful for automated and rapid inspection and has been used successfully in some situations [45] it was worthwhile investigating some reasons for its inaccurate estimation of defect size. Two potential reasons are the subjective determination of image contrast and the limited fields of view that are possible. Figure 30 shows the effect, on one image, of changing the contrast or decreasing the field of view.

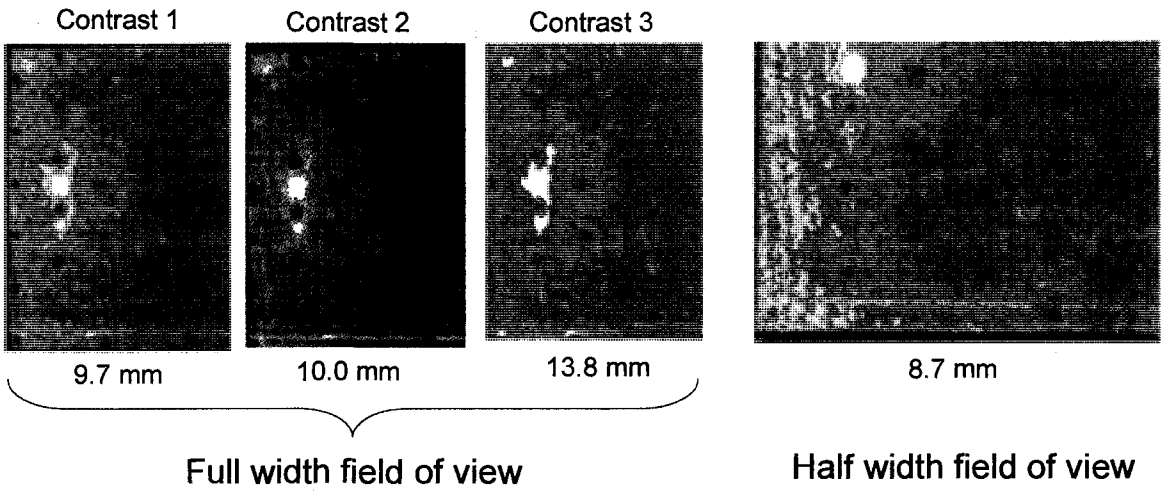

Figure 30 The effect of changing the contrast and field of view on the analysis of thermography images

It is apparent that changing the contrast evoked a change in the apparent extent of the defect which indicated the subjective nature of this method. Also, by using a smaller field of view a greater sensitivity of measurement was achieved. Therefore, more work is needed to develop a process for thermographic inspection that reduces the subjective nature and variability of results.

3.5 Summary

From the results of these tests it was determined that visual inspection was the most effective and efficient method to detect and identify the types and size of defects caused during the experimental trials performed for this work.

Chapter 4 Parametric Study of Process Variables

In order to identify the process variables that have an effect on the evolution of defects in resin-infused parts an investigation was performed where a single process parameter was isolated. The process variables examined included resin viscosity, infusion pressure, and the pattern of holes used to distribute resin through the thickness of the foam core. The trials on the three isolated processing parameters were performed according to the resin infusion process used on the Seawind aircraft. With the exception of these variables all other process parameters were kept constant in order to obtain an accurate indication of the effect of the individual test parameters. Parameters such as temperature, humidity, type and position of distribution medium and ratio of resin constituents potentially have an effect on the infusion results, but were not studied here. Chapter 2 describes the nominal processing conditions used for these trials and Appendix A provides a list of the actual values for the process parameters examined. An explanation of the reasoning behind the choice of process parameter variables follows.

Vinyl ester resin contains an active solvent, styrene, that evaporates with time resulting in an increase in the viscosity of the resin. Therefore, monomeric styrene is added to control the resin viscosity. However, preliminary tests have indicated that styrene has a deleterious effect on the compression modulus of resin-infused laminates [46]. In addition, styrene is a hazardous substance and regulations restrict the level of exposure in the workplace [47],[48]. Therefore, the amount of styrene added to the resin should be minimized without adversely affecting its viscosity. A

series of processing trials were performed to evaluate the effect of viscosity on defect evolution and fill time. In these trials all manufacturing parameters were maintained while varying only the viscosity of the resin. Vinyl ester resin was acquired from the manufacturer with a styrene volume fraction of 42.5% [46]. Styrene was added until a particular viscosity was obtained as measured by a Brookfield DV-E viscometer. Trials were performed at viscosities of 0.147, 0.225, 0.307, 0.320 and 0.510 Pa·s. Based on work performed by Khoun [49], these viscosities correspond to an estimated styrene addition of 16.2%, 9.3%, 6.0%[1], 5.3%, and 0.4%, respectively. The method for calculation of the styrene percent addition will be described in Section 4.2.1.

The effect of infusion pressure on the quality of resin-infused sandwich panels was also examined. The maximum vacuum pressure achieved was -96.5 kPa. The vacuum pressure was then reduced by increments of 10% and parts were visually inspected for defects.

In this work a pattern of holes was used to distribute resin from the top skin through the core. Depending on the spacing, size, and pattern of holes, defects of varying shapes and locations occurred. There was also an effect on the lag time between top and bottom skin saturation. A variety of hole patterns, as shown in Figure 31, were examined.

[1] The test temperature for this data point was not recorded. In this case an average temperature value for all test conditions was used to calculate the additional styrene percent.

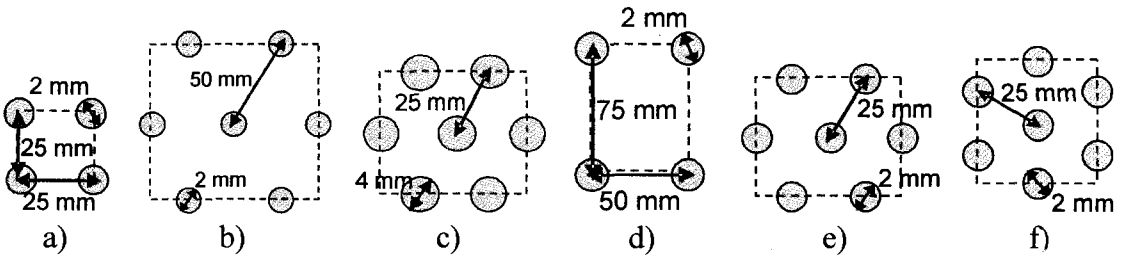

Figure 31 Schematics of hole patterns a) 25 mm square, b) Nominal hexagonal - 50 mm spacing, c) Nominal hexagonal - 4 mm hole, d) 50 mm x 75 m rectangle, e) Nominal hexagonal, and f) Nominal hexagonal - rotated 90°. Schematics are not to scale.

In Figure 31 the dotted lines represent the perimeter of the unit cell. The area fraction of holes in each unit cell is the area of the holes within the perimeter of the unit cell divided by the total area of the unit cell. The calculated area fraction of holes for each unit cell is shown in Table 5.

Table 5 Area fraction of holes in unit cells

Unit Cell	Area fraction of holes (%)
a) 25 mm square	0.50
b) Nominal hexagonal – 50 mm spacing	0.15
c) Nominal hexagonal – 4 mm hole	2.32
d) 50 mm x 75 mm rectangle	0.08
e) Nominal hexagonal	0.58
f) Nominal hexagonal - rotated 90°	0.58

As the area fraction of holes in the unit cell increases so does the resin content in the sandwich panel since resin fills the holes during the infusion process. In aircraft structure weight is a critical constraint and therefore, additional resin that does not add to the structural integrity of the part is undesirable. This effect will be explored further in Sec. 4.2.3. Table 6 contains a list of the values used for the process variables examined. This table identifies the conditions used in this work, but it is not a complete list of all possible parameter variations for this infusion process.

Table 6 Resin infusion process parameters examined

Process Variable	Resin viscosity (Pa·s)	Vacuum pressure (kPa)	Hole pattern (see Figure 31)
Parameter Values	0.147 0.225 0.307 0.320 0.510	-96.5 -86.3 -77.9 -67.7 -57.6 -47.4	a) 25 mm square b) Nominal hexagonal – 50 mm spacing c) Nominal hexagonal – 4 mm hole d) 50 mm x 75 mm rectangle e) Nominal hexagonal f) Nominal hexagonal - rotated 90°

4.1 Experimental Methodology and Data Reduction

Using the experimental set-up and resin infusion process described in Chapter 2 trials were performed to examine the effects of process variables on mould filling time and the evolution of defects. Glass tooling with CCD cameras above and below the standard layup (as shown in Figure 32) captured images every 30 seconds during the infusion. The position of the resin flow front was measured from each image using the software Image Tool. The measurements were calibrated for each panel using the core length of 61 cm.

Figure 32 Image of experimental panel lay-up

The time for the resin flow front to reach its measured position on the panel was plotted versus variations in the process parameter examined. Each trial is represented by one point on the graph. These experimental measurements were then compared to calculations using Darcy's Law described in the following section. It should be noted that the flow front analysis from this work shows trends only since images were acquired every 30 seconds. Measurements were based on a visual determination of the flow front location at any given time and flow fronts were not often straight across the width of the part. Therefore, measurements can be considered to be accurate to within ±15 seconds.

4.2 Simulation of Flow

The flow rates examined during the parametric evaluation of the resin infusion process were compared with a basic calculation of Darcy's Law for uniform, one-dimensional (1-D) flow through a porous medium:

$$v_x = -\frac{K_x}{\mu}\frac{dP}{dx} \qquad \textbf{Equation 1}$$

where v_x is the superficial velocity (m/s), K_x is the permeability of the preform (m^2), μ is the viscosity (Pa·s), and dP/dx is the pressure gradient along the part (Pa/m). The experimental panels were sufficiently wide that edge effects on resin flow could be ignored. Measurements of the resin flow front were taken along the centre of the part in the direction of resin flow. Therefore, for simple analysis of resin flow rate in the axial direction the 1-D relationship in Equation 1 is sufficient to compare with the

measurements of the experimental panels. Manipulation of Equation 1 results in the formula based on Darcy's Law that was used to compare with the experimental results. Assuming that the infusion took place under a constant pressure condition, the formula determines the time for mould filling [36]

$$t_f = \frac{x_f^2 \mu \phi}{2K_x(P_o - P_b)} \qquad \textbf{Equation 2}$$

where t_f is the time to fill the mould (s), x_f is the position of the resin flow front (m), μ is the viscosity (Pa·s), ϕ is the porosity of the preform, K_x is the permeability of the preform (m^2), and P_o-P_b is the pressure difference along the part (Pa).

The nominal input parameters shown in Table 7 were used as the defaults for Equation 2 to compare with the processing trials.

Table 7 Nominal input parameters for evaluation of processing trials by Darcy's Law

Model Input	Value
Inlet pressure, P_o	0 kPa
Outlet pressure, P_b	-96.5 kPa
Mould length	57.2 cm
Porosity	0.5

The inlet pressure was taken to be the vacuum pressure level at the resin inlet which was effectively 0 kPa upon introduction of resin at atmospheric pressure. The outlet pressure was taken to be the vacuum pressure at the vacuum extraction point. The outlet pressure varied for infusion pressure trials. The mould length was taken to be the distance between the resin inlet tube and the end of the distribution medium. For these trials the distribution medium ended approximately 38 mm before the end of the 61 cm core. For simplification of the calculations involving resin flow the

calculations were performed just to the end of the distribution medium. For this work, the nominal porosity used was 0.5. Earlier work by Boukhili, et al. showed that the fibre volume fraction (V_f) of fiberglass panels made with the Seawind infusion process was 0.51 [38]. If the porosity, ϕ, can be estimated by Equation 3 then the porosity is 0.49 or approximately 0.5.

$$\phi = 1 - V_f \qquad \textbf{Equation 3}$$

Using this porosity value with the other parameters in Table 7 and the experimental data a permeability value was calculated by solving Equation 2 for K_x. For the infusion pressure trials K_x was determined to be 9.32×10^{-10} m^2 by averaging the values for each data point. However, it should be noted that only six of the eight values for K_x were used in the average as two of the values were significantly lower than the average value. K_x for the viscosity trials was calculated as $8.38 \times 10^{-10} m^2$ based on three of five data points for reasons similar to those for the infusion pressure trials. By performing a best fit of the permeability data to the experimental results one can easily see any anomalies that may have occurred. The parameters that may have affected consistent results will be discussed later. Equation 2 was then used with the average permeability values and the parameters in Table 7 to calculate the time for mould filling at each experimental data point. The results from these calculations were used to demonstrate trends in the relationships between mould filling and various process parameters as well as to highlight points that did not fit the general trend rather than to dictate absolute values for prediction of mould filling times. Generally, the experimental results fit well with calculated results with the

exception of a few discrepant points. It would be necessary to repeat the trials that resulted in discrepant data to verify the results of these experiments.

4.2.1 Viscosity

The results of the viscosity trials (Figure 33) show that all panels were fully infused without any visible defects. The experiments showed a general trend of an increase in mould filling time with viscosity.

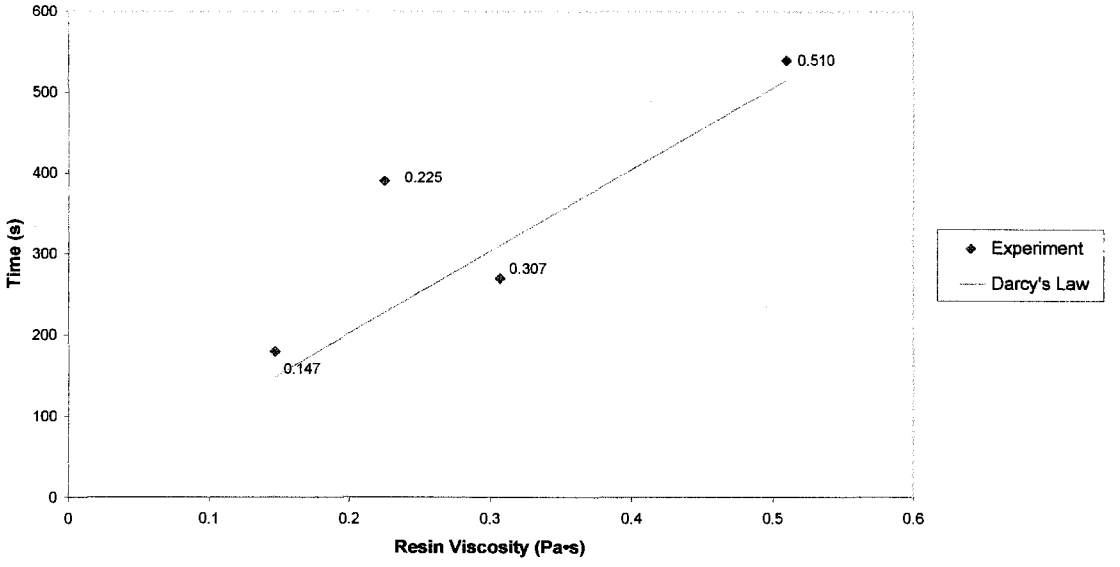

Figure 33 Time for saturation of panel related to resin viscosity

As expected, the calculated results show a linear relationship between time and resin viscosity which would indicate an inverse relationship between resin velocity and viscosity. Figure 33 demonstrates that the results of the experimental trials are generally in agreement with Darcy's Law for 1D flow through a porous medium.

Qualitatively, the results of these trials in general indicate that as long as the gel time is sufficient to saturate the part it is possible to allow a higher resin viscosity than the nominal value of 0.275 Pa·s without causing defects. In fact, it was possible to use a viscosity of 0.51 Pa·s and saturate the trial panel to the end of the distribution medium within 9 minutes. With the resin mixing ratio used for these trials the approximate gel time was 30 minutes at a temperature of 25°C. Using Equation 2, the theoretical maximum flow front position that can be filled prior to gelation was determined. The results are shown in Figure 34.

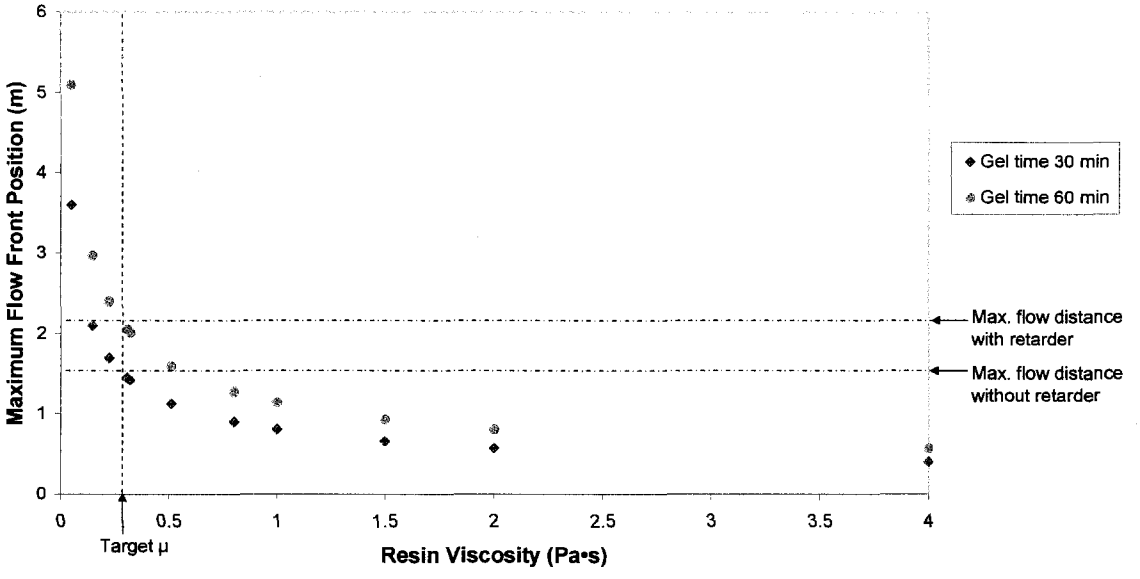

Figure 34 Position of the resin flow front related to the resin viscosity

By adding a retarder to the resin mixture to increase the gel time to 60 minutes it is possible to increase the potential saturation length. Overall, the increase in saturation length is theoretically 41% with the addition of 0.035 phr of retarder 2, 4 Pentanedione (2, 4-P). Therefore, the greatest effect on the actual distance traveled is

seen at the lower resin viscosities. In other words, at 0.05 Pa·s, the saturation length with retarder is 5.1 m compared to 3.6 m without retarder while at 4 Pa·s the difference in saturation length is on the order of 17 cm. At the target viscosity of 0.275 Pa·s the increase in saturation length with retarder is approximately 64 cm. The reason for this appears to be that the effect of resin viscosity on the saturation time decreases as resin viscosity increases. The calculation also shows that a maximum viscosity of approximately 1.5 Pa·s can be used to fully saturate the 61 cm part. Above approximately 2 Pa·s an increase in viscosity does not have as large an effect on the maximum flow front position as at the lower viscosity levels.

Figure 34 indicates that at a viscosity of 0.05 Pa·s a part between 3.5 m and 4 m can potentially be saturated. The following semi-empirical relationship may be used to determine the amount of styrene necessary to obtain a particular viscosity at a given temperature [49],

$$\ln \mu = \ln \mu_o + \frac{E}{RT} + (b_o + bT)\ln St\% \qquad \textbf{Equation 4}$$

where μ is the viscosity (cP), T is the temperature (K), and St% is the percentage weight of styrene in the resin. The constants in Table 8 were calculated by Khoun for the Derakane Momentum 411-350 resin system [49].

Table 8 Values for Equation 3 constants from Ref. [49]

Constant	Value
μ_o	1.96×10^5 cP
E/R	2857.853 K
b_o	-2.38979
b	-0.00601

By solving for St% in Equation 4 it is found that it would be necessary to have a styrene content of 71% to achieve 0.05 Pa·s. This is an addition of ~30% styrene by weight over the as-manufactured value.

Under these conditions, there is a trade-off between the use of styrene additions to achieve a longer resin saturation length within the gel time or allowing a shorter saturation length by eliminating the need for styrene additions to the benefit of the health of the operators performing the process. An additional benefit arises from the improved compressive properties of the part. Khoun showed that an increase in the styrene by approximately 10% above the as-manufactured value decreased the Young's Modulus by approximately 5 GPa [49].

4.2.2 Infusion Pressure

Trials performed while varying the infusion pressure resulted in panels exhibiting incomplete resin infiltration defects. These defects occurred when the pressure difference between the resin inlet and vacuum extraction was reduced by 20% or more from the maximum pressure difference of 96.5 kPa. Defects of the form described in Section 3 were present on the tool surface of the parts. As the pressure difference was reduced defects appeared to become more severe. Examples of these defects are shown in Figure 35.

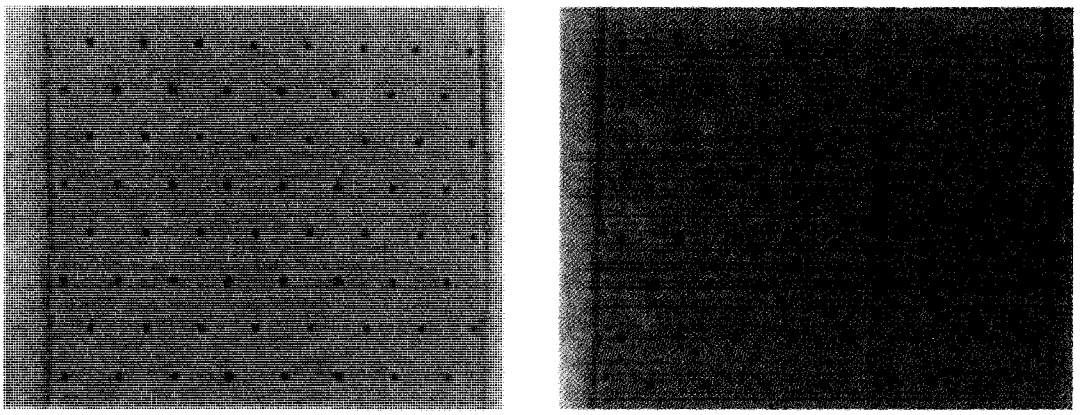

a) b)

Figure 35 Examples of incomplete resin infiltration defects caused by reduced vacuum pressure a) 57.6 kPa, and b) 47.4 kPa

These defects increased in severity closer to the vacuum extraction end, similar to what was reported by Haque et al. [28], but disappeared at the location corresponding to the end of the distribution medium. It is possible that at this point the change in the velocity of the resin flow front leads to a decrease in the creation of macrovoids.

Similar to the viscosity trials the time to saturate the part to the end of the distribution medium was plotted versus the infusion pressure difference. The viscosity and pressure of each experimental data point were used to calculate a corresponding point according to Darcy's Law. Two experiments were performed for each pressure difference of 57.6 and 96.5 kPa and therefore, two Darcy's Law predictions were made using the viscosity level of each of the experimental trials. As before, there was a good fit with Darcy's Law with some anomalous results. As shown in Figure 36 between pressure differences of 47.4 and 77.9 kPa, for which defects were apparent, the saturation time reduction was proportional to the pressure difference increase. However, the time to saturate the panel was not the cause of defects in these

situations. Trials performed at higher pressure differences of 86 and 96 kPa in some cases had longer infusion times, but did not have associated defects. Therefore, the infusion pressure difference can be used to predict the likely occurrence of incomplete infiltration defects.

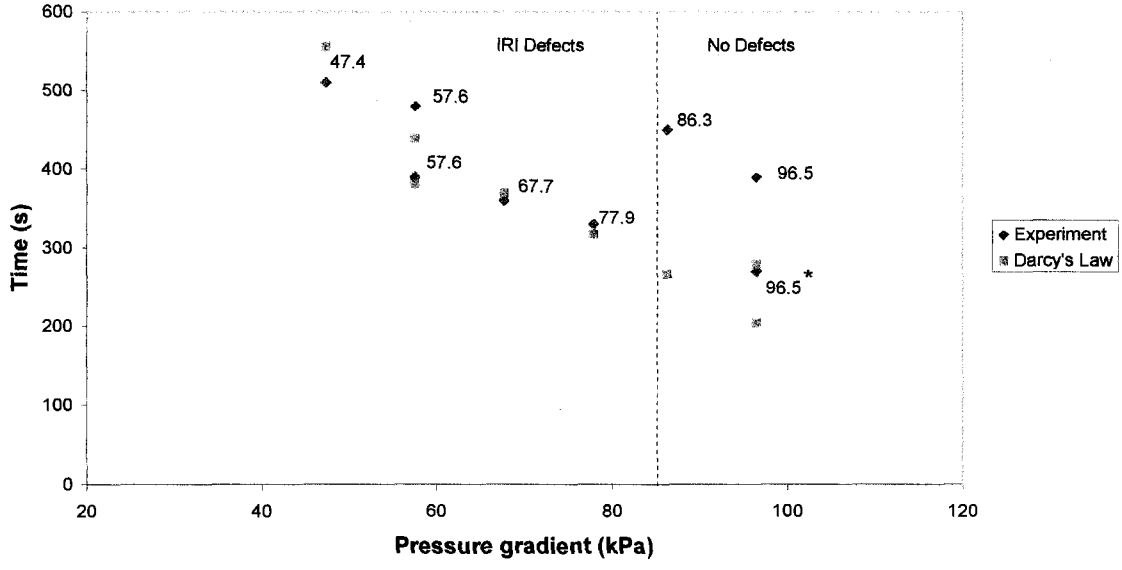

Figure 36 Time for saturation of panels versus the vacuum pressure during resin infusion. *Duplicate trial for 96.6 kPa.

The mould filling time for pressure differences of 86.3 and 96.5 kPa were not close to the predicted times; therefore, a duplicate trial at 96.5 kPa was performed to verify the deviation of the original result from Darcy's Law. The duplicate result has closer agreement with Darcy's Law and indicated there was another process variable that had an influence on the results. The source of the variability is unknown, but since viscosity was controlled by the addition of styrene and it was difficult to obtain the same value consistently this variable was examined by normalizing the pressure with the viscosity values. Figure 37 shows that there was a slight effect of viscosity

variations on mould filling that affected the fit of some of the points, but the general trend was not influenced.

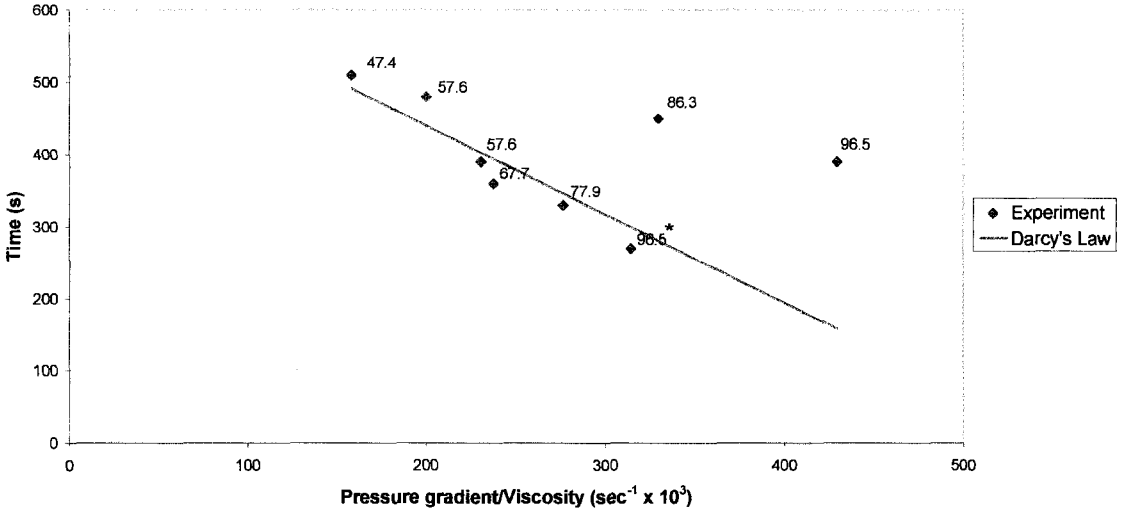

Figure 37 Panel saturation time versus vacuum pressure normalized for resin viscosity. *Duplicate trial for 96.5 kPa.

At the moment the source of the variability of the 86.3 and 96.5 kPa values is unknown. It would be useful to perform an investigation of how the compaction and permeability are affected by changes to the infusion pressure. Since the permeability is affected by the porosity of the preform, higher infusion pressures produce higher compaction, and thus, permeability decreases. Therefore, more comprehensive data acquisition at varying infusion pressures to measure preform compaction would demonstrate the opposing influence of these process parameters.

4.2.3 Core Hole Patterns

The mechanism used for the distribution of resin through the closed cell foam core was holes drilled through the thickness of the core. By changing the pattern of holes

in the core (see Figure 31) a change in resin flow on the tool surface was affected. It was shown from the original trials using foam cores with varying patterns of holes that the location and shape of defects were directly associated with these patterns. Under nominal processing conditions as described in Section 2.3 the rectangular pattern in Figure 31(d) resulted in incomplete infiltration defects along the panel in the position shown in Figure 38. These defects were approximately 4 to 5 mm in diameter. The hexagonal pattern with 50 mm hole spacing (Figure 31(b)) also had incomplete infiltration and slight dry spot defects that were between 5 and 10 mm in diameter. These were present on the tool side at the vacuum end of the panel 15 mm from the end of the core. The remaining hole patterns did not affect defect evolution under nominal processing conditions. An explanation of how the hole pattern may influence defect evolution will be discussed further in Chapter 5.

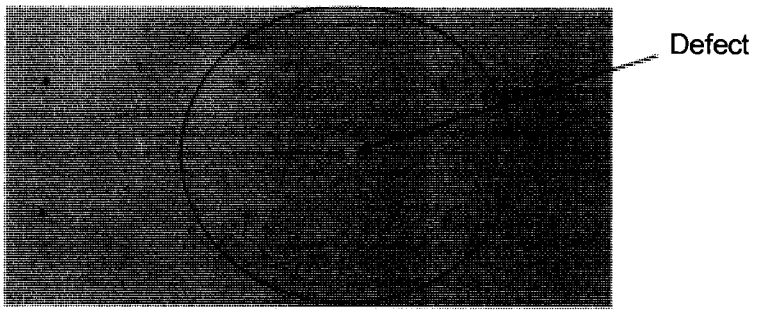

Figure 38 Evolution of incomplete infiltration defect in panel using hole pattern d) (Figure 31)

An analysis of the fill time for the cases shown in Figure 31 is summarized in Figure 39. The time for saturation of the part up to the end of the distribution medium on the top surface of each panel was compared to the saturation time on the bottom (tool) surface. The saturation time was normalized with viscosity.

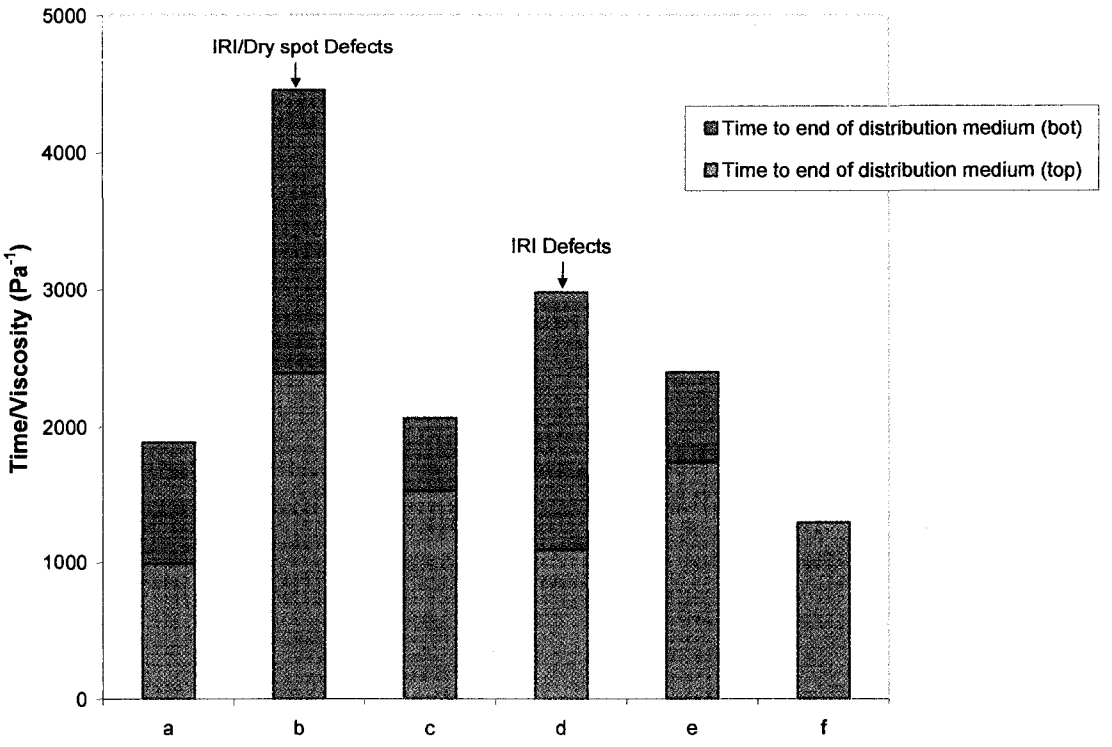

Figure 39 Results of resin infiltration time for various hole patterns[1]. a) 25 mm square, b) Nominal hexagonal - 50 mm spacing, c) Nominal hexagonal - 4 mm hole, d) 50 mm x 75 m rectangle, e) Nominal hexagonal, and f) Nominal hexagonal - rotated 90°.

Hole patterns b) and e), hexagonal patterns with 50 mm hole spacing and nominal hole spacing, respectively, had higher saturation times on the bag side of the panel compared with the remaining hole patterns. In comparison, the rectangular pattern d) and pattern b) had holes with the greatest spacing between them and took longest to fill the tool side of the panel. The longer saturation time on the tool side is likely because of the lower through-thickness resin flow. These panels were also the only two with corresponding defects. The part with hole pattern c), 4 mm holes, had a higher through-thickness resin flow that likely resulted in a slower flow through the top skin, but a shorter lag with the bottom skin. Increasing the hole size can result in

[1] Refer to Figure 31 for core hole patterns.

a more uniform flow front on the top and bottom surface. The disadvantage in this case was that, similar to the square pattern a), the part had an approximately 5% higher resin content than the nominal hexagonal pattern shown in Figure 31e). It should be noted that for hole pattern f) the panel was fully saturated after infusion, but the video record of the infusion stopped prior to saturation. Therefore, the time to the end of the distribution medium on the bottom of the panel could not be measured.

What was indicated by these trials is that there is an optimum hole pattern, size and spacing to avoid defects and saturate the part efficiently. For example, the square hole pattern a) contained no defects and had one of the shortest infusion times. However, the disadvantage of this pattern is the increased resin content of the final part. In contrast, the part with hole pattern b), hole spacing double that of the nominal hexagonal pattern, had a resin content ten times lower, but also had the highest infusion time. An optimized pattern has yet to be determined by a combination of experimental trials and process modelling.

4.3 Summary

It was found from infusion processing trials that the development of defects in closed-cell foam core sandwich panels was limited to a range of processing parameters. These included infusion pressure differences lower than 86 kPa. Defects were also developed due to certain patterns in the holes through the foam core. In the case of the rectangular pattern the resin flow front was affected to the extent that incomplete infiltration defects were formed where air was trapped between multiple saturated

flow fronts. Variations in viscosity for the ranges examined did not contribute to the occurrence of defects. However, there was an effect on the part saturation time due to resin viscosity that was also predicted by calculations based on Darcy's Law. These calculations closely followed the experimental results for the viscosity trials as well as the infusion pressure trials with the exception of some anomalies. These anomalous results appear to have been affected by an unknown process parameter or combination of parameters.

While there is an attempt to keep all fixed parameters constant during the experimental trials there is still variability between trials that results in experimental error. Only the parameters in the previous section were studied for their effect on trial results, but as shown in Appendix A there are a number of other parameters that may have contributed to the variability. For example, four different operators prepared and performed the experiments. There may have been some variability in layup and bagging techniques between the operators that resulted in the different results. Variations include placement of the vacuum extraction tube relative to the fiberglass which ranged in distance from 25 to 38 mm. For most trials the position of the flow front when the resin and vacuum tubes were clamped would not be a contributing factor since flow front position was measured only up to the end of the distribution medium and the tubes were clamped after this point was reached. However, for the trials investigating core hole patterns the effect of clamping may have been evident in the measurements of the flow front on the bottom of the panel if the resin tube was clamped prior to saturation of the core. The fabrication of two

panels at one time compared with a single panel may also have had an effect on the saturation time due to the use of longer resin and vacuum tubes and splitting of the resin and extraction flow. Finally, if the temperature changed enough during the processing trial to affect the viscosity, there would have been an effect on saturation time. Since temperature and viscosity were both measured prior to infusion, it is unknown if this factor had an effect on the results.

As will be shown in Chapter 5, the behaviour of the resin flow front on the tool surface, which varied due to the hole pattern, had an effect on the evolution of defects. However, infusion pressure trials showed that defects would also develop with the hexagonal hole pattern if conditions were not ideal.

Chapter 5 Flow Image Analysis

During the infusion trials CCD cameras captured the progression of the resin flow front for the purposes of both measuring the flow rate and analyzing flow front behaviour. Trials using the process described in Chapter 2 with various patterns of holes through the foam core showed the effect of the hole distribution pattern on the resin flow rate on the top surface compared to the bottom. Since the majority of common defects occur on the tool surface of the parts, further investigation was performed to analyze the effect of hole patterns on the path of the resin flow front. Images were examined at various stages during infusion of parts containing different hole patterns. The results are summarized in the following sections.

5.1 Unidirectional Flow Analysis

During infusion, if the resin flow front is not parallel to the vacuum extraction tube, there is a possibility for the resin to encapsulate voids or air in the preform. In the case of the sandwich structure where resin flows through the thickness of the part by means of a pattern of holes through the foam core there is the possibility of a non-uniform resin flow path related to the hole pattern. Figure 40a), b), and c) show time-elapsed photos of the resin flow fronts for the hole patterns shown in Figure 31 f), d), and a). It is clear from these figures that there is a direct effect of the hole pattern on the shape of the resin flow front on the tool surface of the part.

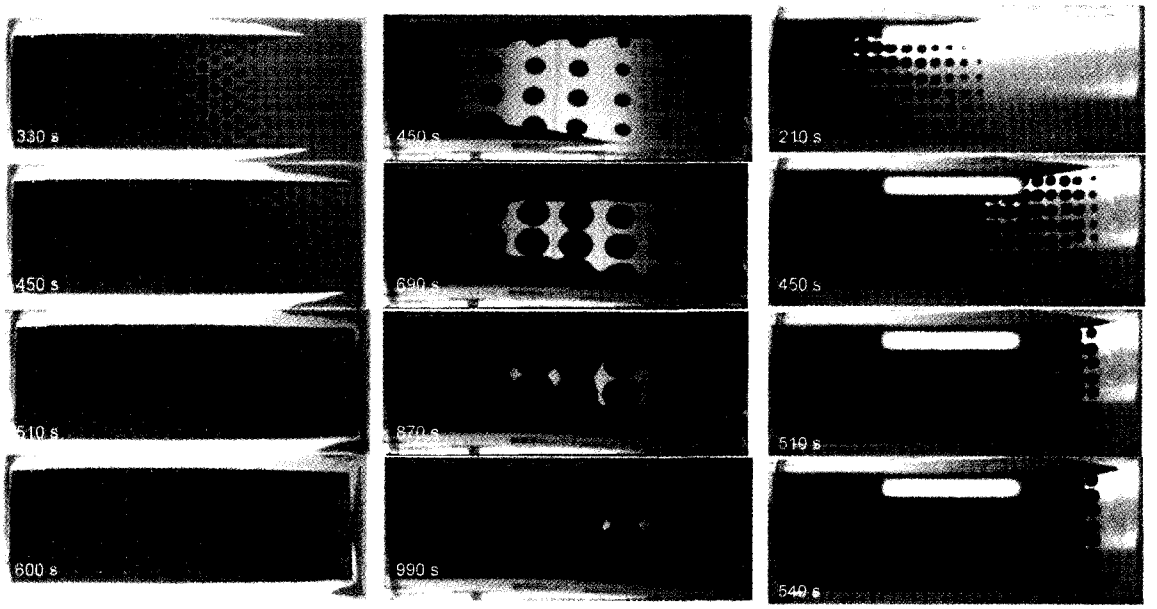

a) b) c)

Figure 40 Time elapsed images of resin saturation on tool surface of panels with hole patterns (e), (d), and (a) from Figure 31

For these experiments, parts contained repeating unit cells of the hole patterns. The size of the unit cell dictated how many cells were contained across the width of the part, which was limited by the tool size. Some racetracking occurred along the edges of the parts, but since this edge effect would vary with the size of an actual part it was ignored for the purposes of this analysis. Figure 40a) shows the hexagonal pattern with resin flow appearing through multiple holes simultaneously. However, the maximum distance between holes was only 44 mm with overlapping flow fronts in between so saturation was effective under normal processing conditions. In this image white spots are visible in the saturated portion of the panel. These spots correspond to light on the opposite side of the panel from the camera shining through the holes in the foam core.

Figure 40b) shows that because of the separation distance of the holes in the rectangular pattern there was more resin available for distribution on the bag side of the part, resulting in an increased lag time between the saturation of the bag side compared to the tool side. Since the leading edge of the flow was so far ahead of the saturated flow front on the tool side, the result was several saturated flow fronts on the tool side initiated at each line of holes through the foam core. The flow fronts moved outward from the distribution holes in all directions, but faster in the direction of the vacuum extraction. Once the flow front on the bag side reached the vacuum port the flow fronts on the tool side had only the pressure difference between them to induce saturation. Therefore, the resin flow fronts trapped air or voids that appeared as incomplete resin infiltration defects at approximately the midpoint of the hole pattern in the cured parts. Since a large area of the tool surface needed to be saturated by resin flowing in the opposite direction to the applied vacuum pressure difference, an inefficient saturation mechanism developed. The same is true for the hexagonal pattern, but because of the close proximity of the holes the occurrence of defects was limited. Based on the results of this flow analysis it may be useful to perform a trial with the rectangular hole pattern rotated so that the distance between the holes in the direction of the flow is shorter than the transverse distance which will prevent multiple flow fronts from forming.

Figure 40c) shows a square pattern of holes spaced one inch apart. Due in part to the proximity of the holes and also to the fact that the flow front did not form a saturated flow path that was parallel to the vacuum tube, but multiple "fingers" of resin along

the length of the part, there were no apparent defects with this hole pattern. This trial demonstrated that it is best to produce a resin flow path that does not allow a saturated flow front to progress in front of an unsaturated region of the part.

Based on these results, a metric of the location of defects relative to the holes patterns was developed.

5.2 Development of Unit Cells

Parts fabricated and cured were examined for the occurrence of defects caused by the pattern of holes used for distribution of resin on the tool side of a sandwich structure. Each hole pattern has a distinct unit cell that repeats over the surface of the part to form an array of holes. These unit cells are shown in Figure 41 with a black line or point indicating the typical locations and shapes of defects. These defects were either observed from various processing trials or estimated based on the observation of the resin flow front behaviour.

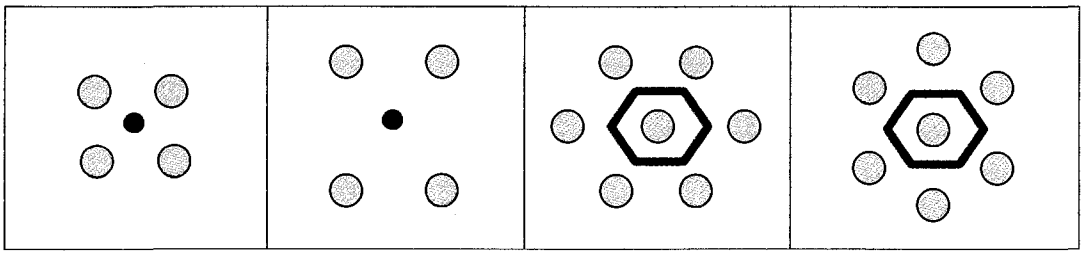

Figure 41 Schematics of potential defect locations for hole patterns a), d), e), and f), Figure 31

In the case of the hexagonal hole pattern defects which only occurred outside of the standard processing conditions would appear as smaller concentric hexagons or

partial hexagons. The defects did not consistently occur on one side of the holes, but for the pressure variation trials they were along the two sides of the hexagon perpendicular to the vacuum extraction tube. The rectangular hole patterns resulted in defects occurring as points either centered within the unit cell or slightly closer to the vacuum end. This asymmetry resulted from resin flowing against the vacuum pressure difference. The square hole patterns would likely have similar defects compared to the rectangular pattern, but because of the closely spaced holes the likelihood of defects was low. In almost all cases, the defects that resulted were incomplete resin infiltration defects that did not appear as dry fibres on the tool surface of the part. This indicates that dry spot defects are the result of more severe deviations in the resin infusion process. The results of these trials showed that based on the pattern of the holes used for distribution of resin through the thickness of a foam core sandwich panel it is possible to predict the types, potential locations, and shape of defects that are likely to occur under process deviations.

5.3 Orthogonal Flow Analysis

5.3.1 Experimental Trials

Further to the trials in the previous section, trials were performed to evaluate the effect of resin flow in two orthogonal directions through a sandwich part with holes used for through-thickness resin distribution. These trials examined the effect of square and rectangular hole patterns as described in Figure 31a) and d).

Two experiments were performed using the same materials used for the unidirectional flow trials as described in Chapter 2. The layup that was used is shown in Figure 42.

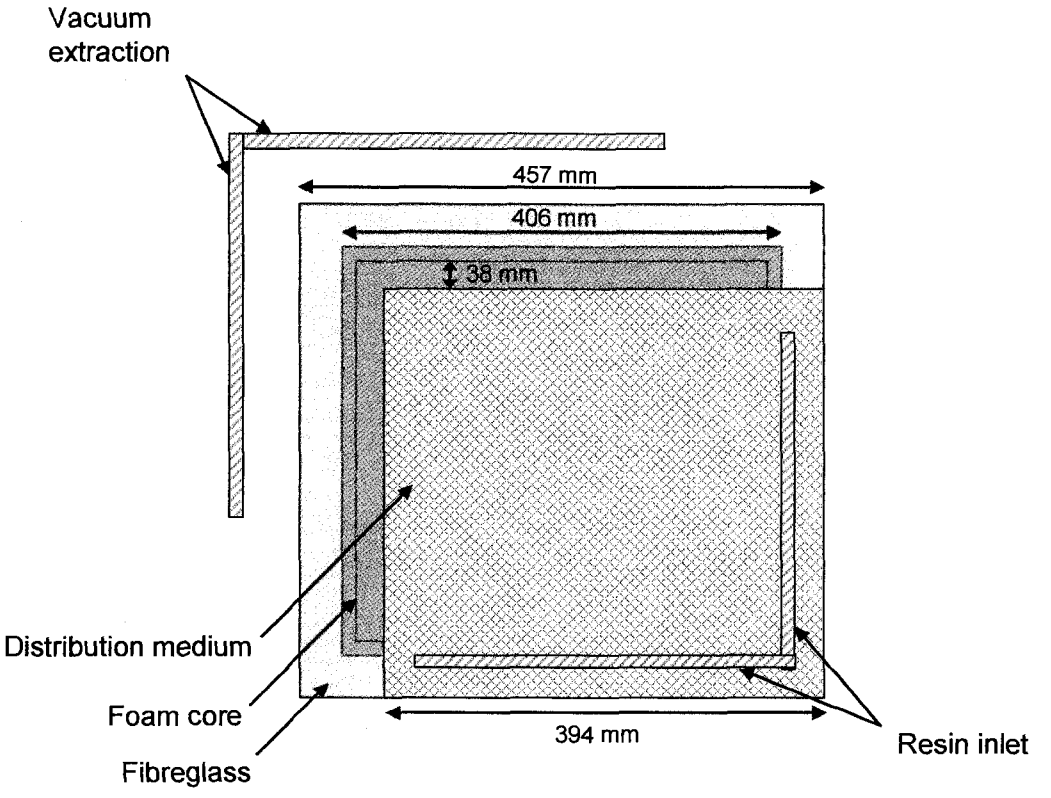

Figure 42 Schematic of lay-up for orthogonal flow trials

Experiments were performed on a 30.5 cm by 30.5 cm glass tool. The dimensions of all layup materials were equal in the length and width directions. A video camera captured the infusion on the top and bottom surface through the use of a mirror positioned under the glass tool to reflect the bottom of the panel. Resin was introduced at the corner of the two inlet tubes and extracted along the opposite two edges of the panel. The spiral tubes used for the inlet and extraction ranged in length from 30 to 36 cm. The resin viscosity for the trial with the square hole pattern was 0.300 Pa·s and the rectangular hole pattern was 0.320 Pa·s. The pressure difference along the part was approximately 96 kPa.

5.3.2 Defect Evolution and Prediction

For the panel with the square hole pattern an increased amount of accelerator was used to prematurely gel the resin during the infusion. Since the square pattern was unlikely to form defects under standard processing conditions, the premature gelation allowed closer observation of the resin flow behaviour. It is clear from Figure 43 that the same resin "fingers" form in both directions of the panel even with resin flowing on an angle relative to the square pattern. Additionally, the saturated flow front occurred behind the leading edge of the resin flow which decreased the chances of defects forming. However, it appears that if defects did form due to process excursions they would consist of a dry spot defect in the corner of the unit cell closest to the corner where the two vacuum extraction tubes met.

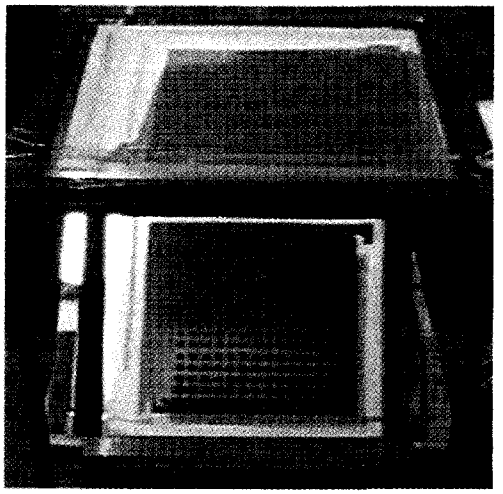

Figure 43 Image of experimental set-up for orthogonal flow trial using hole pattern a) from Figure 31

For the panel with the rectangular pattern two different resin flow front behaviours were observed depending on the orientation of the rectangle. Where the resin flow

front was perpendicular to the longitudinal axis of the rectangle saturated flow fronts occurred simultaneously at various positions across the panel. Where the resin flow front was parallel to the longitudinal axis the resin flow behaviour was similar to that for the square hole pattern. These behaviours can be seen in Figure 44.

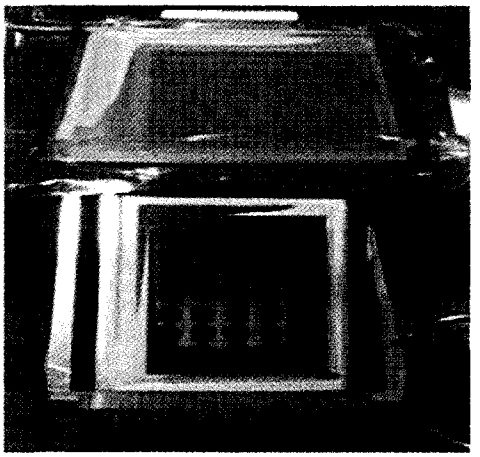

Figure 44 Image of experimental set-up for orthogonal flow trial using hole pattern d) from Figure 31

5.4 Summary

From these experiments it is clear that the orientation of the resin flow front relative to asymmetric hole patterns is important to the resin flow behaviour. In the case of the rectangular pattern where defects developed during unidirectional experiments under standard processing conditions, reorientation of the pattern could result in successful infusion under the same conditions. Therefore, it is important to perform a careful analysis of distribution mechanisms relative to the principal flow front direction during planning of the manufacturing process of a resin-infusion part.

Chapter 6 Mechanical Testing

Previous work has investigated the effect of impact damage on the compression strength of coupons made using the resin infusion process outlined in this paper [50],[51]. For comparison, similar coupons containing defects, rather than impact damage, were tested to evaluate the effect of defects on the compression strength. Specimens were selected from the processing trials for the presence of dry spot and incomplete resin infiltration defects.

6.1 Procedure

Prior to the fabrication of test coupons, the selected parts were post-cured at 70°C for 8 hours to complete the manufacturing process used for production parts. Specimens were cut to the dimensions of 152 mm by 102 mm on a circular diamond saw. The saw rotation rate was reduced to avoid overheating the foam core. Specimens were then tested in the Boeing Compression After Impact Compression Test Fixture BSS 7260 according to SACMA Recommended Methods test standard 2 (SRM 2R-94) [52]. A description of the test procedure and a schematic of the test specimen are contained in Appendix B. A picture of a specimen installed in the fixture is shown in Figure 45.

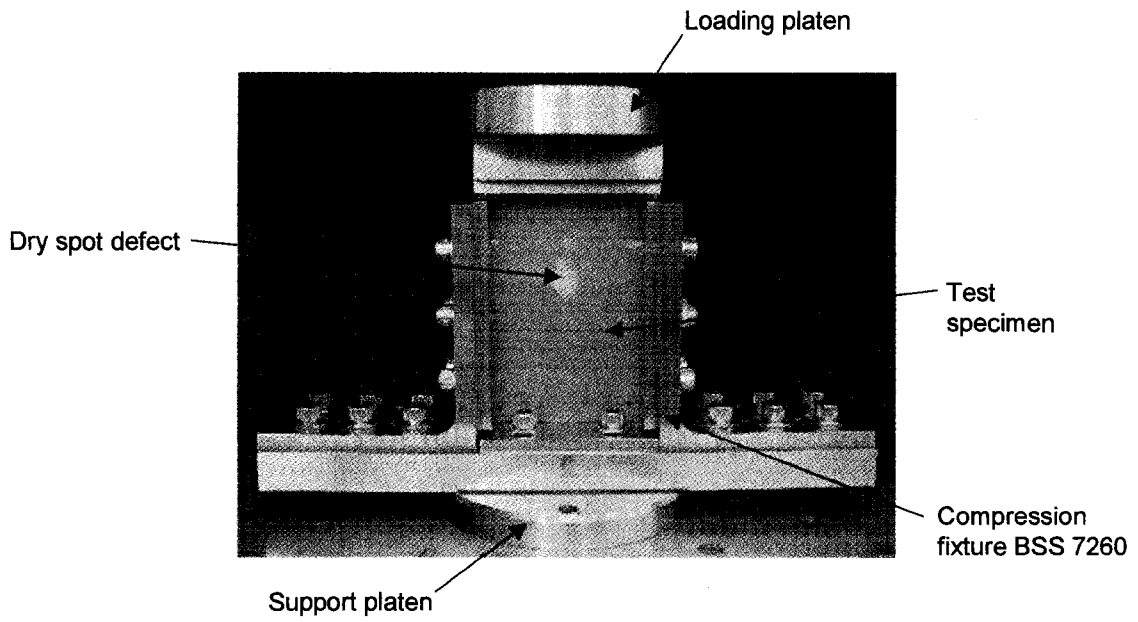

Figure 45 Compression after impact test fixture with specimen inserted

The fixture was aligned between the loading and support platens of an Instron Model 1125 System 7887 test frame using MTS TestWorks 4 software to acquire data during the tests. Initially, a self-aligning gimbal was used in place of the upper platen. The gimbal appeared to lead to amplification of bending in the unsupported area of the specimen above the anti-buckling guides. Failure of two specimens, 070104-1 and 070104-2, occurred in this manner and the use of the gimbal was discontinued.

After using a plum bob to determine the centre of the loading path the position of the fixture on the lower platen was marked for repeatable placement. Crosshead movement was used in place of strain gages for measuring displacement of the specimen. The lack of strain gages also meant that out-of-plane bending was not evaluated during loading of the specimens. Table 9 shows a list of the panel numbers and the associated defects that were examined by the compression tests.

Table 9 Condition of panels tested in compression

Panel	Characteristics
072604	Reduced pressure (-57.6 kPa) resulting in formation of incomplete infiltration defects
080604	Reduced pressure (-47.4 kPa) resulting in formation of incomplete infiltration defects
112603	Controlled formation of dry spot defects
121603 #2	Controlled formation of dry spot defects
081104	Controlled processing conditions, no visible defects
070104	Visually observed tranverse defect on bag surface (after demoulding)

The following section describes the position of the coupons on each panel and the failure morphology of the coupons after testing.

6.2 *Failure Morphology Results*

The following section describes the results of compression trials on coupons containing incomplete resin infiltration defects.

6.2.1 Incomplete Resin Infiltration

During the unidirectional flow trials the infusion pressure difference was reduced to determine its effect on defect evolution. The resulting specimens contained incomplete resin infiltration defects that increased in severity with proximity to the vacuum extraction port and with reduction in the pressure difference. Near the resin infiltration port the specimens contained no visible defects. Coupons from both the defective and non-defective regions of the specimens fabricated at pressure differences of 47.4 kPa and 57.6 kPa were tested in compression. Figure 46 shows the location of the coupons on each specimen.

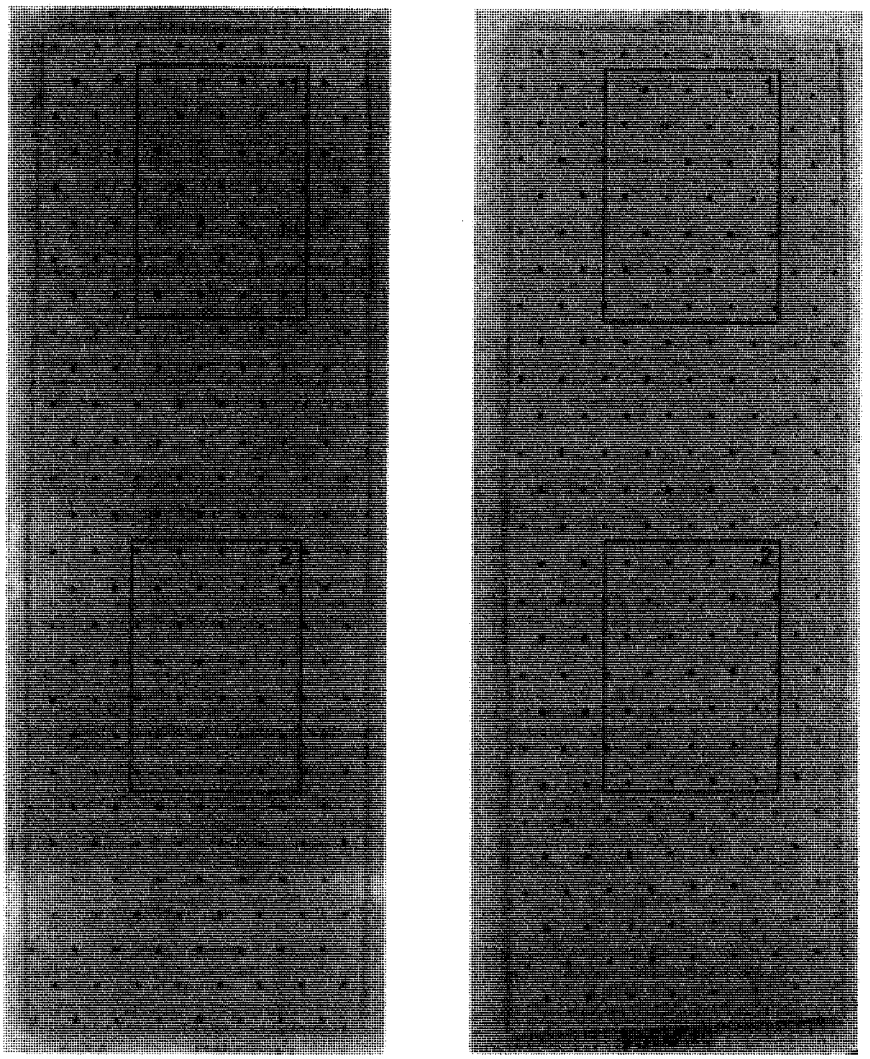

a) 080604 – 47.4 kPa b) 072604 – 57.6 kPa

Figure 46 Location of coupons in panels fabricated using reduced vacuum pressure during resin infusion

The coupons were selected to represent the areas containing the most severe defects and defects of lower severity. These coupons were tested as outlined in Section 6.1 and the locations of the compression failure relative to the defect locations on both the tool and bag side of the panel are shown in Figure 47 and Figure 48.

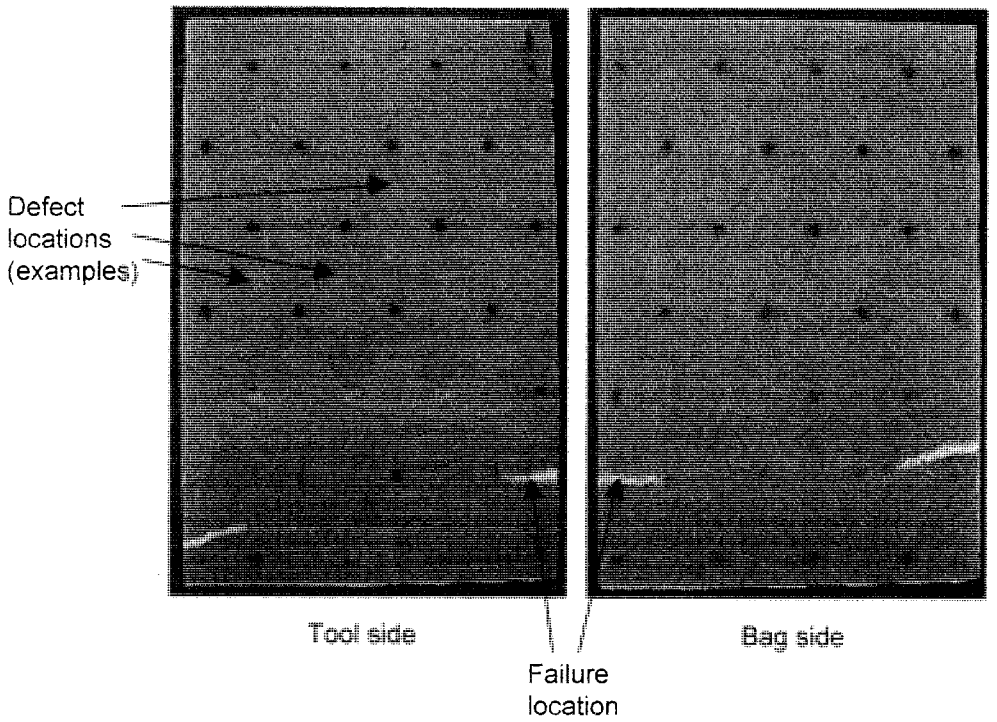

a) 072604-1 (57.6 kPa)

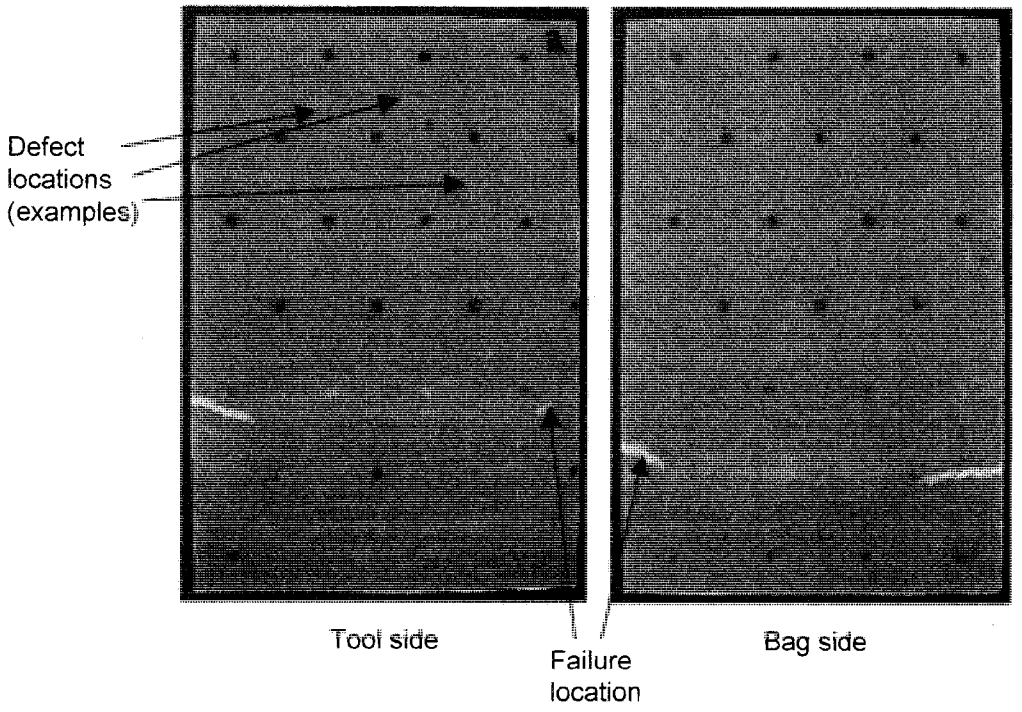

b) 072604-2 (57.6 kPa)

Figure 47 Specimens infused at pressure difference of 57.6 kPa and tested in compression a) Specimen 1 on panel 072604 (Figure 46) and b) Specimen 2 on panel 072604 (Figure 46).

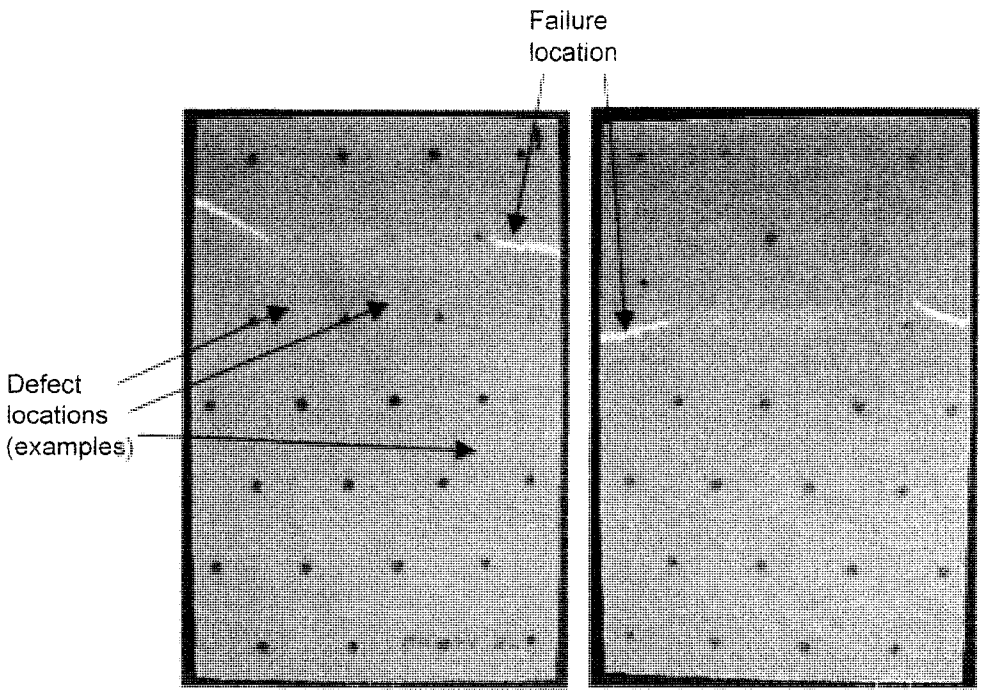

080604-1 (47.4 kPa)

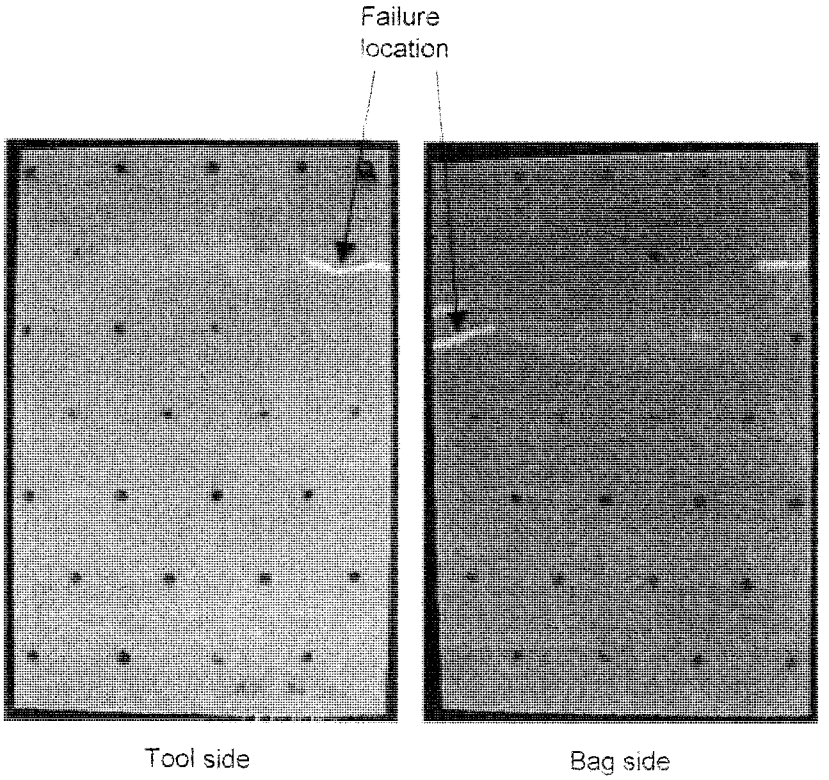

080604-2 (47.4 kPa)

Figure 48 Specimens infused at pressure difference of 47.4 kPa and tested in compression a) Specimen 1 on panel 080604 (Figure 46) and b) Specimen 2 on panel 080604 (Figure 46).

These coupons showed no strong evidence that the failure location corresponded to the defect location. Failure locations varied along the length of the coupons and appeared to consist of a short fibre fracture at each edge of the coupon and a region of facesheet buckling in the area between. However, the failure appeared to occur instantaneously during testing and therefore, the progression of failure is unknown.

6.2.2 Dry Spots

Specimens containing dry spots were fabricated as described in Section 3.1. The severity of the dry spot defect varied depending on its location on the specimen. Specimens were cut into test coupons with the dry spots located near the centre of the coupons. A coupon without visible defects was tested for comparison. Figure 49 shows the location of each test coupon.

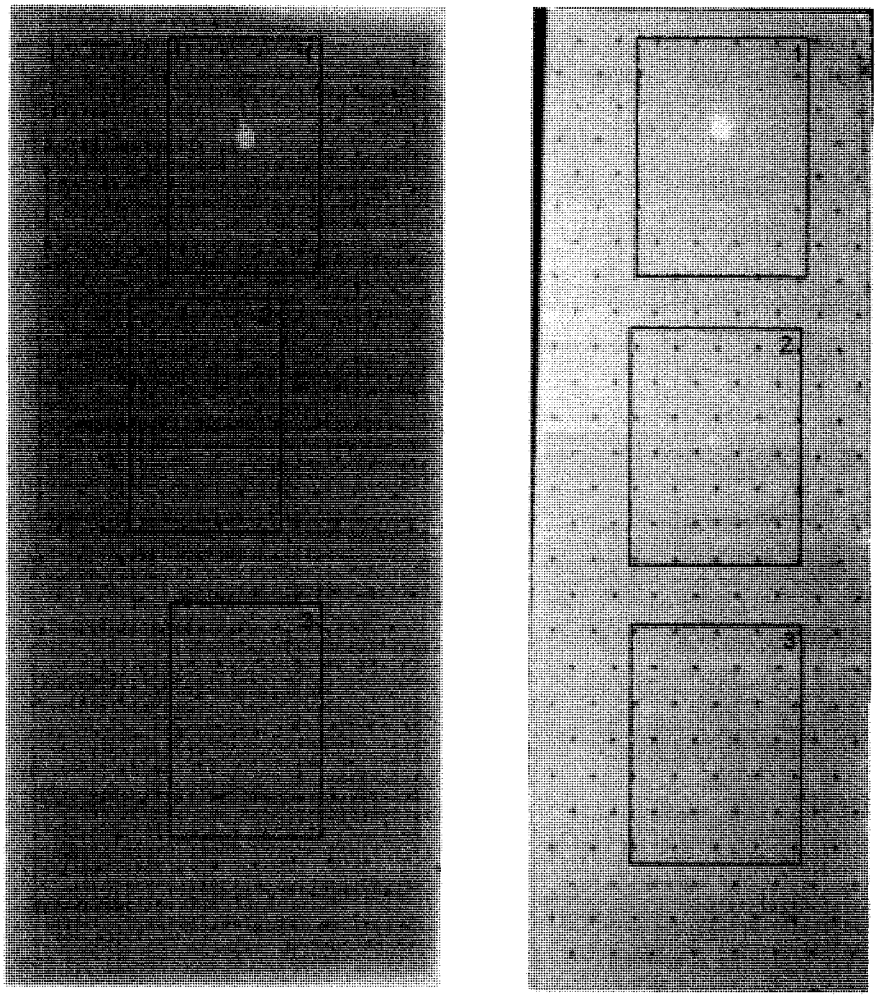

112603 121603#2 -

Figure 49 Location of coupons in panels fabricated with dry spot defects

Specimen number 1 from each panel contained the most severe dry spot defect followed by specimens 2. Specimens 3 were selected from an area that appeared to have no visible defects. Figures 50-55 show the failure location on each coupon after compression testing.

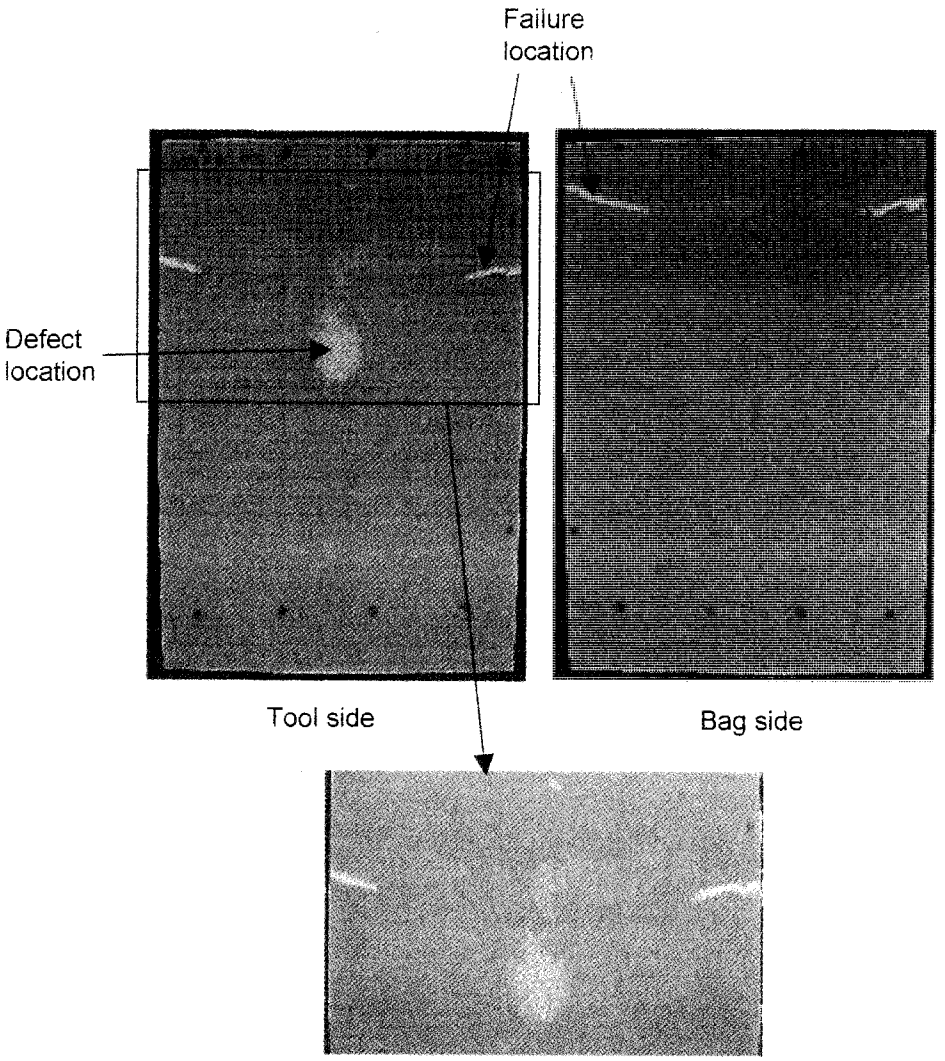

Figure 50 Specimen 1 on panel 112603 after compression testing (Figure 49)

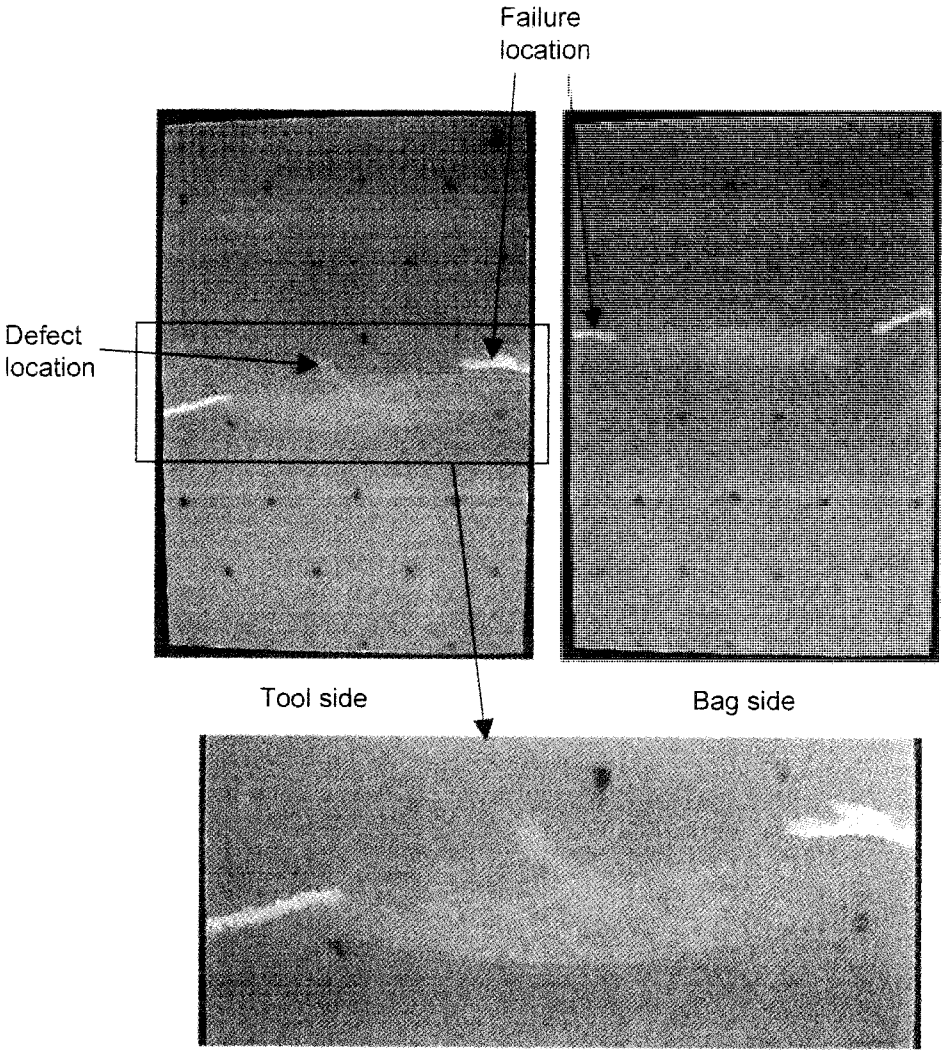

Figure 51 Specimen 2 on panel 112603 after compression testing (Figure 49)

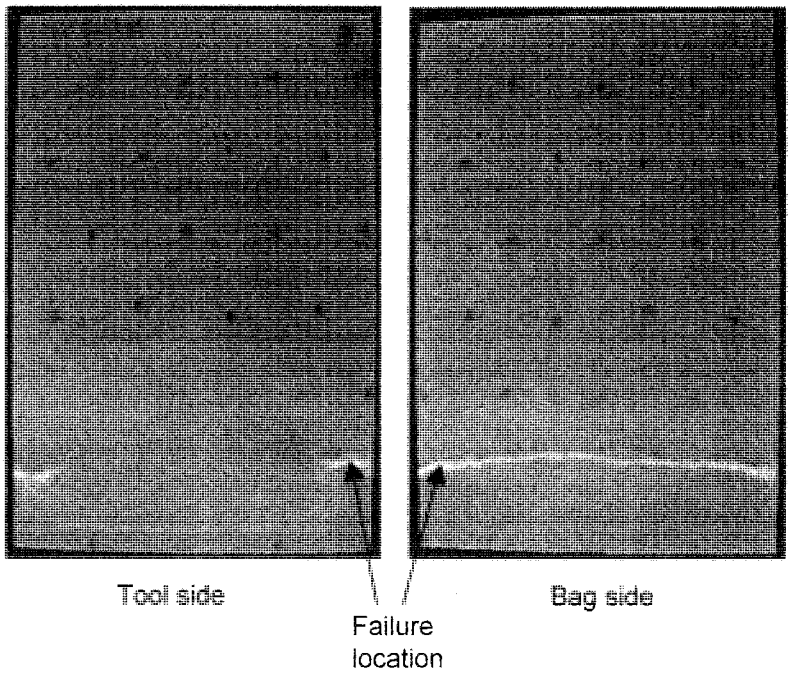

Figure 52 Specimen 3 on panel 112603 after compression testing (Figure 49)

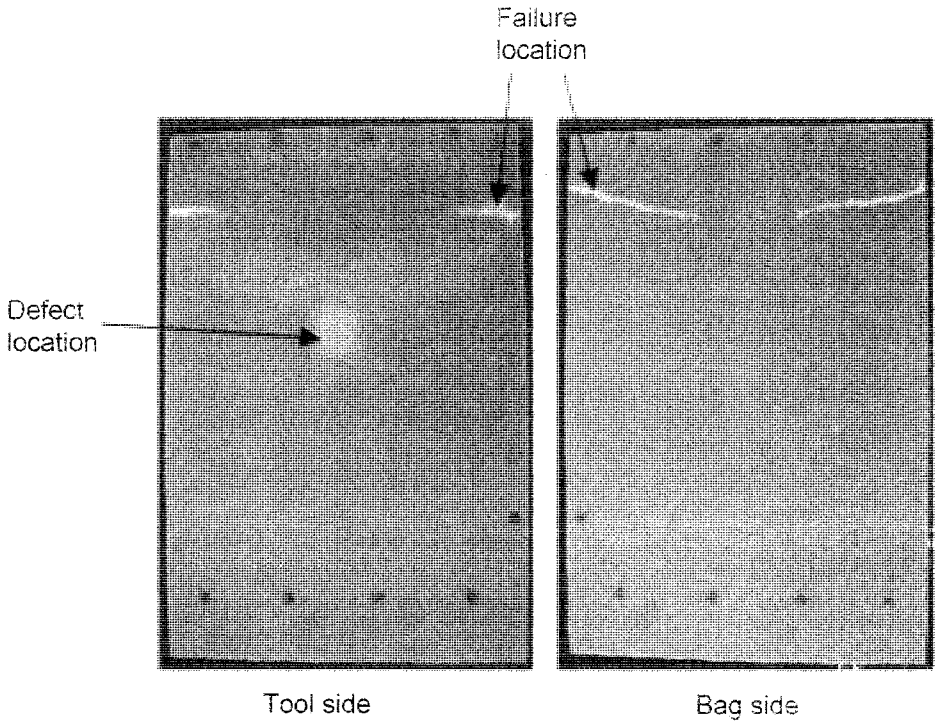

Figure 53 Specimen 1 on panel 121603#2 after compression testing (Figure 49)

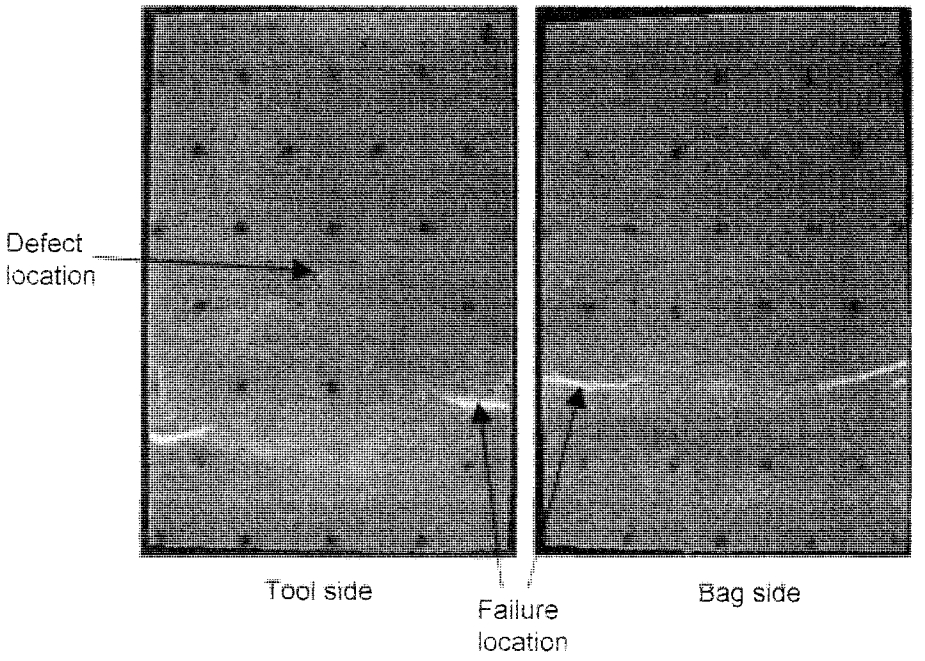

Figure 54 Specimen 2 on panel 121603#2 after compression testing (Figure 49)

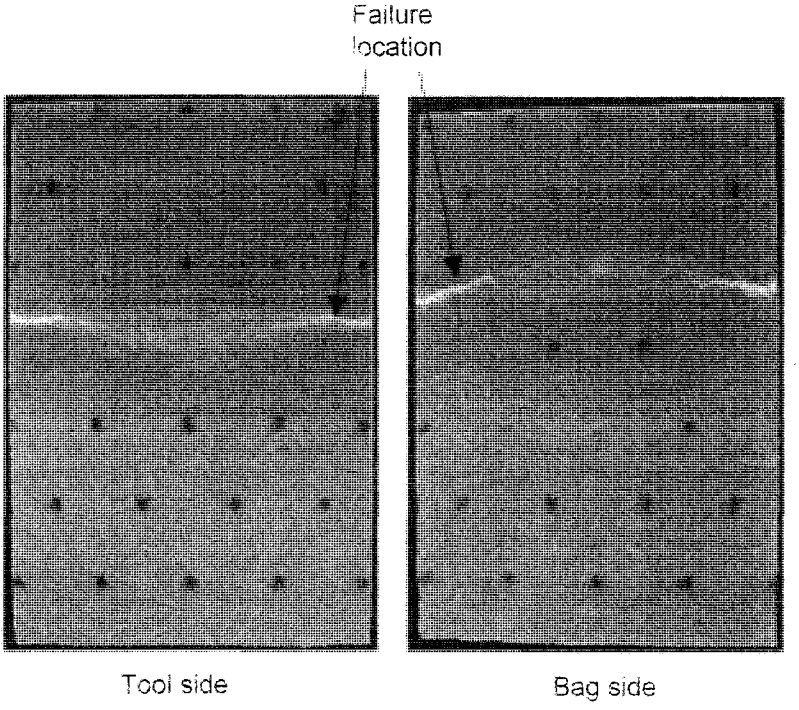

Figure 55 Specimen 3 on panel 121603#2 after compression testing (Figure 49)

The failure morphology for the coupons with dry spots was similar to that for incomplete resin infiltration where edge cracks were found on either side of facesheet buckling. However, in this case the facesheet buckling appeared to lead to a greater extent of delamination between the facesheet and core than for the incomplete resin infiltration specimens. While the cracks were not always directly related to the position of the defects, this delamination was often present over the area of the dry spot.

For comparison, a specimen without any visible defects was tested in compression. Figure 56 shows the failure morphology of this specimen.

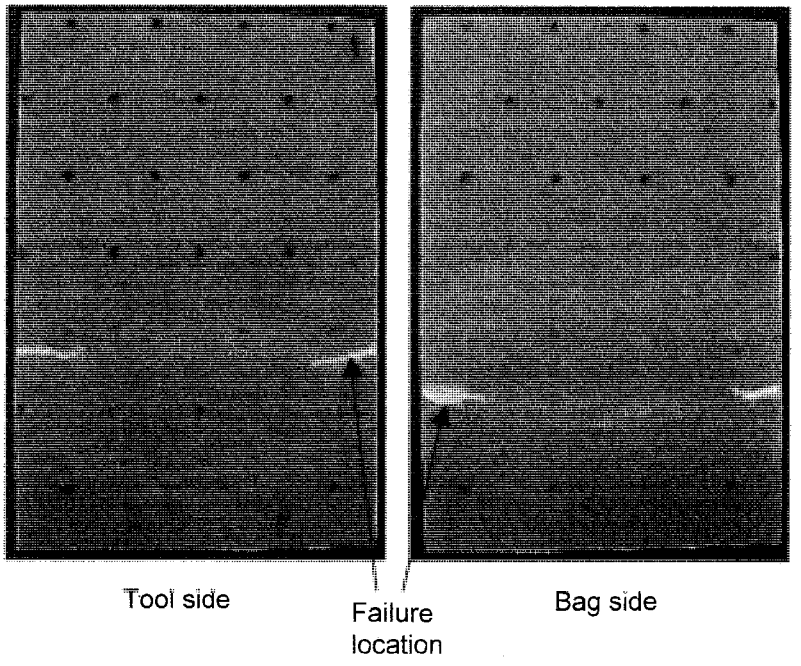

Figure 56 Specimen with no visible processing defects as it appears after compression testing

The failure morphology is very similar to the coupons containing process defects. There is a region of fibre cracking and facesheet buckling on both the tool and bag side of the specimen. To further evaluate the effect of process-induced defects on the coupons the compression strength was calculated and compared. A summary of the quantitative results is contained in the following section.

6.3 Summary of Results

An example of a typical stress versus displacement curve for a compression specimen is shown in Figure 57 .

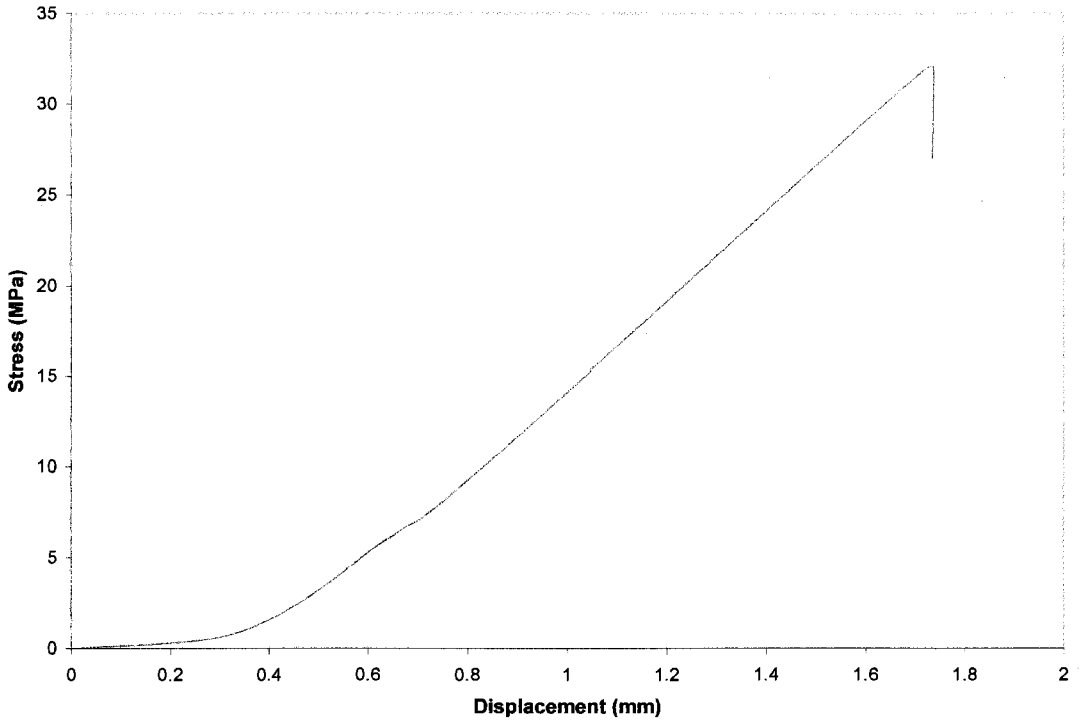

Figure 57 Example of a typical stress versus displacement curve obtained from compression testing

The ultimate compressive strength σ_{ult} (MPa) resulting from this test can be expressed as follows:

$$\sigma_{ult} = \frac{P}{bt} \qquad \textbf{Equation 5}$$

where P is the ultimate compressive load (N), b is the average specimen width (mm), and t is the average specimen thickness (mm). Equation 6 is used to find the maximum stress in the fiberglass facesheet [51].

$$\sigma_{facesheet} = \frac{P}{2bt_f} \qquad \textbf{Equation 6}$$

where P is the ultimate compressive load (N), b is the average specimen width (mm), and t_f is the average skin thickness (mm). Facesheet thickness was determined by subtracting the nominal core thickness from the overall measured thickness of the sandwich panel. Table 10 shows the results for the calculations of compressive strength for each specimen.

Table 10 Results of compression testing

Panel	Type of defect and approximate size	Approximate fracture location - measured from top of specimen on tool side (cm)	Overall maximum stress (MPa)	Facesheet maximum stress (MPa)
081104-1	No defect	9.7	39.31	239.08
072604-1	IRI – 15 mm x 4 mm	1.3[2]	32.04	169.22
072604-2	IRI – 15 mm x 4 mm	10.3	34.83	183.98
080604-1	IRI – 15 mm x 4 mm	3.5	33.37	182.92
080604-2	IRI – 15 mm x 4 mm	3.3	36.49	191.84
112603-1	Dry spot – 20 mm x 15 mm	3.7	34.49	197.96
112603-2	Dry spot – 13 mm x 3 mm	7.0	32.34	187.93
112603-3	No defect	13.1	35.78	194.32
121603-1	Dry spot – 15 mm x 13 mm	2.7	33.05	201.32
121603-2	Dry spot – 5 mm x 4 mm	11.0	32.93	196.02
121603-3	No defect	6.1	32.45	190.11
Average			**34.50**	**194.06**
Standard Deviation			**2.20**	**17.32**
COV			**6.38%**	**8.92%**

Figure 58 shows a comparison between the results for specimens with no defects compared with specimens that had either dry spot or incomplete resin infiltration defects.

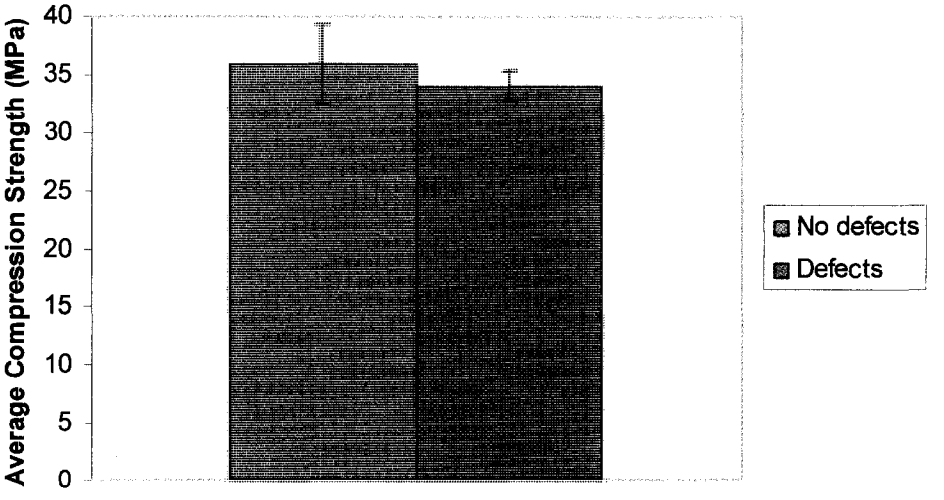

Figure 58 Comparison of average compression strength for panels with and without defects

[2] Due to the proximity of this failure to the antibuckling guides, this result was not included in the calculation of the average stress.

As is apparent from Figure 58 these trials showed no significant difference in the compression strength of specimens with or without defects. The only difference is that the specimens without defects had a slightly higher variation in compression strength. Specimens 072604-1, 121603#2-1, 112603-1 failed very close to or on the edge of the anti-buckling guides. Since these failures were not considered legitimate they were not included in the calculation of the average compression strength.

The average facesheet stress for all specimens tested in this work is similar to the results found for specimens in Gordon and Boukhili's work with no impact damage, 194 MPa versus approximately 200 MPa [50]. The sandwich panels in each of the two studies were fabricated from the same materials by the same method. The only difference was in the layup of the facesheets; instead of using three fabric plies for a layup of $[0/90]_3$, the facesheet in Gordon and Boukhili's work used a layup of [±45, 0/90, ±45] [50]. The different layups could have resulted in the difference in compression strengths between Gordon and Boukhili's work compared with this work. There was also likely an effect on the compression modulus, but this was not examined here. In Gordon and Boukhili's work specimens were subjected to a range of impact energies to study the effect of damage severity on the compression after impact strength. It was found that the presence of damage on the non-impacted facesheet reduced the residual strength of the specimen by 90 to 100 MPa and that barely visible impact damage (BVID) on the impacted face only resulted in a reduction of residual compression strength of approximately 55 to 85 MPa. BVID was defined by the occurrence of matrix microcracking. In comparison, specimens

with dry spot and incomplete infiltration defects had no significant effect on the compression strength of the facesheet. These results show that the absence of resin or the presence of severe voiding in the matrix does not affect the columnar compressive strength of the sandwich panel.

Chapter 7 Conclusions and Recommendations

The purpose of this work was to analyze defects and how they arise during the fabrication of sandwich structures using a low-cost resin infusion technique. In order to perform this study the author developed a trial matrix and set default parameters for a controlled experimental approach. The design of the trial panel was given to three other operators to perform the axial flow trials. The author analyzed the saturation times and flow fronts for these trials using Image Tool software. The orthogonal flow trials were both designed and performed by the author. Analysis of these trials as well as the effects of defects on the compression strength also formed part of this work.

The following conclusions were made:

- Visual observation of defects was the most accurate and efficient method to identify and characterize defects in sandwich structures made with fiberglass skins and PVC foam core.
- Defects during resin infusion arise in the form of incomplete resin infiltration, dry spots, air ingression and premature gelation. Air ingression and premature gelation were due to process excursions outside the scope of this work.
- Viscosity affects the mould saturation time in agreement with Darcy's Law for 1-D flow through a porous medium. However, no defects were observed to arise from variations in viscosity.

- Infusion pressure results in incomplete resin infiltration defects below infusion pressure differences of 86.3 kPa when the nominal core hole pattern is used.
- At any infusion pressure difference, variations in core hole pattern can result in incomplete resin infiltration defects and possibly dry spot defects.
- Analysis of the flow front shows that it is the pattern of resin flow due to the core hole patterns that affects the evolution of defects.
- Orthogonal flow analysis indicates that a more complex flow front has the potential to overcome the problems seen in axial flow.
- Compression testing of specimens containing defects showed that there was no significant impact of either incomplete resin infiltration defects or dry spot defects on the compression strength.

The following recommendations were developed as a result of the work that was performed:

- This work investigated the evolution of defects due to a single process variable. In most cases no defects arose due to the single variable being studied. Therefore, it would be useful to examine parametric interactions to determine the combination of variables that result in defects.
- Since each experimental trial is labour-intensive and costly, it would be beneficial to develop a design of experiments (DOE) approach to study the interaction of the parameters.

- The use of numerical evaluation of the results would be necessary to keep the number of trials to a minimum since attribute-based DOE is difficult to evaluate. For example, the percent and size of defects, resin flow rate, and part mass could be used as evaluation measures.
- This work demonstrated that the types of defects evolved for a given process condition were not highly variable. However, the resin flow rate results indicated that there was a variability that could not be explained by the process parameters studied. Future work should focus on determining the cause of this variability. It may be useful to limit the experimental trials to a single operator to eliminate this potential source of variability.
- Since there was no significant effect of defects on the static compressive strength of the specimen it is recommended to evaluate these specimens in the form of long-beam sandwich panels under flexural testing conditions. Also, based on studies by Haque et al. [28], fatigue tests on structures containing defects may also be more appropriate due to the effect of void content on fatigue properties.

Appendix A

The following tables contain the actual process parameters used for each of the experimental trials.

Table 11 Summary of processing parameters for resin viscosity trials

Parameters	Resin Viscosity			
Trial	310cP	320cP	150cP	500 cP
Date	12/07/04	04/29/04	06/11/04	3/4/2005
Notes		may have been an air leak		
Operator	Khoun	Khoun	McGrath, Petrescue	St-Amant
Core length (cm)	61	61	61	61
Core width (cm)	20	20	20	20
Core mass (g)	46.8	67.9	71.8	61.2
Fibreglass length (cm)	65	65	65	65
Fibreglass width (cm)	24	24	24	24
# of plies	6	6	6	6
Peel ply length (cm)	76	76	76	76
peel ply width (cm)	25	25	25	25
peel ply mass (g)	20.5	12.2	12.2	20.4
resin tube length - panel to T connector (cm)	n/a	69	n/a	n/a
resin tube length - T connector to pot (cm)	91	51	119	119
spiral tube length (cm)	20	20	20	20
vacuum tube length - panel to T connector (cm)	n/a	69	n/a	n/a
vacuum tube length - T connector to pot (cm)	91	51	119	119
media length from taper (mm)	38	38	38	38
media width (cm)	19	19	19	19
media mass (g)	20	-	18.3	21.4
Distance between vacuum tube and end of fibreglass (mm)	25	-	38	38
resin tube location	At taper	-	At Taper	At taper
infusion pressure (kPa)	96.5	94.8	94.8	91.4
temperature (°C)		22	20.7	21.7
flow front location when clamping resin tube		-	fully saturated core	fully saturated core
flow front location when clamping vacuum tube		-	fully saturated fibres	fully saturated fibres
mass of trigonox 239A (g)	4.5	-	4.11	5.6
mass of cobalt (g)	2.8	-	2.49	3.5
mass of derakane resin (g)	430.7	420	411.6	530
viscosity of resin after mixing (Pa•s)	0.307	0.32	0.147	0.51
panel mass (g)	574.5		589.3	570
defects	no defect	not infused completely	surface discolouration	no defect

Table 12 Summary of processing parameters for infusion pressure difference trials

Parameters	Infusion Pressure Gradient						
Trial	96.5 kPa	86.3 kPa	77.9 kPa	67.7 kPa	57.6 kPa		47.4 kPa
Date	08/11/04	08/13/04	06/09/04	08/10/04	07/26/04	08/04/04	08/06/04
Notes							
Operator	McGrath	McGrath	McGrath, Petrescue	McGrath	McGrath	McGrath	McGrath
Core length (cm)	61	61	61	61	61	61	61
Core width (cm)	20	20	20	20		20	20
Core mass (g)	57.6	54.7	71.9	55.7	51.4	57.3	54.5
Fibreglass length (cm)	65	65	65	65	65	65	65
Fibreglass width (cm)	24	24	24	24	24	24	24
# of plies	6	6	6	6	6	6	6
Peel ply length (cm)	76	76	76	76	76	76	76
peel ply width (cm)	25	25	25	25	25	25	25
peel ply mass (g)	20.8	20.1	13	20.7	12.3	21.8	20.8
resin tube length - panel to T connector (cm)	n/a	n/a	n/a	n/a	n/a	n/a	n/a
resin tube length - T connector to pot (cm)	119	119	119	119	119	119	119
spiral tube length (cm)	20	20	20	20	20	20	20
vacuum tube length - panel to T connector (cm)	n/a	n/a	n/a	n/a	n/a	n/a	n/a
vacuum tube length - T connector to pot (cm)	119	119	119	119	119	119	119
media length from taper (mm)	38	38	38	38	38	38	38
media width (cm)	19	19	19	19	19	19	19
media mass (g)	20.4	19	17.9	20	19	19.4	17.9
Distance between vacuum tube and end of fibreglass (mm)	25	25	38	25	on top of edge of fibers	38	25
resin tube location	At taper	At taper	At Taper	At taper	At Taper	At taper	At taper
infusion pressure (kPa)	96.5	86.3	77.9	67.7	57.6	57.6	47.4
temperature (°C)	22.3	23	22.9	22.1	22	22.1	22.6
flow front location when clamping resin tube	fully saturated core and fibers	core fully saturated	fully saturated core	fully saturated core, and fibers	Fuly saturated core	fully saturated core	fully saturated core
flow front location when clamping vacuum tube	fully saturated fibers	fibers were fully saturated	almost fully saturated fibres	Fully saturated fibers	fully saturated fibers	fully saturated fibers	fully saturated fibers
mass of trigonox 239A (g)	4.7	2.77	5.97	4.7	3.89	4.115	4.23
mass of cobalt (g)	2.8	4.62	3.58	2.82	2.33	2.47	2.54
mass of derakane resin (g)	467.4	462.4	597.2	470	390.4	411.5	423
viscosity of resin after mixing (Pa•s)	0.225	0.262	0.282	0.285	0.288	0.25	0.3
panel mass (g)	577.8		575.3	592.5	549.4	572.6	547.9
defects	no defect	no defect	mild IRI + other surface defects	IRI and air ingression after infusion	IRI near end of distribution media	IRI near end of distribution media	dry spot at one of the side edge near resin inlet + IRI

Table 13 Summary of processing parameters for core hole pattern orthogonal flow trials

Parameters	Core Hole Patterns					Orthogonal Flow	
Trial	50 mm hole spacing	4mm hole size	90° rotation of existing pattern	uniforme pattern 25 mm x 25 mm	rectangular pattern 50 mm x 75 mm	Square Pattern 25 mm x 25 mm	Rectangular Pattern 50 mm x 75 mm
Date	12/08/03	12/05/04	07/06/04	12/14/2004	12/14/04	02/20/05	03/03/05
Notes			Small amount of air bubbles			Laid up on 17Feb05, vacuum bag became slightly brittle; used Co 12% ; resin gelled prematurely, did not saturate fully	
Operator	Petrescue	Khoun	McGrath	Khoun	Khoun	Petrescue	Petrescue
Core length (cm)	61	61	61	61	61	41	41
Core width (cm)	20	20	20	20	20	41	41
Core mass (g)			75.5	60.2	60		
Fibreglass length (cm)	65	65	65	65	65	46	46
Fibreglass width (cm)	24	24	24	24	24	46	46
# of plies	6	6	6	6	6	6	6
Peel ply length (cm)	69	76	76	76	76	55	55
peel ply width (cm)	25	25	25	25	25	55	55
peel ply mass (g)	17.4		11.8	20.7	20.7		
resin tube length - panel to T connector (cm)	51	69	69	69	69	119	119
resin tube length - T connector to pot (cm)	89	51	51	51	51	n/a	n/a
spiral tube length (cm)	20	20	20	20	20	36+36	30+30
vacuum tube length - panel to T connector (cm)	n/a	69	69	69	69	119	119
vacuum tube length - T connector to pot (cm)	n/a	51	51	51	51	n/a	n/a
media length from taper (mm)	24	38	38	38	38	38	38
media width (cm)	19	19	19	19	19	39	39
media mass (g)	14.7		22.6	18.1	19.4		
Distance between vacuum tube and end of fibreglass (mm)		25	on top of fibers edge	25-38	25-38	25	32
resin tube location		At taper	At Taper	At Taper	At Taper	at taper	at taper
infusion pressure (kPa)			94.8	94.8	94.8	96.5	94.8
temperature (°C)			22.5	15.5	15.5	19.9	21.6
flow front location when clamping resin tube		Fully satured core	not fully saturated core,clamped 3/4inch after media	fully saturated core	fully saturated core-dry spot on the botom side	when resin gelled in beaker	fully saturated fibres
flow front location when clamping vacuum tube		fully satured fiber	fully saturated	fully saturedted	fully saturated	after 30 min	fully saturated fibres
mass of trigonox 239A (g)	7.7		6.3	7.8	7.8	5.57	4.8
mass of cobalt (g)	2.8		3.8	5	5	0.28	0
mass of derakane resin (g)	770		634	740.4	740.4	552.88	479.63
viscosity of resin after mixing (Pa•s)	0.276	0.334	0.255	0.302	0.302	0.3	0.32
panel mass (g)		574.8	556.5				
defects	IRI/dry spot at vacuum end	no defect	no defect	no defect	IRI defect along panel length	gelled before saturation	no defect

Appendix B

Compression test coupons were measured for cross-sectional area and perpendicularity using the following procedure:

1. Check for perpendicularity using 3" precision square (Mitutoyo Square 50x75mm),
2. Measure width at 3 locations using Vernier Calipers CD-8" (Mitutoyo BMD-1" DM Caliper Micrometer),
3. Measure length at 3 locations using Vernier Calipers CD-8",
4. With Mitutoyo Micrometer 0-1" (Mitutoyo Micrometer 1-2") take 4 measurements of thickness around defect location, but not close enough to include effect of defect on thickness.

An 81 piece set of Gauge Blocks, Grade B (AS-2), were used to check the calibration of the calipers and micrometer. A schematic of the specimen requirements according to AITM 1.0010 is shown in Figure 59.

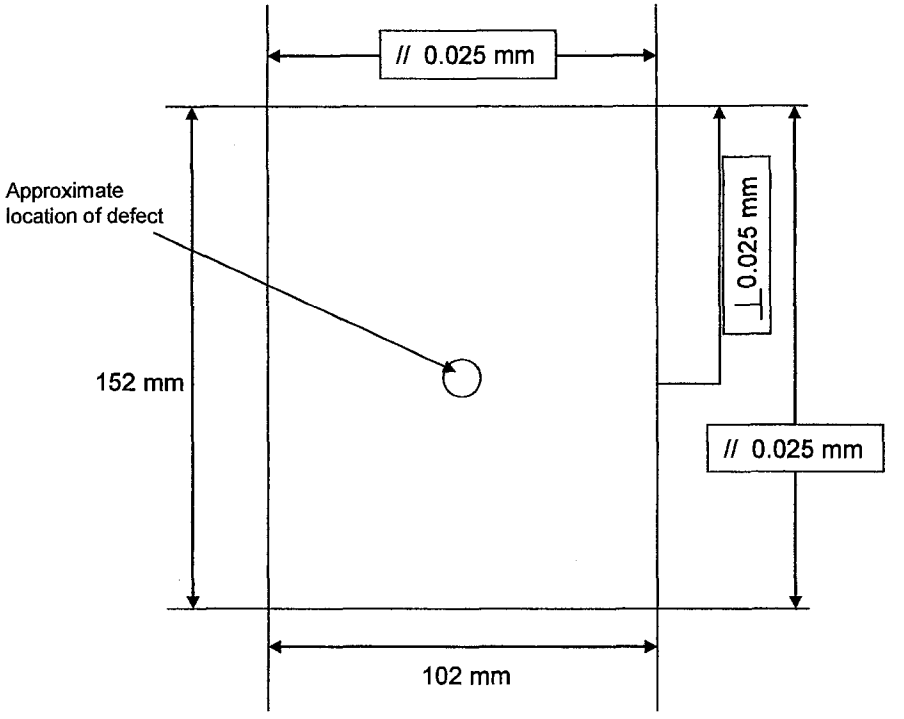

Figure 59 Schematic of compression after impact test specimen [53]

According to Figure 59, the required tolerance for specimen perpendicularity and parallelism in AITM 1.0010 was 0.025 mm, but due to limitations of the machining equipment a standard deviation of 0.127 mm in the length measurements and 0.102 mm in the width measurements was achieved.

References

[1] W.D. Callister, Jr, *Materials Science and Engineering: An Introduction*, John Wiley & Sons, Inc., New York (1994).

[2] D. Hull and T.W. Clyne, *An Introduction to Composites Materials*, Cambridge University Press, Cambridge (1996).

[3] M.G. Bader and C. Lekakou, Processing for Laminated Structures in *Composites Engineering Handbook*, (Edited by P.K. Mallick), 394-454, Marcel Dekker, Inc., New York (1997).

[4] C. Wittman, Hand Lay-up Techniques in *Handbook of Composites*, (Edited by G. Lubin), 321-367, Van Nostrand Reinhold Company, Inc., NewYork, New York (1982).

[5] S. Lee, *Dictionary of Composite Materials Technology*, Technomic Publishing Co., Inc., Lancaster, PA (1989).

[6] J.E. Sumerak, The Pultrusion Process for Continuous Automated Manufacture of Engineered Composite Profiles in *Composites Engineering Handbook*, (Edited by P.K. Mallick), 549-552, Marcel Dekker, Inc., New York (1997).

[7] www.jamco.co.jp/e/e-components/adp.html, Cutting-edge technology for lighter, stronger aircraft structural components. *Advanced Pultrusion (ADP)* (2000-2005).

[8] S.T. Peters and Y.M. Tarnopol'skii, Filament Winding in *Composites Engineering Handbook*, (Edited by P.K. Mallick), 515-545, Marcel Dekker, Inc., New York (1997).

[9] www.plastech.co.uk/Mtrtm.html, Resin Transfer Moulding (RTM) (2005).

[10] A. le Compte, Method and Apparatus for producing a thin-walled article of synthetic resin, in particular a large sized article, *United States Patent 4,359,437*, November 16, 1982.

[11] C. Williams, J. Summerscales and S. Grove, Resin infusion under flexible tooling (RIFT): a review. *Composites Part A*, **27A**, 517-524 (1996).

[12] V.M. Karbhari, D. Wang, and Y. Gao, Processing and performance of bridge deck subcomponents using two schemes of resin infusion. *Composite Structures*, **51**, 257-271 (2001).

[13] I.E. Muskat, Method of Molding, *United States Patent 2,495,640*, January 24, 1950.

[14] S.G. Advani and E.M. Sozer, Liquid Molding of Thermoset Composites. *Comprehensive Composite Materials*, **2**, 807-844 (2000).

[15] C.D. Williams, S.M. Grove and J. Summerscales, The compression response of fibre-reinforced plastic plates during manufacture by the resin infusion under flexible tooling method. *Composites Part A*, **29A**, 111-114 (1998).

[16] www.mdacomposites.org/mda/psgbridge_cb_mgf_print.html, Composites Basics: Composites Manufacturing, *American Composites Manufacturers Association*, Downloaded December 14, 2006.

[17] www.netcomposites.com/education.asp, Downloaded December 13, 2006.

[18] M. Allende, R.V. Mohan, and S. M. Walsh, Experimental and Numerical Analysis of Flow Behavior in the FASTRAC Liquid Composite Manufacturing Process. *Polymer Composites*, **4**, 384-396 (2004).

[19] G. Marsh, Putting SCRIMP in context. *Reinforced Plastics*, **January**, 22-26 (1997).

[20] W.H. Seemann, III, Plastic Transfer Molding Techniques for the Production of Fiber Reinforced Plastic Structures, *United States Patent 4,902,215*, February 20, 1990.

[21] M. Kleineberg, U. Wenner, and M. Hanke, Cost Effective CFRP-Fuselage Manufacturing with Liquid Resin Infusion (LRI) – Technologies. Institute of Composite Structures and Adaptive Systems, German Aerospace Center (2002).

[22] L.R. Thomas, A. K. Miller, and A.L. Chan, "Fabrication of Complex High-Performance Composite Structures at Low Cost using Vartm. *Proceedings of the 47th International SAMPE Symposium and Exhibition*, 1317-1329, Long Beach (2002).

[23] B.A. Gama, H. Li, W. Li, A. Paesano, D. Heider, and J.W. Gillespie, Jr., Improvement of Dimensional Tolerances During VARTM Processing. *Proceedings of the 33rd International SAMPE Technical Conference*, 1415-1427, Seattle (2001).

[24] B. Daval and S. Bickerton, Exploring the potential for laminate quality control using VARTM. *Proceedings of the 36th International SAMPE Technical Conference*, San Diego (2004).

[25] E.J. Rigas, T.J. Mulkern, S.M. Walsh, S.P. Nguyen, Effects of Processing Conditions on Vacuum Assisted Resin Transfer Molding Process (VARTM). *ARL-TR-2480*, Army Research Laboratory (2001).

[26] V. Rohatgi, N. Patel, and L. J. Lee, Macro and microvoid formation in liquid composite molding. *Proceedings of Advanced Composites Technologies Conference*, 81-98, Dearborn, Michigan (1993).

[27] M.K. Kang, W.I. Lee, and H.T. Hahn, Analysis of vacuum bag resin transfer molding process. *Composites: Part A*, **32**, 1553-1560 (2001).

[28] A. Haque, J. Johnson, U.K. Vaidya and S. Jeelani, Fatigue damage of glass/vinyl ester thick composites. *Proceedings of the ASME,* **24**, NCA (1997).

[29] T.J. Wu and H.T. Hahn, Mechanical Properties of E-Glass/Vinyl Ester Composite Fabricated by VARTM. *Proceedings of the 42nd International SAMPE Symposium*, Anaheim, California (1997).

[30] Y. Wang, J. Li, and P.B. Do, Properties of Composite Laminate Reinforced with E-glass multiaxial non-crimp fabrics. *Journal of Composite Material*, **29**, No.17, 2317-2333 (1995).

[31] J. Dai and H. T. Hahn, Flexural behavior of sandwich beams fabricated by vacuum-assisted resin transfer molding. *Composite Structures*, **61**, 247-253 (2003).

[32] A.P. Mouritz and R.S. Thomson, Compression, flexure and shear properties of a sandwich composite containing defects. *Composite Structures*, **44**, 263-278 (1999).

[33] R.S. Thomson, et al., Shear properties of a sandwich composite containing defects. *Composite Structures*, **42**, 107-118 (1998).

[34] P. Majumdar, et al., Effect of processing conditions and material properties on the debond fracture toughness of foam-core sandwich composites: experimental optimization. *Composites Part A: applied science and manufacturing*, **34**, 1097-1104 (2003).

[35] J. Dai, D. Pellaton, and H.T. Hahn, A comparative study of vacuum-assisted resin transfer molding (VARTM) for sandwich panels. *Polymer Composites*, **24**, No. 6, 672-685 (2003).

[36] R. Mathur. S.G. Advani, B.K. Fink, Optimization of Channel Design in VARTM Processing. *Specialized Moulding Techniques*, Plastics Design Library, 209-215 (2001).

[37] Part V: Airworthiness - Chapter 523: Normal, Utility, Aerobatic and Commuter Catergory Aeroplanes, *Airworthiness Manual*, Canadian Aviation Regulations (2006).

[38] R. Boukhili, et al., Mechanical Properties for Low Pressure Resin Infusion Processed Vinyl-Ester/Glass Composites, *Final Report prepared for Flight Dynamics Corporation, CDT project 2731,* École Polytechnique de Montréal, QC (2002).

[39] P. Hubert, L. Khoun, L. Petrescue, S. Gordon, and A. Johnston, Processing variability in low-cost VARTM aeronautical structures. *Proceedings of the SAMPE Europe 26th International Conference, Paris, France* (2005).

[40] M. Brothers, Personal communication (2004).

[41] http://iar-ira.nrc-cnrc.gc.ca/smpl/smpl_5d2_3.html, Enhanced Visual Techniques: Edge of Light (2005).

[42] R. Gould, T. Marincak, and J. Komorowski, TM-21-95: MICRO-INSPECTION TECHNOLOGY. *Canadian Police Research Centre* (1995).

[43] P.K. Mallick, Nondestructive Tests in *Composites Engineering Handbook*, (Edited by P.K. Mallick), 1157-1171, Marcel Dekker, Inc., New York (1997).

[44] M. Genest and D.S. Forsyth, NDE of foam core sandwich structures by thermography. *Proceedings of the Fifth Canadian-International Composites Conference*, Vancouver, Canada (2005).

[45] N.P. Avdelidis, B.C. Hawtin, and D.P. Almond, Transient thermography in the assessment of defects of aircraft composites. *NDT&E International*, **36**, 433-439 (2003).

[46] P. Hubert, L. Khoun, L. Petrescue, S. Gordon, A. Johnston, Processing Variability in Low-Cost VARTM Aeronautical Structures. *Proceedings of the 26th International Conference and Forums*, Paris, France (2005).

[47] G. Marsh, Shut it! – moving into closed moulding. *Reinforced Plastics*, **46**, No. 5, 18-24 (2002).

[48] G. Marsh, Cutting down on styrene – the resin solution. *Reinforced Plastics*, **October**, 36-42 (1999).

[49] L. Khoun, Influence of the styrene content on the chemical and mechanical properties of a vinyl ester resin used in VARTM. *DEA Report* (2004).

[50] S. Gordon and R. Boukhili, Damage tolerance of composite sandwiches: Impact damage characterization. *Proceedings of the Fifth Canadian-International Composites Conference*, Vancouver, Canada (2005).

[51] S. Gordon and R. Boukhili, Damage tolerance of composite sandwich: fatigue behaviour. *Proceedings of the Fifth Canadian-International Composites Conference*, Vancouver, Canada (2005).

[52] SRM 2R-94, SACMA Recommended Test Method for Compression after impact properties of oriented fiber-resin composites. *Suppliers of Advanced Composites Materials Association* (1994).

[53] AITM 1.0010, Airbus Industrie Test Method: Determination of compression strength after impact. *Airbus Industrie* (1994).